Realia et naturalia

DISSERTATIONES
CHIMICAE
UNIVERSITATIS
TARTUENSIS
139

ELO KIBENA

Electrochemical grafting of glassy carbon, gold, highly oriented pyrolytic graphite and chemical vapour deposition-grown graphene electrodes by diazonium reduction method

TARTU ÜLIKOOL · UNIVERSITAS TARTUENSIS · 1632

DISSERTATIONES CHIMICAE UNIVERSITATIS TARTUENSIS
139

DISSERTATIONES CHIMICAE UNIVERSITATIS TARTUENSIS
139

ELO KIBENA

Electrochemical grafting of glassy carbon, gold, highly oriented pyrolytic graphite and chemical vapour deposition-grown graphene electrodes by diazonium reduction method

UNIVERSITY OF TARTU
PRESS
1632

Institute of Chemistry, Faculty of Science and Technology, University of Tartu, Estonia

Dissertation is accepted for the commencement of the degree of Doctor of Philosophy in Chemistry on June 17th, 2014 by the Council of the Institute of Chemistry, University of Tartu.

Supervisor: Assoc. Prof. Kaido Tammeveski
Institute of Chemistry, University of Tartu, Estonia

Opponent: Assoc. Prof. Lasse Murtomäki
Department of Chemistry, Aalto University, Finland

Commencement: August 27th, 2014 at 10:00 in Tartu, Ravila 14a, room 1021.

Publication of this dissertation is granted by FMTDK.

ISSN 1406-0299
ISBN 978-9949-32-619-8 (print)
ISBN 978-9949-32-620-4 (pdf)

University of Tartu Press
www.tyk.ee

TABLE OF CONTENTS

I. LIST OF ORIGINAL PUBLICATIONS

This thesis consists of six original articles listed below and a review. The articles are referred in the text by Roman numerals I–VI.

I **E. Kibena**, U. Mäeorg, L. Matisen, K. Tammeveski, Electrochemical behaviour of ABTS on aryl-modified glassy carbon electrodes, *Journal of Electroanalytical Chemistry* 661 (2011) 343–350.

II **E. Kibena**, U. Mäeorg, L. Matisen, P. Sulamägi, K. Tammeveski, A study of glassy carbon electrodes modified with azobenzene derivatives, *Journal of Electroanalytical Chemistry* 686 (2012) 46–53.

III **E. Kibena**, M. Marandi, U. Mäeorg, L.B. Venarusso, G. Maia, L. Matisen, A. Kasikov, V. Sammelselg, K. Tammeveski, Electrochemical modification of gold electrodes with azobenzene derivatives by diazonium reduction, *ChemPhysChem* 14 (2013) 1043–1054.

IV **E. Kibena**, K. Tammeveski, L. Matisen, U. Hasse, F. Scholz, $OH^{\bullet}$ radical degradation of blocking aryl layers on glassy carbon and gold electrodes leads to film thinning on glassy carbon and pinhole films on gold, *Electrochemistry Communications* 29 (2013) 33–36.

V **E. Kibena**, M. Mooste, J. Kozlova, M. Marandi, V. Sammelselg, K. Tammeveski, Surface and electrochemical characterisation of CVD grown graphene sheets, *Electrochemistry Communications* 35 (2013) 26–29.

VI **E. Kibena**, M. Marandi, V. Sammelselg, K. Tammeveski, B.B.E. Jensen, A.B. Mortensen, M. Lillethorup, M. Kongsfelt, S.U. Pedersen, K. Daasbjerg, Electrochemical behaviour of HOPG and CVD-grown graphene electrodes modified with thick anthraquinone films by diazonium reduction (2014, submitted).

Author's contribution:

Paper I: The author has performed all electrochemical measurements, analysis of data and is mainly responsible for writing the paper.

Paper II: The author has performed all electrochemical measurements, analysis of data and is mainly responsible for writing the paper.

Paper III: The author has participated in the electrochemical measurements, analysis of data and writing the paper.

Paper IV: The author has performed all electrochemical measurements, analysis of data and is mainly responsible for writing the paper.

Paper V: The author has participated in the electrochemical measurements, analysis of data and is mainly responsible for writing the paper.

Paper VI: The author has performed all electrochemical measurements, analysis of data and is mainly responsible for writing the paper.

2. ABBREVIATIONS AND SYMBOLS

A	geometric surface area of an electrode
A_r	real surface area of an electrode
AB	azobenzene
ABD	azobenzene diazonium tetrafluoroborate
ABTS	2,2`-azino-bis(3-ethylbenzothiazoline-6-sulphonic acid) diammonium salt
ACN	acetonitrile
AFM	atomic force microscopy
AP	4-aminophenyl
APOH	hydroxylaminophenyl
AQ	9,10-anthraquinone
AQD	9,10-anthraquinone-1-diazonium tetrafluoroborate
Au/AB	gold electrodes electrografted with azobenzene groups
Au/FBK	gold electrodes electrografted with 2,5–dimethoxy–4–([4–nitrophenyl]azo)benzene groups
Au/GBC	gold electrodes electrografted with 2–methyl–4–([2–methylphenyl]azo)benzene groups
C^o	concentration in the bulk solution
C_{dl}	double-layer capacitance
C_f	the sensitivity factor of the crystal
$c_{O_2}^b$	concentration of oxygen in the bulk solution
CP	4-carboxyphenyl
CPD	4-carboxyphenyldiazonium salt
CV	cyclic voltammetry
Cu-Gra	chemical vapour deposition-grown graphene on copper foil
Cu-Gra/AQ	chemical vapour deposition-grown graphene on copper foil electrografted with 9,10-anthraquinone groups
CVD	chemical vapour deposition
D	diffusion coefficient
D_{O_2}	diffusion coefficient of oxygen
DEA	4-diazo-N,N-diethylaniline
$E_{Fc^+}^0$	standard potential of the Fc^+/Fc couple
E_p	peak potential
$E_{1/2}$	half-wave potential
EC	electrochemical-chemical
EIS	electrochemical impedance spectroscopy
ET	electron transfer
EQCM	electrochemical quartz crystal microbalance
F	Faraday constant
FBK	2,5–dimethoxy–4–([4–nitrophenyl]azo)benzene
GBC	2–methyl–4–([2–methylphenyl]azo)benzene

GC	glassy carbon
GC/AB	glassy carbon electrografted with azobenzene groups
GC/AQ	glassy carbon electrografted with 9,10-anthraquinone groups
GC/CP	glassy carbon electrografted with 4-carboxyphenyl groups
GC/FBK	glassy carbon electrografted with 2,5–dimethoxy–4–([4–nitrophenyl]azo)benzene groups
GC/GBC	glassy carbon electrografted with 2–methyl–4–([2–methylphenyl]azo)benzene groups
GC/NP	glassy carbon electrografted with 4-nitrophenyl groups
GO	graphene oxide
HOPG	highly oriented pyrolytic graphite
HOPG/AQ	highly oriented pyrolytic graphite electrografted with 9,10-anthraquinone groups
I	current
I_D	disk current
I_d	diffusion-limited current
I_k	kinetic current
I_{pa}	the anodic peak current
I_{pc}	the cathodic peak current
I_{rel}	relative blocking efficiency
j	current density
k	electrochemical rate constant
k° (or k_{app}°)	standard heterogeneous electron transfer rate constant
K-L	Koutecky-Levich
LSV	linear sweep voltammetry
n	number of electrons
NAB	nitroazobenzene
NADH	β-nicotinamide adenine dinucleotide
NBD	4-nitrobenzenediazonium tetrafluoroborate
Ni-Gra	graphene grown on nickel by chemical vapour deposition
Ni-Gra/AQ	chemical vapour deposition-grown graphene on nickel substrate electrografted with 9,10-anthraquinone groups
NMR	nuclear magnetic resonance
NP	4-nitrophenyl
OCP	open circuit potential
$OH^\bullet$	hydroxyl radical
ORR	oxygen reduction reaction
PAA	4–diazophenylaceticacid tetrafluroborate
PMMA	poly(methyl methacrylate)
Q	charge
Q_{dl}	constant phase element involving an n exponent to represent double-layer capacitance
Q_{lf}	constant phase element at the low-frequency limits
R	universal gas constant

RDE	rotating disk electrode
rGO	reduced graphene oxide
RMS	root-mean-square
rpm	revolutions per minute
R_{ct}	resistance of the charge transfer
R_s	solution resistance
R_p	the overall reflection coefficient for in-plane polarised lights
R_s	the overall reflection coefficient for out-of-plane polarised lights
SAM	self-assembled monolayer
SCE	saturated calomel electrode
$TBABF_4$	tetrabutylammonium tetrafluoroborate
UV	ultraviolet
v	kinematic viscosity of the solution
XPS	X-ray photoelectron spectroscopy
Γ_{AQ}	surface concentration of 9,10-anthraquinone groups
Γ_{NP}	surface concentration of 4-nitrophenyl groups
ΔE_p	peak potential separation
Δf	resonance frequency shift
Δm	change of mass per unit area
Δ_g	ellipsometric parameter of the grafted substrate (the phase shift)
Δ_s	ellipsometric parameter of the bare substrate (the phase shift)
ψ_s	ellipsometric parameter of the bare substrate (the amplitude ration upon reflection)
ψ_g	ellipsometric parameter of the grafted substrate (the amplitude ratio upon reflection)
v	potential scan rate
ω	electrode rotation rate

3. INTRODUCTION

Often, the functionalisation of electrode surface with organic (aryl) groups is necessary in order to achieve desired electrochemical properties which differ from that of the bulk material. A versatile way to do that is to use the electrochemical reduction of corresponding aryldiazonium salts. This method allows the modification of various electrode materials with desired functional groups and most importantly, strong (covalent) bonding between the underlying substrate and organic molecules is obtained [1].

The electrode modification by diazonium chemistry has found many potential applications including (bio)sensors, electrocatalysis and electroanalysis [2–4]. Although the practical output is highly necessary, the fundamental studies (including the blocking and electrocatalytic properties of aryl-modified electrodes) are important as well. Even though the modification of different electrode materials by diazonium reduction has already been the subject of research over two decades [1], there are still some controversies, which need to be explored. For example, the electrochemical behaviour of different substrate materials during electrografting, the stability of the aryl films (especially on gold), the nature of the aryl layers formed on the underlying substrate (e.g. mono- or multilayer) and last but not least, the morphological and electrochemical properties of the aryl-modified electrodes (including comparison between highly oriented pyrolytic graphite and graphene).

Therefore, the main purpose of this PhD thesis was to modify different electrode materials including glassy carbon (GC), gold, highly oriented pyrolytic graphite (HOPG) and graphene grown by chemical vapour deposition (CVD) method through electrochemical reduction of corresponding diazonium salts to further investigate their morphological and electrochemical properties.

The present thesis comprises three chapters. Firstly, a brief literature overview is made for better understanding of the electrode materials, diazonium salts and electrografting method selected for this particular work. Thereafter, a full description of experimental work followed by results and discussion is given. The main part of the work was divided into three sections. First, the electrochemical behaviour of ABTS, which is most common redox mediator for enzyme-based electrodes, was studied on 4-nitrophenyl-, reduced 4-nitrophenyl- and 4-carboxyphenyl-modified GC electrodes in aqueous solutions of various pH [I]. The second part of the work focused on comparison studies of GC and Au electrodes modified with three different azobenzene derivatives [II,III]. In addition, the aryl film degradation on GC and Au electrodes was further investigated by $OH^{\bullet}$ radicals attack [IV]. The third part of the work involved the morphological and electrochemical investigations of bare HOPG and CVD-grown graphene electrodes [V] followed by electrografting with thick anthraquinone layers on HOPG and graphene-based electrodes [VI].

4. LITERATURE OVERVIEW

4.1. The diazonium reduction method

The modification of different electrode materials with organic films has been a widely studied area because of their prospective applications for example in (bio)sensors, corrosion protection, smart surfaces, electroanalysis and electrocatalysis [1]. It is of paramount importance to obtain a strong (covalent) bond between the underlying substrate surface and organic group. In terms of that, the reduction of aryldiazonium salts has received much attention and is currently one of the most commonly used surface derivatisation methods [4]. Mostly because it is a versatile tool to functionalise the electrode surfaces (including carbon, metals and semiconductors) with different aryl groups bearing various functionalities *via* strong (covalent) bond [5, 6]. This literature overview summarises briefly the diazonium reduction method (both on carbon- and metal-based electrodes) including the selection of substrate materials and diazonium salts. Furthermore, morphological and electrochemical properties of aryl-modified electrodes will be discussed.

4.1.1. Electrode materials for electrografting

Before the modification, the choice of the substrate material is important. Many types of electrode surfaces have been modified by diazonium reduction: carbon (e.g. glassy carbon (GC), highly oriented pyrolytic graphite (HOPG), carbon nanotubes, graphene), metals (e.g. gold, nickel, copper) and even insulators (e.g. organic polymers) [4]. Taken into account the used substrates in this thesis, an overview about GC, HOPG, graphene and Au electrodes is given. While graphene is rather new material, a longer description about this substrate will be given.

The main advantages of the electrodes based on carbon materials are as follows: low-cost, conductive surface, mechanical stability and wide potential window in electrochemistry [7]. Among bulk carbon electrodes, GC has been the most frequently used and extensively studied substrate material in electrochemistry research [8]. GC provides a stable surface to attach organic and biomolecules and also it has a reproducible surface for film formation, which is extremely important in the field of modification [9]. The surface of GC is expected to be a mixture of edge and basal plane sites [7]. Furthermore, the heterogeneous electron transfer rate constant (k°) of polished GC electrode for the most commonly used redox probe (ferri/ferrocyanide) is relatively high. Based on the different reports the value of k° for polished GC has measured to be 0.012 cm s^{-1} [10] or 0.076 cm s^{-1} [11] which makes this material suitable for studying the blocking properties of aryl layers.

The most ordered carbon material is highly oriented pyrolytic graphite (HOPG) [7]. HOPG has been used for several applications due to its extreme

smoothness and easily renewable surface by an adhesive tape [12]. In addition, HOPG has a good conductivity, but this material is mechanically quite fragile [12]. It has been proposed that if an adhesive tape is used for the removing of HOPG layers, this method may introduce defects on the surface of HOPG [12], which may have a great impact on the electrochemical properties of this material itself. The reactivity of HOPG has been widely studied by McCreery and co-workers [13–15]. It has been well established that the electrochemical kinetics is faster on the edge sites than on the basal plane of HOPG [12]. For example, the electrochemical behaviour of edge plane HOPG towards ferricyanide reduction is rather similar to that of bare GC, whereas basal plane HOPG is rather inactive [13, 15, 16], which makes this substrate attractive for studying the electrocatalytically active materials. Based on the literature, the k° value measured on defect-free basal plane HOPG is less than 10^{-6} cm s^{-1} for the ferricyanide reduction [17] or even as low as 10^{-9} cm s^{-1} [16]. It is also important to note that HOPG is the closest material to a novel carbon material, graphene, because well-defined HOPG consists of single layered graphene sheets [18, 19].

As mentioned above, one of the newest member of the carbon family is graphene. With its extraordinary electrical, optical, thermal and chemical properties, graphene has attracted particular attention since its discovery by Novoselov *et al*. [19, 20]. In a simplified way, graphene may be considered as a two-dimensional one-atomic thin layer of graphite, where the sp^2-hybridised carbon atoms are hexagonally arranged like in a honeycomb lattice. According to the literature, high-quality mono- or few-layer graphene layers can be prepared by mechanical exfoliation of HOPG using the Scotch tape method [19, 20]. For research applications this method works excellently but on a commercial scale it will hardly ever be applicable [20]. There are some other methods employed for graphene synthesis, for example epitaxial growth, chemical exfoliation (e.g. Hummers' method) and chemical vapour deposition (CVD), the latter being the most promising and frequently used method to synthesise graphene on a larger scale [21, 22].

By controlling synthesising parameters, mono-, bi-, few- or multilayer graphene can be made by CVD on different catalytic metal substrates (Pt, Ru, Ni, Cu, Ir or Co). The choice of the metal substrate greatly depends on the cost and therefore the low-cost polycrystalline Ni has been widely employed in order to synthesise graphene by CVD [23]. Zhou´s group has compared the graphene formation on single crystal Ni(111) and on polycrystalline Ni substrate by CVD method [24]. The authors revealed that on single crystal surface the monolayer or bilayer graphene was formed because of the atomically smooth underlying surface and the absence of grain boundaries, whereas multilayer graphene was formed on polycrystalline Ni presumably due to the grain boundaries in Ni which enables the multilayer growth [24]. Just for the clarification, multilayer graphene can be viewed as more than three and less than ten layers of graphene nanosheets [25].

In general, graphene has a broad range of promising applications including (bio)sensors, nanocomposite materials and protection against corrosion [26]. For example, it has been shown that graphene films grown on catalytic substrates (for example on Ni) by CVD can be used to protect the underlying surface from the oxidation [27, 28]. Furthermore, graphene is also a good model material to be modified because of its novel interesting properties [29].

In contrast to the multilayer graphene formation on Ni substrate, graphene synthesis by CVD on Cu generally yields a uniform thickness and single-layer graphene films due to the low solubility of carbon in Cu. It has also been suggested that graphene growth on Cu is self-limiting [30].

Although carbon-based substrates (especially GC) have some advantages (usually low-cost) over metals, metal-based (particularly gold) electrodes have also gained much interest [31]. It has been claimed that gold has a lower capacitance than carbon materials [32]. Furthermore, the surface of Au can be easily cleaned and while it can be produced very flat (even as a single crystal), this substrate material is suitable for various surface-sensitive techniques such as atomic force microscopy (AFM), ellipsometry and X-ray photoelectron spectroscopy (XPS) [6].

4.1.2. The selection of diazonium salts

In general, the aryldiazonium salts (with the general structure of $RC_6H_4N_2^+$, where R can be $–NO_2$, –COOH, etc.) are widely used in organic synthesis in order to generate a large variety of organic compounds including the production of dyes [6]. For example, aromatic azo compounds are known as a basis for the production of dyes [33]. One of the most common azo compounds is azobenzene. Because of its characteristic colour and photoresponsive properties, azobenzene and its derivatives have received considerable attention. In addition, they are known for their reversible *trans–cis* photoisomerisation [34]. Thus, these compounds have a wide variety of potential applications such as optical storage media, chemosensors and photochemical molecular switches [35, 36].

In general, aryldiazonium salts have many advantages. For example, a lot of them are commercially available. Also, the synthesising process of diazonium salt is quite easy and if necessary, it can be prepared rapidly *in situ* from the corresponding aromatic amine [5].

Recently, the diazonium salts have attracted much attention from the modification of electrode materials point of view. There is a wide variety of diazonium salts which have been used for surface modification. Among the other aryldiazonium salts, 4-nitrobenzenediazonium salt (NBD) is one of the most widely used and studied diazonium compounds for modifying different electrode surfaces (e.g. GC, Au, graphene) with nitrophenyl (NP) groups [37, 38]. It has quite a simple structure which generally allows the formation of densely packed aryl film on the substrate material [39, 40]. Furthermore, the NP groups are electroactive and therefore it is possible to estimate the surface

concentration of the NP molecules attached to the electrode surface [5, 41]. Furthermore, NP groups can be further reduced in protic media *via* electrochemical or chemical reduction to aminophenyl groups [42, 43], which are important ”bridges” for covalently immobilised biomolecules (e.g. enzymes, redox proteins, DNA) to surfaces for biological sensing. Also the 4-carboxyphenyldiazonium salts (CPD) have attracted much attention in order to form 4-carboxyphenyl (CP) layers on electrode surfaces for sensing applications [44, 45]. Furthermore, the CP-derivatised electrodes have been employed/ studied for the corrosion inhibitors on metal surfaces [46].

In addition, a lot of interest has been shown in diazonium salts containing anthraquinone (AQ) derivatives. Generally, AQ has been frequently used in dyes [47] but it is also an important redox molecule for electrochemical applications, including redox mediation [1]. Because of this feature AQ-functionalised substrates have shown promising applications in (bio)sensors [48–50], biofuel cells [51], and electrocatalysis, including the production of hydrogen peroxide *via* the oxygen reduction reaction (ORR) [52–57]. In addition, similarly to NP groups, it is possible to determine the surface concentration of AQ groups attached on the substrate material.

4.1.3. The mechanism of electrode surface modification *via* diazonium reduction

The electrode surface modification method *via* the electrochemical reduction of aryldiazonium salts was first introduced by Pinson and co-workers in 1992 [41]. In general, this process follows a two-step pathway and the proposed reaction mechanism of that is depicted in Scheme 1.

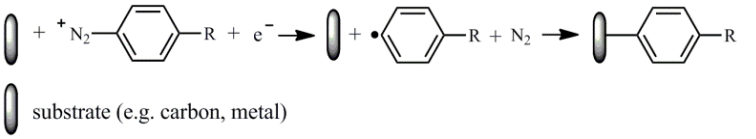

Scheme 1. Proposed reaction mechanism for electrografting by diazonium reduction [5].

In the first step (Scheme 1), the formation of aryl radical and evolution of nitrogen occurs during the one-electron reduction of aryldiazonium compound [1]. Thereafter, the formed aryl radical reacts with the electrode surface, giving a strong bond between the electrode surface and modifier [1]. In case of carbon materials it has been proposed that during the electrografting, the surface carbons bearing the aryl group most likely pass from a sp^2 to a sp^3 hybridisation [58].

The surface grafting with aryldiazonium salts can be performed spontaneously or electrochemically. The spontaneous grafting is achieved by

dipping the electrode into a solution of the diazonium salt for a certain time period [59] and this method has proven to be very useful for modification for example graphene sheets [60]. In contrast, the electrochemical grafting involves the potential cycling or electrolysis at certain potential by applying the potential with a potentiostat [4]. Although spontaneous modification is easier than electrochemical grafting, the first method usually lacks control during the modification, is time-consuming and is not very reproducible [5, 7]. Therefore, the latter method (electrografting) is more preferable due to the better control of the formation of an aryl film on the electrode surface. Usually, the electrografting is performed in a narrow potential range using potential cycling. On the first cycle, single and broad, one-electron wave is observed at potentials close to 0 V (vs. SCE) [1]. It has been proposed that this reduction wave corresponds to the formation of an aryl radical which reacts with the electrode surface. On the subsequent cycles, this reduction wave disappears, which is indicative of the blocking of the electrode surface by the organic groups [5].

The electrochemical reduction of aryldiazonium salts can be carried out both in aprotic (e.g. acetonitrile) or in aqueous acidic solutions. It has been proposed that the grafted aryl-layers on Au surface in aqueous solution are less compact than those grafted in acetonitrile [32]. Based on the Brooksby and Downard study [40], the aryl-film formation on pyrolysed photoresist films in aqueous acid medium yielded lower surface coverage as well as thinner films compared to the aryl films formed in acetonitrile.

The diazonium reduction method has been applied to different electrode materials [7]. One of the most important issues concerns the nature of the bond between the aryl group and electrode surface. Generally, it has been suggested that one of the advantages of the diazonium reduction method is the long-term stability of the aryl layer on electrode surface which indicates that this method allows a strong (covalent) bond between the surface modifier and substrate. It is well established that aryl groups are covalently bonded to the GC surface [61]. This finding has been supported by Raman spectroscopy [62, 63] or time-of-flight secondary ion mass spectroscopy [64]. Also, the calculated bonding energy is very high between the aryl group and carbon electrode surface (105 kcal mol^{-1}) indicating the formation of covalent bond [65]. However, the nature of the bond between an aryl group and HOPG (especially basal plane) is still not fully clear. Liu and McCreery have reported about the chemisorbed (covalently attached) aryl groups on both basal and edge plane HOPG by the electrochemical reduction of the corresponding diazonium salts [62, 66]. In addition, Saveant and co-workers have claimed that the aryl radicals are able to attach to both edge and basal plane graphite [41, 58]. Furthermore, Ray and McCreery concluded that the chemisorption of aryl radicals formed during the diazonium reduction may form both basal and edge regions but more rapidly at edge sites [67]. Very recently, Kirkman *et al.* [68] proposed that aryl groups are covalently attached both basal plane and step edge sites of HOPG. In contrast, Ma *et al*. [69] presented an interesting finding on the attachment of aryl groups

onto HOPG *via* diazonium reduction and these authors concluded that there is no clear evidence for covalent attachment of aryl groups to basal plane HOPG.

There is also a disagreement about the nature of the bonding (covalent or noncovalent bond) between the aryl group and graphene surface. One point of view is that grafting the graphene (including the basal plane graphene) by diazonium reduction yielded a covalent carbon-carbon bond between the aryl group and graphene surface [60, 70, 71]. In contrast, Jiang *et al*. concluded in their paper that the isolated phenyl groups might be weakly bonded on the basal plane graphene *via* diazonium reduction although a carbon-carbon bond is formed between the aryl group and graphene converting a sp^2-carbon in the graphene sheet to sp^3 [72]. Furthermore, it has been proposed that the diazonium reduction appears more rapidly at edges and the reactivity of the sp^2 sites is much higher for single layer than bilayer graphene and decreases further as the number of graphene layers increases and it is still not clear how aryl radicals bind to multilayer graphene [69, 73].

It has been proposed that the modification by the reduction of diazonium salts on metal surfaces (including Au) is more complex and difficult than that of carbon electrodes [5]. The first attempt of modifying metal electrodes (including Au) by diazonium salts was reported by Ahlberg *et al.* already in 1980 [74]. However a systematic characterisation of diazonium-functionalised Au was first reported by Laforgue *et al*. [75]. It has been considered, that for Au substrate, the nature of the bond on Au surface is also controversial and there is still lack of information about the electrochemical grafting process and the physico-chemical properties of the deposited layer [32]. In general, it has been shown that the reduction of aryldiazonium salts on Au surface leads to the formation of Au–C bonds [76]. Furthermore, the Au–C bond formed by diazonium-based radical during electrografting is more stable and stronger compared to the Au–S (sulphur) bond produced by self-assembled monolayers (SAMs) of thiols on gold [44, 77–79]. Laurentius *et al*. [76] have claimed that the interaction between the organic layer derived from diazonium chemistry and Au substrate is Au–C covalent bond, which was confirmed by surface-enhanced Raman scattering studies. It has been claimed that the calculated bonding energy between the organic molecule and Au surface is 24 kcal mol^{-1} [80], which is much higher than that reported for thiol SAMs on Au (5 kcal mol^{-1}) [5], but at the same time it is much lower than that calculated in case of carbon-based materials (105 kcal mol^{-1}). Besides the strong bond between aryl layer and substrate, and the presence of azo bonds inside the multilayer films, the formation of Au–N=N–C bonds is also evident [81].

In general, the attachment of the aryl films on electrode surface is strong and persistent. In order to remove the organic films from the surface, a mechanical abrasion is required. It has been shown that the aryl films on GC and Au surface are even able to withstand ultrasonication in different solvents and long time exposure to ambient conditions [5]. Lately, Lee *et al*. [82] studied the stability of aminophenyl films electrografted on GC and Au surfaces and the results

revealed that the aryl films grafted on Au surface were more stable than those grafted to GC.

An interesting study has been carried out by Scholz *et al*. [83] where the authors showed that SAMs of thiols on gold and mercury electrodes were degraded by hydroxyl radicals ($OH^{\bullet}$). It is known that $OH^{\bullet}$ radical is a highly reactive species degrading almost all kinds of organic compounds. Usually, the $OH^{\bullet}$ radicals are used in advanced oxidation processes for removal or degradation of pollutants, e.g., azo compounds (dyes) in different wastewaters. $OH^{\bullet}$ radicals can be produced by Fenton reactions or UV photolysis of water and hydrogen peroxide. In the Fenton process, $OH^{\bullet}$ radicals are generated in acid media from H_2O_2 in the presence of Fe^{2+} ions [84]. As shown by Scholz workgroup, $OH^{\bullet}$ radicals were able to degrade SAMs of thiols on Au [83] and in addition to remove surface asperities from mechanically polished Au electrodes [85] whereby active centres were knocked out [86]. Therefore, it would be highly interesting to study the degradation of aryl layers on GC and Au substrate by $OH^{\bullet}$ radicals in order to get some insight into the stability of the aryl layers formed on either GC and Au substrate and it was performed recently [IV].

4.1.4. Mono- or multilayer formation of aryl films

Electrochemical reduction of diazonium salts often yields submonolayers, monolayers or multilayers on electrode surfaces, depending on the choice of the substrate, aryldiazonium salt and the modification procedures used. Furthermore, an insulating (when diazonium compounds are not electroactive) or conducting aryl film may form on the electrode surface. The insulating layers can be functionalised with electroactive molecules (e.g. ferrocene) [77]. Both (mono- and multilayers) have potential applications in many fields including biosensing, corrosion protection, electrocatalysis, etc. [5].

It is necessary to obtain a sufficiently thin (rather a monolayer) and well-conductive aryl layer on the electrode surface in order to attach biomolecules for the construction of biosensors [87]. Taking into account the substrate nature (e.g. GC), it is suggested that highly ordered monolayers could not form on the GC surface due to its roughness [88], rather a structurally disordered monolayer containing defects or microscopic pinholes may form [89]. However, there is a discrepancy in the literature. According to the study by Downard and Prince, even if the monolayer is very thin, it can be rather blocking towards electron transfer decreasing the electron transfer rate [89]. Whereas others suggest that the monolayer is not expected to significantly decrease the ferri/ferrocyanide electron-transfer rate [75, 90].

While aryl radicals are highly reactive, the formation of multilayers is usually observed. The resulting organic layers bring new properties to the covered substrate, leading to applications in many areas such as corrosion, insulating material and catalysis [91]. Different mechanisms for aryl film

growth and multilayer formation have been proposed. The most common explanation is that the multilayer formation on electrode surface may occur due to the highly reactive free radicals in the solution generated during the electrografting which might react with already formed aryl layer on electrode surface (see Scheme 2) [17]. This might indicate that the initial aryl layer could become sufficiently conductive to reduce further diazonium ions in the solution [92]. As can be seen from Scheme 2, the formed aryl radical may attack already grafted aryl group on the electrode surface. It has been even proposed that during this process, cyclohexadienyl radical may form which may further react with an aryl radical or diazonium cations [1, 5]. In order to recover the aromaticity, the cyclohexadienyl radical should lose a hydrogen radical [5]. Furthermore, it has been proposed that during the multilayer formation, the azo bonds within the aryl film may form [1]. Another explanation has been given by Brooksby and Downard, where the multilayer formation may occur due to the penetration of diazonium precursor in aryl film defects/pinholes/pores [93]. Solak *et al*. [94] proposed that if the electrons could transfer only through pinholes, they would be rapidly clogged and multilayer formation would be inhibited. In general, the multilayers formed on the electrode surface are rather disordered than closely packed (e.g. *para*-substitution) [10, 17]. However, the thickness of the aryl film formed can be controlled by several parameters (see Section 4.1.5).

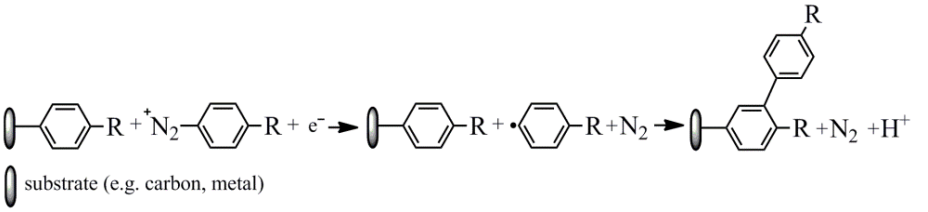

Scheme 2. Proposed mechanism for the formation of multilayer on electrode surface by aryldiazonium reduction [5].

4.1.5. The formation of thick organic films by diazonium reduction

There are several factors which influence the thickness of aryl films formed on electrode surface by the electrochemical reduction of diazonium salts: the number of potential cycles applied, electrolysis (modification) time, applied potential, potential sweep rate, the type of electrode material, the type of aryl diazonium salt, the concentration of the diazonium salt solution [40]. For example, the aryl film thickness can be varied through controlled potential electrolysis. Downard [95] investigated the aryl film formation using different electrolysis potentials as well as different electrolysis time. The results revealed that the surface concentration of aryl groups (e.g. nitrophenyl) depends greatly on the modification potential. The surface coverage increased as the electrolysis potential became more negative, however using the same potential but different

electrolysis time the film formation seemed to be self-limiting (e.g. 10 min was enough instead of 100 min) [95]. In addition, the film growth stopped at each potential used and submonolayer coverage was obtained [95]. Moreover, Kariuki and McDermott [10] claimed that thick aryl films (15–25 nm) can be obtained using high diazonium concentration as well as long periods of deposition time (10–30 min).

A step forward is the formation of thick organic film on the electrode surface. Very recently, this strategy was fully explored by Daasbjerg and coworkers [96–98] who reported about the formation of thick covalently attached conducting organic layers on different substrates (GC, gold and stainless steel) *via* electrochemical reduction of various aryldiazonium salts (including 4-nitrobenzenediazonium tetrafluoroborate and 9,10-dioxo-9,10-dihydroanthracene-2-diazonium salt). In order to form conductive organic films of high thickness, the main factors are as follows: the aryldiazonium salt should contain redox active functionality in order to maintain the charge propagation in the growing film; the sweeping of potential is essential during the electrografting process to avoid the clogging of the physisorbed species in the electrolyte channels in the film; usually a higher sweep rate than 500 mV s^{-1} is preferred and last but not least, the selection of the switching potential during the surface modification is important [96–98]. For example, when the electrografting of AQ moieties on Au substrate was carried out in the potential range where only the reduction pre-wave of the diazonium salt appeared, the layer thickness of the organic film was almost 10 times lower compared to the one where the switching potential was set to more negative direction where the first redox wave of the AQ moiety was observed as well [98]. Furthermore, the formation of thick conducting films depends on the substrate and aryldiazonium salt used [96]. To date, there has been no report on systematic studies about the formation of thick organic layers on CVD-grown graphene or HOPG as yet. Therefore it has been done recently in the frame of this PhD thesis [VI].

4.2. Surface morphology characterisation of aryl-modified electrodes

After surface derivatisation with aryl groups, it is necessary to ascertain the presence of an aryl film on electrode surface [5]. The characterisation of the aryl-modified surfaces can be achieved by various analytical or spectroscopic methods, including X-ray photoelectron spectroscopy (XPS), atomic force microscopy (AFM), ellipsometry, Raman spectroscopy, electrochemical quartz crystal microbalance [4, 5, 99].

One of the most popular surface characterisation method is X-ray photoelectron spectroscopy. This method has been widely used for the elemental composition analysis of surface films. There is a large variety of functional groups (e.g. F-, Br-, I-) that can be detected in the aryl film by XPS [5]. Most

widely studied are the modifiers containing nitro groups. The latter give a clear signal in the XPS spectra at about 406 eV [1]. In addition, further reduction of $–NO_2$ groups give a peak at about 400 eV [1], which usually corresponds to the aminophenyl groups. The XPS peak at ca 400 eV can be also attributed to azo groups or azo bonds, which may form during the electrografting and additionally confirm the multilayer presence on the electrode surface [4].

Atomic force microscopy has been widely used for the observation of modification of surfaces after electrografting. The AFM images clearly evidence the formation of an aryl layer of variable height and roughness (depending on the grafting conditions). AFM can be also used for estimating the aryl layer thickness by the "scratching" method [5]. Ellipsometry has been also used for measuring the film thickness [100]. It has been proposed that ellipsometry can be applied to film thicknesses from monoatomic up to mircometer [101]. In 1994, Wall *et al*. [102] measured the thickness of thin poly(phenyleneoxide) film (the latter was electrochemically deposited onto HOPG) by AFM and spectroscopic ellipsometry and the results showed that the ellipsometry measurements were more or less concordant with AFM measurements.

Raman spectroscopy is also a very useful technique in characterising the surface groups [5]. For example, McCreery and co-workers modified the (both edge and basal plane) HOPG and GC surfaces with 4-azobenzene (AB) or 4-nitroazobenzene (NAB) groups by diazonium reduction and studied the aryl-film composition by Raman spectroscopy [62, 67]. The authors demonstrated that the attachment of AB or NAB layers on GC and HOPG was observed through a complete assignment of the spectra [5]. In addition, Raman spectroscopy is a powerful tool to characterise the quality of HOPG and CVD-grown graphene [103].

Electrochemical quartz crystal microbalance (EQCM) is a good technique in order to study the formation of mono- or multilayers. Gold substrates are suitable for these measurements. For example, the EQCM results on aryl-modified Au substrates have shown a mass increase higher than a monolayer even after the first half cycle during the electrochemical grafting, which increased progressively also in the subsequent cycles indicating the formation of multilayer on Au substrate [104].

4.3. Electrochemical properties of aryl-modified electrodes

Aryl groups grafted to an electrode surface may have a great impact on the underlying material itself, therefore it is important to study the electrochemical properties of these functional layers [105]. In order to do that, electrochemistry (e.g. cyclic voltammetry, rotating disk electrode method, electrochemical impedance spectroscopy) provides a convenient tool to study the electrochemical properties of aryl films deposited onto electrode surface. Using the

solution-based redox probes at aryl-modified surfaces, it is possible to study the blocking properties or in contrast, electrocatalytic effect on the electron transfer reactions.

4.3.1. Studies of redox systems on aryl-modified electrodes

Based on the literature, different redox probes have been used to investigate the electrochemical properties (especially barrier properties) of aryl-modified electrodes compared to bare surfaces [7, 8, 61].

One of the interesting redox probes is $ABTS^{2-}/ABTS^{\bullet-}$ (2,2`-azino-bis(3-ethylbenzothiazoline-6-sulphonic acid), ABTS). ABTS has been widely used as an electron transfer (ET) mediator for O_2 reduction on laccase-modified electrodes to ensure the effective electron transfer communication between the redox centres of the enzyme and the underlying electrode [106, 107]. For clarification, laccase is an enzyme, which belongs to the copper-containing oxidases and which catalyses the reduction of oxygen to water [108]. Therefore, laccase is also one of the most commonly studied enzymes in the applications of biofuel cells [109]. Based on the recent review, there is an enormous number of reports concerning studies about the (bio)electrochemical properties of laccase-modified electrodes in the presence of ABTS in solution or co-immobilised with ABTS [109]. However, only few studies have focused on the electrochemical behaviour of ABTS itself. For example, early work on the ET process of ABTS on GC electrodes has been studied by Scott *et al*. [110]. The authors reported that ABTS undergoes reversible oxidation from the colourless dianion ($ABTS^{2-}$) to coloured (intensely blue-green) radical ($ABTS^{\bullet-}$) [110]. Furthermore, it is now well established that ABTS undergoes two consecutive one-electron oxidations at 475 mV and 885 mV (vs. Ag/AgCl), which correspond to the reactions of redox couples of $ABTS^{2-}/ABTS^{\bullet-}$ and $ABTS^{\bullet-}/ABTS$, respectively [110–112]. Quan *et al*. [113] studied the pH dependence of redox properties of ABTS on platinum electrode and the results revealed that the oxidation of ABTS is almost pH independent. Very recently, Zeng *et al.* [114] investigated systematically the kinetic parameters of $ABTS^{2-}/ABTS^{\bullet-}$ redox reaction on bare GC electrodes using cyclic voltammetry and the rotating disk electrode method. Among other things, the authors determined the rate constant to be $k° = 4.6\times10^{-3}$ cm s^{-1} which was close to the value obtained by Palmore and Kim [106]. However, the diffusion coefficient of ABTS (4.4×10^{-6} cm^2 s^{-1}) [114] was different from that of Di Fusco *et al*. study, where the diffusion coefficient of ABTS was determined to be 3.4×10^{-6} cm^2 s^{-1} in case of platinum electrode [115]. In recent years it has been shown that laccase can be covalently immobilised onto electrode surfaces that are modified with aryl groups by diazonium reduction [116–120]. However, the literature about the electrochemical behaviour of ABTS on electrodes modified with aryl groups (especially the aryl-modified electrodes which can be used in the attachment of biomolecules, e.g. aminophenyl or carboxyphenyl) is still scarce. Therefore it

was necessary to study the electrochemical behaviour of ABTS on aryl-modified electrodes and it has been done as part of this thesis [I].

In general, the ferri/ferrocyanide ($Fe(CN)_6^{3-/4-}$) couple is probably the most often used redox system to evaluate the electrochemical properties of modified electrodes [7]. The $Fe(CN)_6^{3-/4-}$couple is an inner sphere redox system and therefore can be used as a redox probe to analyse the pinholes and defects on the aryl-modified electrode surfaces [90]. The diameter of the $Fe(CN)_6^{3-}$ ion is ca 0.6 nm [121] and it has rather hydrophilic properties [89]. Furthermore, ferricyanide is negatively charged and may be repelled from the electrode surface by the carboxylate species at the electrode surface [77]. For example, a systematic investigation of the pH dependence of the electron transfer kinetics for four redox probes (including the $Fe(CN)_6^{3-}$ probe) on electrochemically grafted 4-diazo-*N,N*-diethylaniline (DEA) on GC electrode has been performed by Schauff *et al*. [122]. The authors reported that the electron transfer process on the DEA-modified GC electrode depends on the chemical nature of the redox species. It was shown that the blocking effect of the grafted layer was strong for the $Fe(CN)_6^{3-/4-}$ redox couple, while others (for example, the $Ru(NH_3)_6^{2+/3+}$ redox system) were barely affected by the DEA grafted layer. However, for the $Fe(CN)_6^{3-}$ probe, a major blocking effect was demonstrated at pH 10, while the DEA grafted electrode suppressed the response of $Ru(NH_3)_6^{2+/3+}$ at pH 2. Furthermore, Kullapere *et al*. [123] have studied the blocking properties of aryl-modified GC electrodes using the $Fe(CN)_6^{3-/4-}$ redox probe and in addition, the electrochemical behaviour of these electrodes was investigated towards oxygen reduction. The overall results showed that the ferricyanide reduction on aryl-modified GC electrodes was blocked to a much larger degree than oxygen reduction and in addition the blocking effect varied significantly depending on the aryldiazonium salt used [123].

Gui *et al*. [31] investigated the electrochemical properties of sulfophenyl-grafted GC and Au electrodes. The authors suggested that if the aryl layer (e.g. sulfophenyl) should give a negatively charged layer, then it is expected to provide an electrostatic barrier to the electrochemistry of soluble negatively charged redox species (like ferri/ferrocyanide ions). The effect of blocking occurs if the electrochemical response of the redox probe is suppressed on 4-sulfophenyl-grafted GC electrodes [31]. If it is not (as in case of gold grafted with 4-sulfophenyl groups), then the aryl layer is not as closely packed as it was in case of aryl-modified GC [31].

Based on the above-mentioned results, the electrochemical properties of aryl-modified electrodes depend on the electrode material, modification procedure and redox species [89]. Therefore it is important to use different redox probes in order to make solid conclusions about the nature of the aryl film. Furthermore, it is relevant to perform comparative studies between different underlying materials electrografted with different aryl groups. This has been done recently [II,III].

Besides the investigation of electrochemical behaviour of aryl-modified electrodes, the electrochemical properties of the new material, graphene, need to be studied. As highlighted by Banks and co-workers [124, 125], it is important to investigate the electrochemical behaviour of CVD graphene compared with a material of similar structure (e.g. HOPG). However, there is a disagreement in the literature comprising the electrochemical behaviour between CVD-grown graphene and HOPG. Namely, Brownson *et al*. [126] claimed that the electrochemical behaviour of CVD graphene on Ni substrate (commercially available) towards β-nicotinamide adenine dinucleotide (NADH) and uric acid resembled that of the edge plane HOPG. In contrast, Ambrosi *et al*. [127] showed that the electrochemical response of CVD-grown multilayer graphene transferred to a poly(ethylene terephthalate) substrate towards NADH as well as the $Fe(CN)_6^{3-/4-}$ redox system was similar to that of basal plane HOPG. Therefore it was necessary to study the electrochemical behaviour of CVD-grown graphene compared to HOPG more systematically and it has been done recently [V].

4.3.2. The oxygen reduction studies on aryl-modified electrodes

The ORR has been widely explored because it is an important reaction in fuel cells, metal-air batteries and in the electrochemical synthesis of hydrogen peroxide. Recently, Šljukic *et al.* [128] investigated the reduction of oxygen on GC electrodes modified with azobenzene, hydroazobenzene and Fast Black K salt *via* solvent evaporation. Based on their results, the modified electrodes showed the best electrocatalytic properties towards the ORR in acidic solution (pH 2) compared with bare GC [128]. In addition, these aryl-modified electrodes were suggested to be appropriate for H_2O_2 formation [128].

The investigation of ORR in alkaline medium has received considerable interest [129]. Over many years, a large research has been carried out to investigate O_2 reduction on AQ-modified electrodes in alkaline electrolyte. In our workgroup [53, 54, 121, 130–134] it has been shown that the AQ derivatives covalently attached to GC electrode surfaces can be used as electrocatalysts for O_2 reduction. Moreover, it was demonstrated that O_2 reduction follows a two-electron pathway indicating that the AQ-modified GC electrodes efficiently catalyse the reduction of oxygen to hydrogen peroxide in alkaline solution [53, 54, 121, 130–134]. Furthermore, Sarapuu *et al*. [135] and Kocak *et al*. [136] have studied the reduction of oxygen on AQ-modified HOPG electrodes with the AQ surface concentration (Γ_{AQ}) lower than 1×10^{-10} mol cm^{-2} and 1.3×10^{-10} mol cm^{-2}, respectively. Taking into account that the surface coverage for a closely-packed monolayer of anthraquinonyl groups is 3.45×10^{-10} mol cm^{-2} [137] then these Γ_{AQ} values correspond to submonolayer AQ films on the HOPG surface. Even so, from both studies, the AQ-modified HOPG electrodes catalysed the reduction of oxygen to hydrogen peroxide *via* two-electron pathway [135, 136].

4.3.3. The oxygen reduction studies on graphene-based electrodes

In recent years, there has been an increased interest in O_2 reduction studies on bare and modified graphene-based electrodes because of the excellent properties of graphene itself (e.g. high electrical conductivity, large specific surface area, etc.) [138]. Very recently, Randviir and Banks [139] reported a comparative study of ORR in acidic media using pristine graphene (which is free from surfactants), graphene oxide (GO, synthesised by Hummer´s method) and edge and basal plane pyrolytic graphite electrodes. The results showed that the electrocatalytic activity depended on the underlying substrate [139]. To be more specific, the electrocatalytic activity towards the ORR was higher on GO than on pristine graphene, whereas pristine graphene was less active than basal plane pyrolytic graphite [139]. Lima *et al*. [140] and Matsumoto *et al*. [141] showed, that the reduced graphene oxide (rGO) was more electrocatalytically active for ORR in alkaline solution than GO. In addition, the ORR activity of GO was comparable with edge plane HOPG, whereas basal plane HOPG was less active towards ORR than GO or rGO electrodes [141]. As can be seen, the electrochemical behaviour between differently obtained graphene and pyrolytic graphite electrodes varies. To date, the comparative ORR studies between CVD-grown graphene and HOPG have not been reported as yet, which was for the motivation to investigate that as a part of this thesis [V].

In order to enhance the electrocatalytic activity of graphene towards the ORR, graphene has been used as a catalyst-support for ORR studies [142]. For example, Tiido *et al*. [143] have shown that Pt catalyst supported onto TiO_2 functionalised graphene nanosheets exhibited similar electrocatalytic activity compared with bulk Pt towards O_2 reduction in both acidic and alkaline medium. In addition, nitrogen-doped graphene has received much interest [129]. For example, Vikkisk *et al*. [144] showed that N-doped GO revealed similar electrocatalytic activity towards the ORR in 0.1 M KOH compared to Pt/C catalyst. Furthermore, N-doped GO and mutliwalled carbon nanotube composite materials are good electrocatalysts for ORR as reported by Ratso *et al*. [145].

However, in the literature there are only a few studies concerning the modification of graphene with AQ groups. For example, Yang and co-workers have studied the electrochemistry of rGO modified with AQ moieties covalently attached by electrochemical reduction of the corresponding diazonium salt [146] and noncovalently by adsorption method [147]. The authors also determined the surface concentration of AQ groups attached to graphene: in the first report the surface coverage of AQ groups was 9.58×10^{-10} mol cm^{-2} [146] and in the latter study it was twice lower ($\Gamma_{AQ} = 4.9\times10^{-11}$ mol cm^{-2}) [147], although these electrodes showed good electrocatalytic properties towards the ORR. Moreover, it would be interesting to study O_2 reduction on thick AQ films electrografted on HOPG and CVD-grown graphene electrodes and it has been done recently [VI].

5. EXPERIMENTAL

5.1. Chemicals and materials

2,2`-azino-bis(3-ethylbenzothiazoline-6-sulphonic acid) diammonium salt (ABTS, 98%, Sigma), 4-aminobenzoic acid (99%, Aldrich), 4-aminoazobenzene hydrochloride (97%, TCI), 1-aminoanthraquinone (Sigma-Aldrich), tetrafluoroboric acid (48%, Sigma-Aldrich), potassium hexacyanoferrate(III) ($K_3Fe(CN)_6$, Aldrich or Merck), potassium hexacyanoferrate(II) trihydrate ($K_4Fe(CN)_6 \times 3H_2O$, Merck), KOH pellets (p.a. quality, Merck or BDH, AristaR), KCl (Merck), K_2SO_4 (p.a. quality, Merck), $NaNO_2$ (Merck), KH_2PO_4 (Merck), Na_2HPO_4 (Fluka), $CH_3COONa \times 3H_2O$ (Fluka), CH_3COOH (Sigma-Aldrich), acetonitrile (ACN, HPLC grade, Sigma-Aldrich), isopropanol (Sigma-Aldrich), acetone (Lach-Ner or VWR), methanol and diethyl ether (HPLC grade, Sigma-Aldrich), H_2SO_4 (96%, Merck), HCl (37%, Sigma-Aldrich), sodium tetrafluoroborate ($NaBF_4$, 98%, Sigma-Aldrich), hydrogen peroxide (H_2O_2, 30%, Merck), tetrabutylammonium perchlorate monohydrate ($TBAClO_4 \times H_2O$, 99%, Acros Organics) and tetrabutylammonium iodide (Bu_4NI, Sigma-Aldrich) were used without further purification. Tetrabutylammonium tetrafluoroborate ($TBABF_4$) was purchased from Fluka (98%) or was synthesised using standard procedure [148]. Alumina with the grain size of 1, 0.3 and 0.05 μm was purchased from Buehler.

Three commercially available diazonium salts: 4-nitrobenzenediazonium tetrafluoroborate (NBD, 97%, Aldrich), Fast Garnet GBC sulphate salt (2-methyl-4-([2-methylphenyl]azo)benzenediazonium salt, Sigma–Aldrich), Fast Black K salt (2,5-dimethoxy-4-([4-nitrophenyl]azo)benzenediazonium chloride hemi(zinc chloride), Sigma) and three pre-synthesised diazonium salts: 4-carboxyphenyl diazonium tetrafluoroborate (CPD), azobenzene diazonium tetrafluroborate (ABD) and 9,10-anthraquinone-1-diazonium tetrafluoroborate (AQD) were used for the electrochemical grafting of different electrode surfaces. The latter three diazonium salts were synthesized similarly using previously published procedures [39, 65, 149–154]:

CPD: 4-aminobenzoic acid (0.04 mol) was dissolved in water (56 mL) and 7.2 mL of 37% HCl was added slowly. The solution was maintained at about 0 ºC in an ice bath. Thereafter, a solution containing $NaNO_2$ (0.044 mol) in 16 mL was added and the obtained solution was allowed to stir for 1 h in an ice bath. Afterwards, the solution was filtered and $NaBF_4$ (0.044 mol) was added. The slurry was cooled below 0 ºC, filtered by suction and washed with ice water and cold ether. The synthesised CPD was dried and stored in a desiccator (about 4 ºC). Yield was ca 44%. Additionally, the diazonium functionality was detected by IR spectroscopy at about 2290 cm^{-1} [155] and the purity of CPD was controlled by NMR spectroscopy.

ABD: 4-aminoazobenzene hydrochloride (0.01 mol) was dissolved in 100 mL of the mixture of water and acetone (1:1 by volume). The obtained solution was

maintained at 0~5 ºC in an ice bath. A mixture of $NaNO_2$ (0.01 mol), HCl (0.01 mol) and 50 mL of water and acetone (1:1 by volume) was added to the previously prepared solution. The solution was filtered and $NaBF_4$ (0.01 mol) was added. The slurry was cooled below 0 ºC, filtered by suction and washed with ice water and cold ether. The synthesised ABD was dried and stored in a desiccator (about 4 ºC). Yield was ca 50%. The purity of ABD was controlled by NMR spectroscopy.

AQD: 1-aminoanthraquinone (2.2 mmol) was dissolved in acetone (5 mL) while stirring. Tetrafluoroboric acid (48%, 1 mL) was added and the solution was cooled in an ice bath for 10 min. $NaNO_2$ (2.2 mmol) was dissolved in distilled water (0.5 mL) and the solution was cooled in an ice bath for 10 min. The dissolved $NaNO_2$ was added slowly to the 1-aminoanthraquinone solution and the obtained solution was allowed to stir for 1 h in an ice bath. Afterwards, the solution was filtered and the solid was washed with cold tetrafluoroboric acid, pre-cooled methanol and diethyl ether, followed by recrystallisation from acetone and diethyl ether. The resulting AQD was dried by rotary evaporator and stored at −18 ºC. Yield was ca 60%. The purity of AQD was checked by NMR spectroscopy.

Glassy carbon (GC) and gold electrodes were prepared by pressing GC (GC-20SS, Tokai Carbon) or Au disks (99.99%, Alfa Aesar) into Teflon holders, respectively. The geometric area (A) of these electrodes was 0.2 cm^2 [I–IV].

GC plates (12×12×2 mm) were supplied from NII Grafit (Russia). HOPG (SPI-2 grade, 12×12×2 mm or 10×10×2 mm and ZYB grade, 12×12×1.2 mm) substrates were purchased from SPI Supplies or NT-MDT (Russia). The area of these electrodes exposed to solution was fixed by Kalrez® perfluoroelastomer O-ring yielding the area of 0.64 or 0.38 cm^2 [V,VI].

The synthesis of graphene was performed by chemical vapour deposition (CVD) onto nickel or copper substrates (designation: Ni-Gra or Cu-Gra). The CVD-grown graphene on Ni foil was synthesised at the Institute of Physics of the University of Tartu similarly to the method described in Ref. [156]. In short, prior to deposition the Ni foils (99.9%, Strem Chemicals) were annealed for 40 min. in Ar and H_2 flow with the rate of 100 and 120 sccm, respectively, at 1000 ^oC. Then Ni foils were exposed to a gas mixture of 10% CH_4 in Ar at the same temperature for 40 min. The flow rates of the H_2 and CH_4/Ar mixture were kept at 120 and 40 sccm, respectively. Samples were cooled by moving away of an external heating element and using additional Ar flow with the rate of 100 sccm keeping the H_2 and CH_4/Ar gas flow rates the same as they were during the deposition.

Cu-Gra was prepared by growing graphene onto 50 μm thick Cu foil in a homemade CVD system at Aarhus University (Denmark). The oxygen-free Cu foil was purchased from Advent Research Materials (CU1333) and electro-polished prior to graphene growth [157]. The CVD growth of graphene onto Cu substrate was carried out in a similar way as described by Ruoff and co-workers

[158]. Briefly, the Cu foil was annealed in a split tube furnace at 1030 ºC for 30 min with Ar and H_2 flow at 1470 sccm and 27 sccm, respectively, which was held constant throughout the whole procedure. The temperature was decreased to 1000 ºC and graphene growth was initiated by bleeding 3 sccm CH_4 into the reaction chamber. The growth proceeded for 1 h (pressure = 28 mbar), after which the tube was rapidly cooled to room temperature.

In addition, commercially available CVD-grown graphene on Ni was used. Ni-Gra (10×10 mm) was purchased from Graphene Supermarket with the thin film of Ni itself deposited onto silicon. Bare Cu foil and Ni plates (both 12×12 mm) were used for comparative purposes in the electrochemical experiments.

It should be noted that all current densities in section 6.3.2 were calculated with respect to the A of the individual electrodes. For GC, HOPG (ZYB grade), Cu, Ni, and Cu-Gra, the A was 0.64 cm^2 while for HOPG (SPI-2 grade) and Ni-Gra, it was 0.38 cm^2.

5.2. The electrode preparation before electrografting

Prior the use, the GC substrates were polished to a mirror finish with 1.0 and 0.3 μm alumina slurries on Milli-Q water microcloth pads or with sandpaper grids (P180, P500, P1000 and P2000) followed by polishing with diamond suspensions (grain sizes 9, 3, 1 and 0.25 μm). In case of Au disk electrodes, 1.0, 0.3 and 0.05 μm alumina slurries were used. Thereafter, the GC and Au electrodes were sonicated in Milli-Q water, isopropanol and ACN for 5 min. In addition, the Au electrodes were cleaned electrochemically in Ar- or N_2-saturated 0.5 M H_2SO_4 solution by cycling the electrodes between –0.3 and 1.5 V vs. SCE at a sweep rate (v) of 100 mV s^{-1} until a reproducible cyclic voltammogram was obtained.

The fresh surface of HOPG was prepared prior to each measurement by removing the top layers with adhesive tape.

5.3. Electrochemical reduction of aryldiazonium salts

NBD, CPD, ABD, Fast Garnet GBC sulphate salt, Fast Black K salt and AQD were used in order to functionalise different electrode surfaces with 4-nitrophenyl (NP), 4-carboxyphenyl (CP), azobenzene (AB), 2-methyl-4([2-methylphenyl]azo)benzene (GBC), 2,5-dimethoxy-4-([4-nitrophenyl]azo)benzene (FBK) and 9,10-anthraquinone (AQ) groups, respectively. Scheme 3 illustrates the chemical structures of the diazonium compounds used in this thesis.

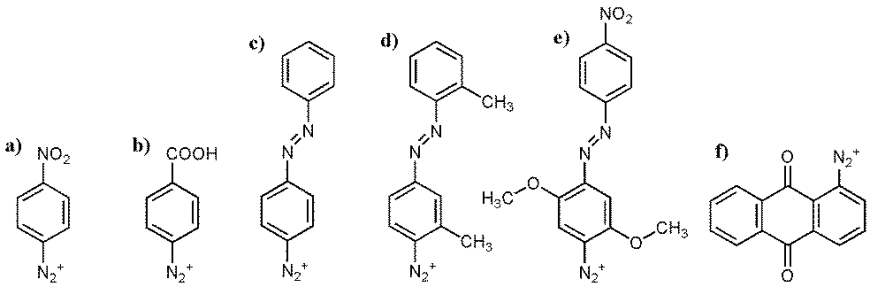

Scheme 3. Chemical structures of the studied diazonium compounds: a) 4-nitrobenzene; b) 4-carboxyphenyl; c) azobenzene; d) Fast Garnet GBC; e) Fast Black K and f) 9,10-anthraquinone.

The electrochemical grafting of carbon-based and Au electrodes was carried out in ACN containing 1 mM or 3 mM of the corresponding diazonium salt and 0.1 M $TBABF_4$ as a base electrolyte. It should be noted that the concentration of the diazonium salts in the solutions was 1 mM and 3 mM in case of carbon-based and Au electrodes, respectively. The exact modification procedures are indicated in the text. After electrochemical grafting, the aryl-modified GC and Au electrodes were sonicated in ACN for 5 min to remove physically adsorbed material. In contrast, the aryl-modified HOPG and CVD-grown graphene electrodes (either on Ni or Cu substrates) were carefully rinsed with ACN in order to avoid the surface damage.

5.4. Electrochemical measurements

Electrochemical measurements were performed using a three-electrode system. Bare and aryl-modified GC or Au electrodes were employed as a working electrode, whereas saturated calomel electrode (SCE) and Pt wire were used as a reference and counter electrode, respectively. In addition, specially designed three-electrode cell with Kalrez® perfluoroelastomer O-ring (DuPont™) was used in case of GC, HOPG and CVD-grown graphene substrates [V,VI]. The O-ring was used in order to avoid leakage of the solution and to ensure the fixed area of the working electrode.

In some organic solvents a Ag/AgI pseudo-reference electrode (a silver wire immersed in ACN of 0.1 M $TBABF_4$ + 0.01 M Bu_4NI) was used. At the end of each experiment the standard potential of the Fc^+/Fc couple, $E^{\circ}_{Fc^+}$, was measured and all potentials were referred against SCE using a previous determination of $E^{\circ}_{Fc^+}$ = 0.41 V vs. SCE in ACN [70]. To facilitate comparison with all the results, all potentials in this thesis are quoted with respect to SCE.

The potential was applied using an Autolab potentiostat/galvanostat PGSTAT128N or PGSTAT30 (Eco Chemie B.V., The Netherlands) and the experiments were controlled with General Purpose Electrochemical System

(GPES) software [I–V]. For some experiments, potentiostat of CH Instruments 660B or 601D were used [VI].

For the electrochemical studies, cyclic voltammetry (CV) or linear sweep voltammetry (LSV) was employed. In some experiments, the rotating disk electrode (RDE) technique was used with an EDI101 rotator and a CTV101 speed control unit (Radiometer, Copenhagen) and the electrode rotation rate (ω) was varied between 360 and 4600 rpm.

The electrochemical behaviour of ABTS was studied in Ar-saturated 50 mM acetate (pH 4 and 5) and phosphate buffers (pH=6–8) containing 0.5 mM ABTS and 0.1 M KCl as a base electrolyte. The electrochemical response towards the $Fe(CN)_6^{3-/4-}$ redox probe was studied in Ar- or N_2-saturated 0.1 M K_2SO_4 or 0.1 M KOH containing 1 mM $K_3Fe(CN)_6$ or 1 mM $K_4Fe(CN)_6$. The O_2 reduction studies were performed in O_2-saturated 0.1 M KOH solution. All buffer and aqueous solutions were prepared in Milli-Q water (Millipore Inc.).

In Section 6.2.3., the electrochemical impedance spectroscopy (EIS) was employed in case of GBC- and FBK-modifed Au electrodes [III]. An Autolab potentiostat/galvanostat (model PGSTAT128N) equipped with a FRA2.X module was used for these EIS experiments. These experiments were conducted at a fixed potential: at an open-circuit potential (OCP) approximately at 0.31 V in the presence of 1 mM $K_3Fe(CN)_6$ with potential perturbation of 25 mV (rms) within a frequency range of 10 mHz to 100 kHz. Care was taken to ensure that AC impedance data corresponded to the interfaces being investigated at high frequencies – namely, the potentiostat employed had faster performance; the highest cutoff frequency was limited to 160 kHz for the FRA2 module, which used a fixed filter when the frequency applied exceeded 19 kHz; cables were short and, akin to the connections, were shielded; the electrochemical cell was placed inside a Faraday cage; the working electrode was positioned in front of and close to a larger Pt plate; and the SCE was placed near to the working electrode. Nova 1.7 Autolab (2009) software was used to simulate the behaviour of equivalent circuits of the interface in the presence of the $Fe(CN)_6^{3-}$ probe and the parameters of these circuits were fitted to the measured spectra using a non-linear least-squares program. The EIS experiments were performed in Federal University of Mato Grosso do Sul, Brazil.

Depending on the purpose, solutions were deaerated with Ar (99.999%, AGA) or saturated with O_2 (99.999%, AGA). All electrochemical experiments were carried out at room temperature (23±1 ºC).

5.5. UV treatment with $OH^{\bullet}$ radicals

The GBC and FBK-modified GC and Au surfaces were treated with $OH^{\bullet}$ radicals generated by UV photolysis of a 10% H_2O_2 solution [IV]. High-pressure mercury lamp (500 W) was used. The solutions were housed in quartz test tubes. The disk electrodes used for electrochemical experiments were

positioned in such way that only some diffuse stray radiation could shine on the electrode surface. In case of the electrodes for AFM measurements, the direct irradiation with the UV lamp of the aryl-modified Au surface was avoided.

5.6. Surface characterisation methods used for bare and aryl-modified electrodes

5.6.1. X-ray photoelectron spectroscopy

X-ray photoelectron spectroscopy (XPS) data were collected with a SCIENTA SES-100 spectrometer using an unmonochromated Mg Kα (incident energy = 1253.6 eV) or Al Kα X-ray source (incident energy = 1486.6 eV) and a take-off angle of 90º. In case of Mg Kα and Al Kα X-ray source, a source power of 300 or 400 W was used, respectively. The operating pressure in the analysis chamber was set below 10^{-9} Torr.

GC plates (1.1×1.1 cm) and Au Arrandee™ (Schröer GmbH, Lienen, Germany) specimens (250±50) nm thick Au film deposited on a (2.5±1.5) nm chromium layer on borosilicate glass slides (1.1×1.1 cm) were used as a substrate material [I–IV]. Prior the electrografting, the latter samples were annealed in a butane flame until a weak dark-red glowing of the surface. After this the Au/glass samples were cooled down to room temperature in N_2 stream, in order to get flat gold terraces with preferential Au{111} orientation [IV].

The surface modification procedures of GC and Au plates for the XPS studies were identical to those used for the electrochemistry measurements [I–IV]. However, the cleaning procedure after electrografting of the Au substrates involved rinsing several times with ACN and dried in a stream of argon gas. The ultrasonic cleaning was not employed due to the risk of delaminating the gold sputtered layer from the glass plate or to damage of the Ni-Gra surface.

The survey spectra of NP- and AP-modified GC samples were recorded between 800–0 eV [I]. In case of AB-, GBC- and FBK-modified GC and Au substrates, the survey scan were obtained between 700–0 eV [II,III] and 600–0 eV [IV]. For bare Ni and Ni-Gra samples, the survey spectra were collected in the energy range of 1000–0 eV. For all cases, pass energy = 200 eV and step size = 0.5 eV were used.

For the high-resolution scan in the N1s region, the energy range was 410–395 eV for the NP-, AP-modified GC [I] or 408–396 eV in case of AB-, GBC-, FBK-modified GC and Au substrates [II–IV]. In addition, pass energy = 200 eV and step size = 0.1 eV were used in all cases.

The XPS measurements were performed by Dr. Leonard Matisen in the Institute of Physics of the University of Tartu.

5.6.2. Atomic force microscopy

The surface morphology of aryl-modified Au, HOPG and CVD-grown graphene electrodes (on either Ni or Cu substrate) was studied by atomic force microscopy (AFM) with a multimode AFM Autoprobe CP II (Veeco) instrument and AFM images were recorded in non-contact mode using a NSG01 (NTMDT) or UL20 (PSI) series cantilevers under ambient conditions. The Gwyddion™ free software (Czech Metrology Institute) ver. 2.27 or 2.34 was employed for image processing and surface roughness calculations. AFM images were processed by the first order flattening for background slope removal, and if necessary, the contrast and brightness were adjusted [III,V,VI]. In some experiments, a DualScope 95–50 microscope (DME, Denmark) in non-contact mode using the Software DME Scan Tool Version 1.2.1.0 was used for the AFM measurements [IV]. Each AFM image presented is a representative of numerous images taken on different locations of the sample.

It should be noted that in some AFM experiments, monocrystalline Au(111) film deposited on mica at elevated temperature using electron beam evaporator VS-17 (Vacuum Service OY) was used as a substrate material [III]. The mica substrates were cleaved just before Au deposition and prior to each surface modification the Au(111) film surface was shortly annealed in H_2 flame [III]. In addition, Au/glass substrates were used similarly to XPS measurements [IV].

The thickness of AB-, GBC-, FBK films on Au and in addition, AQ film thickness on HOPG and CVD-grown graphene electrodes (on either Ni or Cu substrate) was measured with AFM in contact mode using UL20 series cantilevers. For thickness measurements, AFM was used in nanolithography mode to scratch off the modifier layer [III,VI].

The AFM measurements were performed by Dr. Margus Marandi in the Institute of Physics of the University of Tartu [III,V,VI] and Dr. Ulrich Hasse in the Institute of Biochemistry of the University of Greifswald [IV].

5.6.3. Ellipsometry

The thicknesses of AB, GBC and FBK films on Au electrodes were performed using GES-5E ellipsometer with rotating polarizer (Semilab), angle of incidence 65°. Obtained spectra were analysed in the range 1.3–5 eV using WinelliII software [III]. The data for a gold substrate were taken from Ref. [159], the polymer layers approximated as $n = 1.46$ like in Ref. [160].

The thicknesses of AQ films on GC, HOPG and graphene-based electrodes (dried under Ar flow after electrografting) were measured using a rotating analyser ellipsometer (Dre, Germany) [VI]. GC and HOPG substrates were measured at 65° angle of incidence, while Ni-Gra was measured at 70°. The ellipsometric parameters of the bare (Δ_s, ψ_s) and the grafted (Δ_g, ψ_g) substrates were measured in air at ambient temperature, where Δ is the phase shift and $\tan(\psi)$ is the amplitude ratio upon reflection. The complex refractive index of

the bare substrate was calculated from the measured Δ_s and ψ_s values. A three-layer optical model consisting of a substrate with a complex refractive index, the grafted layer with a refractive index and thickness and the surrounding medium (air) was used to calculate the overall reflection coefficients for in-plane (R_p) and out-of-plane (R_s) polarised lights [70].

The real and the imaginary parts of the refractive index of the bare substrate were obtained by measuring the clean plates prior to modification. Ellipsometric measurements were performed on the same area of the plates before and after electrografting. Because the measurements were carried out on a dried and therefore collapsed films, the refractive index of the layer was fixed at a constant value (real = 1.55; imaginary = 0), independent of the thickness. The average and the standard deviation values reported correspond to data points obtained from measuring three spots on each plate [70].

The ellipsometry measurements of AB-, GBC- and FBK-modified Au electrodes were carried out by Dr. Aarne Kasikov in the Institute of Physics of the University of Tartu [III] and the ellipsometry measurements of AQ-modified GC, HOPG and graphene-based substrates were carried out in Department of Chemistry and Interdisciplinary Nanoscience Center, Aarhus University [VI].

5.6.4. Electrochemical quartz crystal microbalance

In section 6.2.3., the GBC and FBK film formation on Au electrodes were studied by electrochemical quartz crystal microbalance (EQCM) method. A Research Quartz Crystal Microbalance (Maxtek) was employed to measure resonance frequency shifts *in situ* in case of GBC- and FBK-grafted Au electrodes [III]. The microgravimetric studies were carried out in a GC-15 three-electrode glass cell that included a CHC-15 crystal holder, clamp and stopper (Maxtek). A 5-MHz AT-cut quartz crystal (25.4 mm in diameter) vertically positioned in front of the counter electrode served as the working electrode (polycrystalline Au), both sides of which were coated with Au sputtered on a Ti layer in a keyhole pattern (geometric area in contact with solution = 1.37 cm^2) (Maxtek). The surface was thoroughly cleaned before electrografting by cycling 30 times in N_2-saturated 0.5 M H_2SO_4 between −0.2 and 1.5 V vs. SCE at 100 mV s^{-1} and, if necessary, changing the solution three times. After this step, the cell and electrodes were washed several times with water followed by rinsing with ACN. The surface modification of the working electrode for EQCM measurements was carried out in 0.1 M $TBAClO_4$/ACN containing 3 mM of Fast Garnet GBC sulphate salt or Fast Black K salt. The reference electrode was separated from the modification solution by a jacket equipped with a sintered glass junction in order to minimise water penetration. The Sauerbrey equation was used assuming that the attached layer of GBC or FBK is rigid and no viscoelastic changes occur at the electrode/solution interface: $\Delta m = -\Delta f / C_f$ [161], where Δm is the change of mass per unit area in g cm^{-2}, Δf is the resonance frequency shift in Hz and C_f is the sensitivity factor of

the crystal in Hz ng^{-1} cm^2 (0.056 Hz ng^{-1} cm^2 in the present case). The EQCM experiments were performed in Federal University of Mato Grosso do Sul, Brazil.

5.6.5. High-resolution scanning electron microscopy

High-resolution scanning electron microscopy (HR-SEM) using Helios™ NanoLab 600 (FEI) instrument was employed for the CVD-grown graphene on Ni foil characterisation [V]. These HR-SEM measurements were performed by Jekaterina Kozlova in the Institute of Physics of the University of Tartu.

5.6.6. Raman spectroscopy

For the characterisation of CVD-grown graphene on Ni foil, Raman spectra were recorded with a Renishaw inVia micro-Raman spectrometer with an incident laser beam wavelength of 514 nm [V].

In order to perform Raman analysis for Cu-Gra, the graphene was transferred from Cu-Gra to Si/SiO_2 (300 nm) wafers using the standard procedure. First, the Cu-Gra substrate was spin-coated with 2% poly(methyl methacrylate) (PMMA) in anisole at 1000 rpm for 45 s, and baked at 150 ºC for 15 min. The Cu-foil was etched with 1 M $FeCl_3$ and the remaining graphene/PMMA was transferred after a short treatment in 1 M HCl and extensive washing with deionised water. The sample was put in the oven to dry at 150 ºC, after which the PMMA was dissolved in hot acetone.

The Raman spectroscopy measurements of bare Ni-Gra electrodes [V] were performed by Jekaterina Kozlova in the Institute of Physics of the University of Tartu. The Raman spectroscopy measurements of bare Cu-Gra (transferred to Si/SiO_2) [VI] were performed in Department of Chemistry and Interdisciplinary Nanoscience Center, Aarhus University.

6. RESULTS AND DISCUSSION

6.1. Surface and electrochemical properties of NP-, CP- and reduced NP-modified GC electrodes

The electrode surface functionalised with 4-aminophenyl (AP) or 4-carboxyphenyl (CP) groups offer the platform for coupling the biomolecules in order to fabricate for example biosensor surfaces [2, 42, 43]. Based on the literature, the blocking properties of NP-, AP- or CP-modified GC electrodes towards the ferri/ferrocyanide couple have been extensively studied [39, 77, 149, 162]. However, while these aryl films (AP or CP) can be used for further attachment of (bio)molecules (e.g. laccase) and ABTS is mostly used redox system studied in laccase-modified electrodes, the electrochemical properties of AP-, NP- and CP-modified GC electrodes towards ABTS oxidation were explored in this section [I].

6.1.1. Electrochemical grafting of GC with NP and CP groups

Figures 1a,b show the cyclic voltammograms recorded during the modification of GC electrodes with 4-nitrophenyl (NP) and 4-carboxyphenyl (CP) groups *via* electrochemical reduction of the corresponding diazonium salts. The electrografting for both diazonium compounds was performed between 0.6 and –0.8 V using a sweep rate (v) of 100 mV s^{-1}. In case of NBD, one (Procedure a) and 20 (Procedure b) potential cycles and in case of CPD, two (Procedure c) and 20 (Procedure d) potential cycles were carried out. The electrodes modified with NP and CP groups are denoted as GC/NP and GC/CP, respectively.

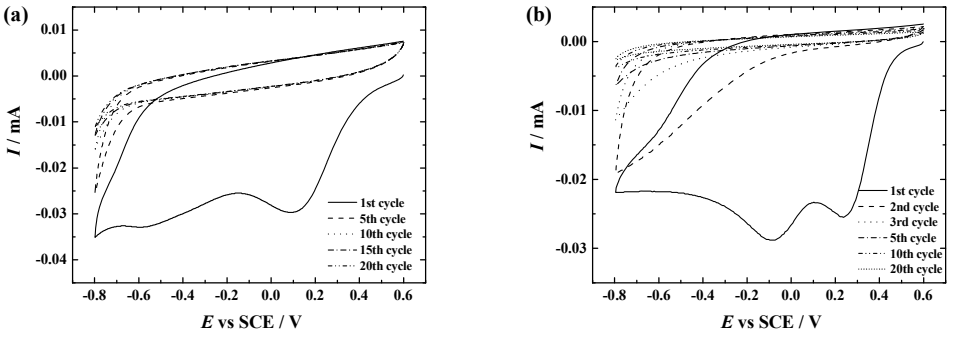

Figure 1. Electrochemical grafting of (a) 4-nitrophenyl and (b) 4-carboxyphenyl groups onto GC electrode in Ar-saturated acetonitrile containing 1 mM of the corresponding aryldiazonium cations and 0.1 M $TBABF_4$ at a sweep rate of 100 mV s^{-1}.

As mentioned in the literature overview (Section 4.1.3.), usually only one reduction peak in a narrow potential range is observed which refers to the

reduction of the aryldiazonium cations to an aryl radical which then reacts with the carbon surface giving a strong covalent C–C bond. However, as can be seen from Figure 1, the first CV of electrografting showed two irreversible cathodic peaks for both aryldiazonium compounds which is in agreement with previous reports [123, 163, 164]. Based on the literature, it has been proposed that the second reduction peak at lower potentials should correspond to the reduction of the aryldiazonium cations to a radical. The origin of the first reduction peak (also assigned as a pre-peak) is still not fully understood [40, 164–166]. During the successive cycling, the reduction peaks diminished by the 20th potential cycle (see Figure 1). This is a typical electrografting behaviour of aryldiazonium salts and the disappearance of the reduction peaks refers to the progressive blocking of the GC surface by an aryl film.

Thereafter, it was of special interest to further reduce the NP groups to aminophenyl (AP) groups. The electrochemical reduction of NP groups was carried out in EtOH–H_2O (1:9 by volume) solution containing 0.1 M KCl as a supporting electrolyte similarly as described in the literature [41, 58, 162]. Briefly, the reduction procedure involved five potential cycles at 100 mV s^{-1} from 0.7 to –1.5 V followed by sonication in EtOH–H_2O for 5 min. The corresponding CVs are shown in Figure 2 and the electrodes are designated as reduced GC/NP.

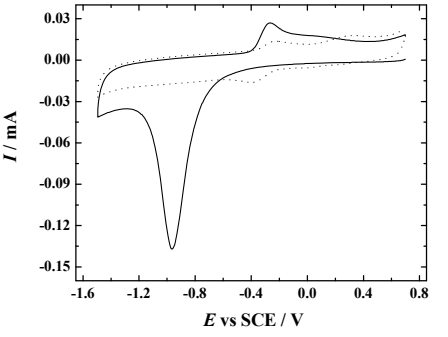

Figure 2. Electrochemical reduction of NP-modified GC electrode in Ar-saturated EtOH–H_2O solution containing 0.1 M KCl (v = 100 mV s^{-1}). First (solid line) and fifth (dotted line) potential cycles are shown.

It has been claimed that a four-electron reduction of NP in protic medium yields hydroxylaminophenyl (APOH) group which may be further reduced to aminophenyl group in the second two-electron step [162]. According to Yu *et al*. [42], the first cycle (see Figure 2) shows a single chemically irreversible reduction and an oxidation process which appears to be two closely spaced peaks. The large reduction peak in the first potential cycle indicates the $6e^-$ reduction of NP to AP groups. A part of NP groups may be reduced to APOH

groups. During subsequent cycles, the reduction peak at –1.0 V disappeared and a small reduction peak at –0.35 V associated with the oxidations appeared. It is suggested that those peaks arise from the APOH/nitrosophenyl couple [162].

While it is known that NP groups are electroactive, the presence of NP groups on GC/NP electrodes was confirmed by electrochemically recording the CVs in Ar-saturated 0.1 M KOH between 0 and –1.2 V (v = 100 mV s^{-1}). The surface concentration of NP groups (Γ_{NP}) was calculated by the charge integration under the voltammetric peaks according to the equation (1) [167]:

$$\Gamma = \frac{Q}{nFA} \quad (1)$$

where Q is the amount of charge consumed, n is the number of electrons involved (n = 2), F is the Faraday constant (F = 96485 C mol^{-1}) and A is the electrode area (A = 0.2 cm^2). Modification with one full potential cycle (Procedure a) and 20 cycles (Procedure b) yielded Γ_{NP} values of 5×10^{-10} and 7×10^{-10} mol cm^{-2}, respectively. Both Γ_{NP} values correspond to less than a monolayer coverage, which is 1.25×10^{-9} mol cm^{-2} [58]. However, the accurate electrochemical determination of the NP groups can be misleading because not all nitro groups may be electroactive (there is a possibility that the electrochemically inaccessible NP groups may be "buried" within the aryl film) [40, 64, 168]. Therefore, the actual surface concentration of NP groups might be higher than that determined from the CV data. From these results it is reasonable assume that a loosely packed NP film may be formed which shows multilayer structure. The surface coverage of other aryl films studied in the present work remains unknown because these modifiers are not electroactive.

6.1.2. Surface characterisation by XPS

XPS measurements were carried out to characterise the elemental composition of NP and reduced NP films. Figure 3 presents the XPS spectra of the N1s region for the as-prepared NP film and for the NP film reduced in EtOH–H_2O, using the modification Procedures (a) and (b), i.e. by applying one and 20 cycles between 0.6 and –0.8 V (see Figure 1a).

It is known that the binding energy values of 406 and 400 eV correspond to $–NO_2$ and $–NH_2$ groups, respectively [169, 170]. The XPS peak at 400 eV can also be explained by the presence of azo linkages (–N=N–) within a multilayer film [75]. As can be seen from Figure 3a, no peak attributed to $–NO_2$ groups (at 406 eV) was observed for reduced GC/NP electrodes modified by Procedure (a), only a large peak at 400 eV was detected, which indicates a complete transformation of NP groups to AP groups and therefore it can be concluded that NP groups of this particular electrode are reduced mainly to AP groups. However, a substantial XPS peak close to 406 eV was observed for reduced GC/NP electrodes modified by Procedure (b), but mostly amino groups of

binding energy of 400 eV dominated (Figure 3b). Both peaks were visible upon surface modification with NP groups, using the modification Procedures (a) and (b) (Figures 3a,b). Besides the azo linkages, the second peak with a lower binding energy close to 400 eV could also arise from chemical transformations of nitro groups during the XPS experiment [169, 170].

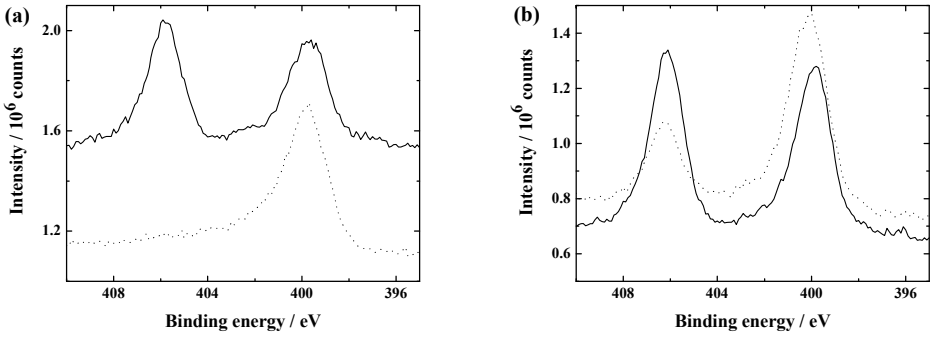

Figure 3. XPS spectra of N1s region of the as-prepared GC/NP (solid line) and reduced GC/NP (dotted line) electrodes, electrografted by: (a) one and (b) 20 cycles.

6.1.3. Electrochemical behaviour towards ABTS oxidation on NP-, CP- and reduced NP-modified GC electrodes

The electrochemical behaviour of ABTS was studied on bare and aryl-modified GC electrodes using cyclic voltammetry (CV) and the rotating disk electrode (RDE) method. First, the CV curves of bare GC electrodes were recorded between 0 and 0.8 V in order to confirm the results obtained in the literature [106, 110]. As can be seen from Figure 4, the CVs showed well-defined one-electron reversible waves which correspond to the $ABTS^{2-}/ABTS^{\bullet-}$ redox couple and in addition, the electrochemical response of ABTS on bare GC was independent of pH. The redox potential of the $ABTS^{2-/\bullet-}$ couple was found to be 0.46 V, which is in good agreement with the previous report [110]. Furthermore, the experiments showed that the peak potential separation (ΔE_p) was determined as 0.08 V in the solutions of various pH (pH=4–8), while Palmore *et al*. [106] reported that in the solution of pH 4, the value of ΔE_p was 0.110 V.

While the electrochemical behaviour towards the $ABTS^{2-}/ABTS^{\bullet-}$ redox probe on bare GC is pH independent, only the representative RDE voltammetry curves for ABTS oxidation on a bare GC electrode at pH 5 are shown in Figure 5. Current plateaux are observed on unmodified GC in the range of potentials between 0.55 and 0.75 V. The theoretical diffusion-limited current was calculated by the Levich equation (2) according to Ref. [167]:

$$I_d = 0.62nFAC^{\circ}D^{2/3}\nu^{-1/6}\omega^{1/2} \quad (2)$$

where I_d represents diffusion-limited current, n is the number of electrons involved (n = 1), F is the Faraday constant (96485 C mol^{-1}), A is the electrode area (0.2 cm^2), $C°$ is the concentration of ABTS in the bulk (0.5×10^{-6} mol cm^{-3}), D is the diffusion coefficient of ABTS (3.4×10^{-6} cm^2 s^{-1} [115] or 4.4×10^{-6} cm^2 s^{-1} [114]), v is the kinematic viscosity of the solution (0.01 cm^2 s^{-1} [171]) and ω is the electrode rotation rate. It is relevant to note that in the paper [I], the theoretical Levich plot was calculated using the value of D as reported by Di Fusco and co-workers ($D = 3.4\times10^{-6}$ cm^2 s^{-1} [115]). However, it was of special interest to see whether the new D value of ABTS (4.4×10^{-6} cm^2 s^{-1} [114]) determined later by Zeng *et al*. could fit with the experimental results obtained in this study. As can be seen from Figure 5 insets 1,2, the oxidation current is equal to the theoretical diffusion-limited current while using the value of $D = 3.4\times10^{-6}$ cm^2 s^{-1} [115] (see Figure 5, inset 1). The half-wave potential ($E_{1/2}$) of ABTS oxidation on bare GC was independent of pH and the $E_{1/2}$ value was 0.46 V, exactly the same as determined from the CV data of bare GC. This is an expected result considering the nearly reversible CV response of ABTS.

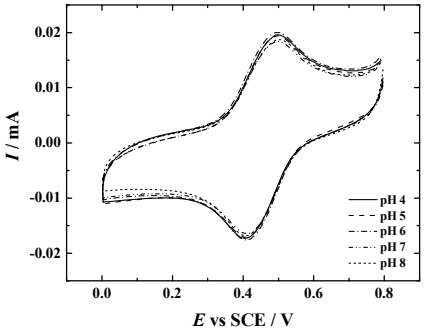

Figure 4. Cyclic voltammograms of a bare GC electrode in Ar-saturated 50 mM acetate buffer (pH 4 and 5) and 50 mM phosphate buffer (pH 6, 7 and 8) containing 0.5 mM ABTS and 0.1 M KCl. v = 100 mV s^{-1}.

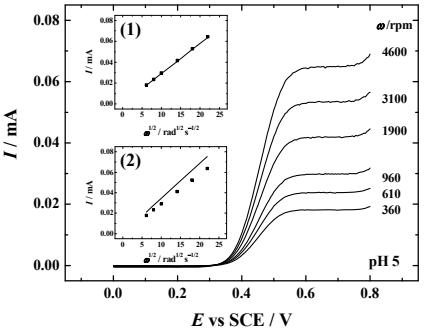

Figure 5. RDE voltammetry curves for ABTS oxidation on a bare GC electrode in Ar-saturated 50 mM acetate buffer (pH 5), containing 0.5 mM ABTS and 0.1 M KCl at various rotation rates. v = 10 mV s^{-1}. The insets show the Levich plot at 0.6 V. The solid line corresponds to the theoretical Levich plot, where the D was used as (1) 3.4×10^{-6} cm^2 s^{-1} [115] or (2) 4.4×10^{-6} cm^2 s^{-1} [114]), respectively.

Figures 6a,c,e,g,i and Figures 6b,d,f,h,j show the CV curves and RDE voltammetry curves towards the $ABTS^{2-/\bullet-}$ redox probe on aryl-modified GC electrodes, respectively. The voltammetric response of bare GC is given for comparison. In addition, the electrochemical data for the $ABTS^{2-/\bullet-}$ couple of

bare GC and differently modified GC electrodes after modification by Procedures (a) and (c) were determined from the CV curves presented in Figures 6a,c,e,g,i and are given in Table 1. One of the parameters, the relative blocking efficiency (I_{rel}), was used for aryl-modified GC electrodes and was defined analogously to Ref. [163]:

$$I_{\text{rel}} = \left(\frac{I_{\text{pa}} \text{ with a film}}{I_{\text{pa}} \text{ for a bare GC}} \right) \times 100\% \quad (3)$$

where I_{pa} is the intensity of the anodic peak current. It should be noted that while using the modification Procedure (b) for GC/NP and reduced GC/NP electrodes and Procedure (d) for GC/CP electrodes, the blocking effect was so strong that the CV peaks were not discernible (see Figures 6a,c,e,g,i) and for these electrodes the parameters to characterise their barrier properties towards the $ABTS^{2-/\bullet-}$ redox couple could not be determined.

According to the values given in Table 1, the $ABTS^{2-/\bullet-}$ redox system exhibits a significant increase of the ΔE_p value and decrease in peak current for NP-modified GC electrode (Procedure a) as compared to bare GC in all solutions. It should be noted that the increase in the separation of peak potentials demonstrates the inhibition of the charge transfer process. But in general, the electrochemical behaviour of ABTS on the GC/NP electrode (Procedure a) was almost the same in the solutions of different pH. Interestingly, the reduced GC/NP (Procedure a) and GC/CP (Procedures c) electrodes showed a rather similar behaviour in the charge transfer process (at pH 4) because the values of ΔE_p were almost the same (see Table 1).

As can be seen from Table 1 and Figure 6, amongst other aryl-modified electrodes studied, some differences were observed in the electrochemical behaviour of ABTS on reduced GC/NP electrodes in different pH solutions as well (Figures 6a,c,e,g,i). It is known that the pK_a of aniline is 4.6 [42, 172], therefore at pH 4 and 5 the AP groups on the modified electrode are protonated. At higher pH (pH >> pK_a) the AP groups are deprotonated and the electron transfer of the $ABTS^{2-/\bullet-}$ couple is somewhat blocked. Furthermore, the reduced GC/NP electrode (Procedure a) showed the lowest barrier properties for the ABTS oxidation in the solutions of different pH (pH=4–8), especially as compared with GC/NP electrodes (Procedure a). This might indicate that the aryl layer of NP is more compact than the reduced NP film where the aminophenyl groups are present (as shown by XPS in Section 6.1.2).

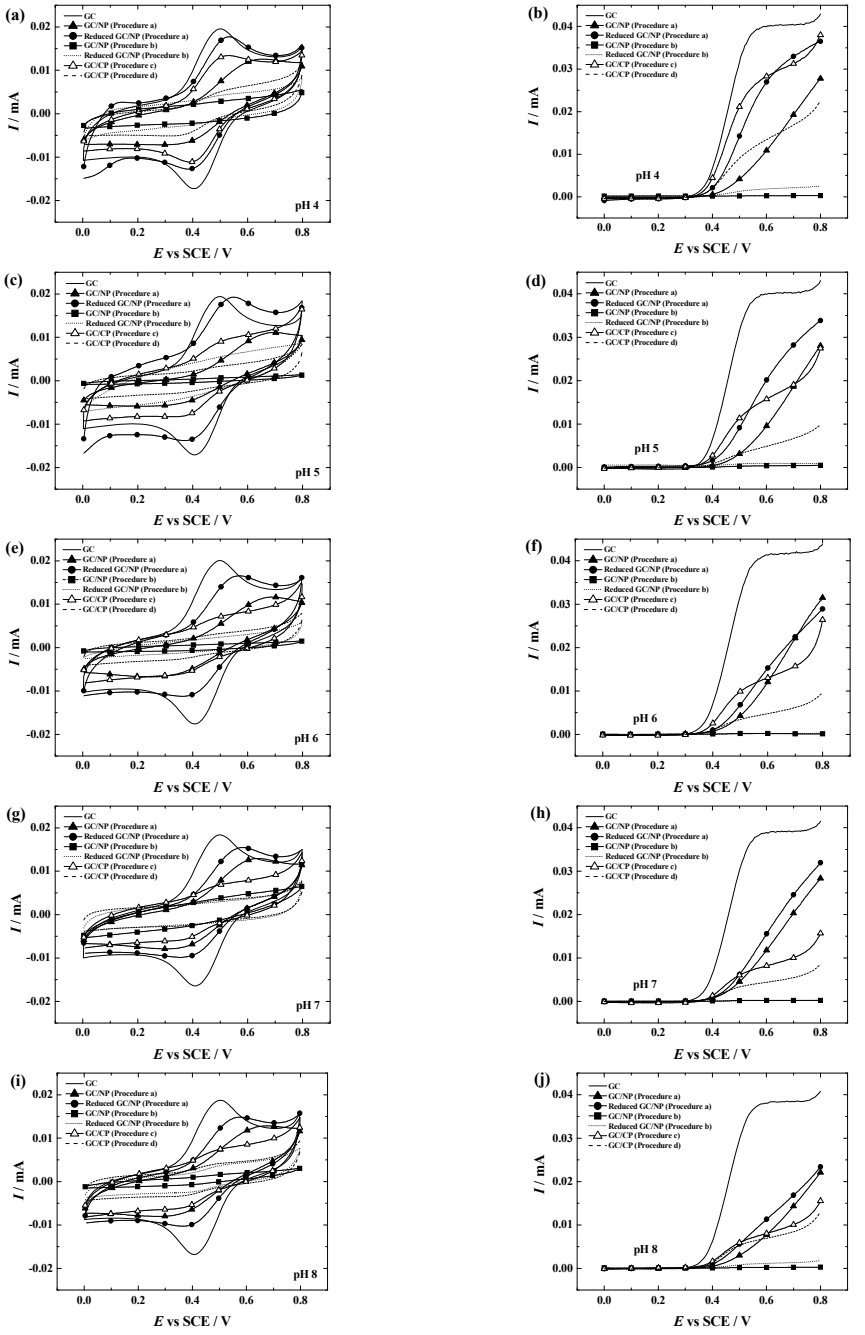

Figure 6. (a,c,e,g,i) CVs and (b,d,f,h,j) RDE voltammetry curves for bare and aryl-modified GC electrodes in Ar-saturated buffer solutions containing 0.5 mM ABTS and 0.1 M KCl at different pH (4–8). (a,c,e,g,i) v = 100 mV s^{-1} and (b,d,f,h,j) v = 10 mV s^{-1} and ω = 1900 rpm.

The electrochemical results are rather controversial compared with literature. Namely, Lyskawa and Bélanger [173] reported the electrochemical behaviour towards ferricyanide reduction of Au electrodes modified with NP or aminophenyl groups by *in situ* generated diazonium salt reduction. The experimental results revealed that the electrochemical response of the $Fe(CN)_6^{3-/4-}$ redox system was more suppressed for AP-modified Au electrodes than for NP-modified Au electrodes [173] and therefore it was further concluded that the aminophenyl layer was more compact than the NP layer [40].

Table 1. Comparison of the CV results of bare GC and aryl-modified GC electrodes, using the modification Procedure a (one cycle) and c (two cycles). CVs were recorded in Ar-saturated 0.1 M KCl solution of various pH (pH=4–8) containing 0.5 mM ABTS. v = 100 mV s^{-1}.

Electrode	pH 4			pH 5			pH 6		
	ΔE_p (V)	I_{pa} (μA)	I_{rel} (%)	ΔE_p (V)	I_{pa} (μA)	I_{rel} (%)	ΔE_p (V)	I_{pa} (μA)	I_{rel} (%)
Bare GC	0.08	13.9	–	0.08	13.8	–	0.08	13.8	–
GC/NP[1]	0.22	7.7	55	0.26	7.7	56	0.27	7.3	53
Reduced GC/NP[1]	0.11	11.3	81	0.13	9.6	70	0.14	9.3	67
GC/CP[2]	0.11	8.6	62	n.d.	n.d.	n.d.	n.d.	n.d.	n.d.
Electrode	**pH 7**			**pH 8**					
	ΔE_p (V)	I_{pa} (μA)	I_{rel} (%)	ΔE_p (V)	I_{pa} (μA)	I_{rel} (%)			
Bare GC	0.08	12.7	–	0.08	13.2	–			
GC/NP[1]	0.22	7.7	61	0.25	7.1	54			
Reduced GC/NP[1]	0.17	9.6	76	0.15	9.2	70			
GC/CP[2]	n.d.	n.d.	n.d.	n.d.	n.d.	n.d.			

[1] These electrodes were modified by Procedure (a); [2] This electrode was modified by Procedure (c); n.d. – *not detectable*

According to the CV and RDE results, the largest pH effect was observed for the GC/CP electrodes (both Procedures c and d). In case of GC/CP electrode modified by Procedure (c), the oxidation peak of ABTS was clearly visible at pH 4 (Figure 6a), while at pH 5 (Figure 6c) the electrochemical response of ABTS was more suppressed and even more at pHs 6–8 (Figures 6e,g,i). Therefore, the electrochemical parameters for GC/CP electrode (Procedure c) at pH>5 could not be determined as can be seen in Table 1. A similar behaviour of CP-modified electrodes has been observed by Saby *et al*. [39] and Abiman *et al*. [174] for the $Fe(CN)_6^{3-/4-}$ redox system in buffer solutions of differing pH. The authors revealed that as the pH of the solution increased, the peak current decreased significantly at the CP-modified electrode. This kind of blocking behaviour was explained by the surface pK_a value of CP groups. Saby *et al*. [39] reported that the apparent pK_a of the 4-carboxyphenyl grafted layer shifted to a lower value (pK_a = 2.8) than the pK_a of solution based benzoic acid (pK_a = 4.2).

It can be said that the CP groups on GC surface are deprotonated at the pHs studied according to the estimated pK_a of 2.8 [39] or 3.25 [174] and thus repel the negatively charged ABTS.

In order to get a better overview of the blocking effect, the differences of the currents of ABTS oxidation at 0.6 V between the electrodes of various aryl films were taken for comparison with that of bare GC. The respective current values are given in Table 2. As can be seen from Table 2, the effect of pH on ABTS oxidation was rather negligible in case of GC/NP (Procedures a,b) and reduced GC/NP (Procedure a) electrodes. Also the electrochemical behaviour towards the $ABTS^{2-/\bullet-}$ redox probe on the GC/NP electrode (Procedure a) was almost the same in the solutions of different pH (see Figure 6). However, the oxidation current values for GC/CP electrode (Procedure d) were higher at pH 4 than in other solutions (pH=5–8), where the current values were almost the same (this was discussed above). The same tendency was also noticed for the reduced NP film by applying Procedure (b).

Table 2. Comparison of oxidation current (I, mA) values at the potential of 0.6 V for a bare and aryl-modified GC electrodes obtained by the RDE method in Ar-saturated solutions of various pH (pH=4–8) containing 0.5 mM ABTS and 0.1 M KCl. ω = 1900 rpm, v = 10 mV s^{-1}.

Electrode	ABTS oxidation current (mA)				
	pH 4	pH 5	pH 6	pH 7	pH 8
Bare GC	0.0399	0.0397	0.0399	0.0386	0.0390
GC/NP (Procedure a)	0.0109	0.0096	0.0120	0.0118	0.0077
GC/NP (Procedure b)	0.0002	0.0004	0.0002	0.0002	0.0002
Reduced GC/NP (Procedure a)	0.0270	0.0214	0.0153	0.0155	0.0113
Reduced GC/NP (Procedure b)	0.0018	0.0009	0.0001	0.0001	0.0011
GC/CP (Procedure c)	0.0283	0.0158	0.0130	0.0082	0.0080
GC/CP (Procedure d)	0.0134	0.0048	0.0048	0.0044	0.0069

The blocking action towards ABTS response increased with the number of modification cycles. The largest blocking effect towards ABTS was observed for a GC/NP electrode (Procedure b) in the solution of different pH (shown in Figure 6), but also for reduced GC/NP (Procedure b) electrodes as can be seen from Table 2. The GC electrodes modified with NP, CP and AP groups using Procedures (b) and (d) showed a similar response towards the $ABTS^{2-/\bullet-}$ couple at various pHs and yielded a stronger blocking effect as compared to the electrodes modified by Procedures (a) and (c). This is obviously related to the differences in the surface concentration of aryl groups.

In addition, the barrier properties of the aryl-modified electrodes can be explained by electrostatic interaction between charged groups and ionic redox probes according to the study by Schauff *et al.* [122] and as discussed in

Section 4.3. Besides the electrostatic interactions the barrier properties are strongly influenced by surface coverage of the modifier film. The structure of the aryl films has not been studied in the present work. However, previous investigations have shown that the blocking properties of aryl films depend on the modification conditions and even on the post-deposition treatment [8]. In addition, the presence and distribution of pinholes in the film might considerably influence its barrier properties. All these aspects are important for the practical application of aryl-modified electrodes in electroanalysis.

6.2. Surface and electrochemical properties of GC and Au electrodes modified with azobenzene derivatives by diazonium reduction

One of the important questions is whether the stability of aryl layer on Au surface is as high as that of the layer on carbon surface. Another issue concerns the electrochemical behaviour during electrografting between carbon and Au substrate. And last but not least, how different is the electrochemical behaviour between aryl-modified GC and Au electrodes. Comparative studies on GC and Au electrografted with NP, CP or 4-sulfophenyl groups have been performed by Gooding and co-workers [31, 38, 44, 77]. According to our knowledge, a comparative study between GC and Au surface electrografted with different azobenzene diazonium salts has not been reported as yet. Therefore, in this section, the electrochemical properties (including electrochemical behaviour during electrografting) of GC and Au electrodes modified with azobenzene derivatives *via* electrochemical reduction of the corresponding diazonium salts are compared [II,III]. Since the electrochemical grafting of GC and Au with aryl groups yielded robust layers, which inhibited the electrochemical response of the $Fe(CN)_6^{3-}$ probe and in addition, the aryl layers were difficult to remove without mechanical treatment on both GC and Au substrates [II,III], it was of special interest to further explore the degradation effect of aryl films on GC and Au surface by $OH^{\bullet}$ radicals generated by UV photolysis of H_2O_2 [IV].

6.2.1. Electrochemical grafting of GC and Au electrodes with different azobenzene derivatives

GC and Au electrodes were modified with AB, GBC and FBK groups *via* electrochemical reduction of the corresponding diazonium salts. These specific diazonium compounds were chosen due to the differences in their structure (see Scheme 3c-e). For both substrates, three different modification procedures were used with each diazonium compound: (1) one cycle, (2) 10 cycles and (3) 10 cycles after which the electrode was held at –0.2 V for 10 min. In all cases, the potential cycling was performed between 0.6 and –0.4 V with a scan rate of

100 mV s^{-1}. For the clarification, the GC and Au substrates electrografted with AB, GBC and FBK groups are designated as GC/AB, GC/GBC, GC/FBK and Au/AB, Au/GBC, Au/FBK, respectively.

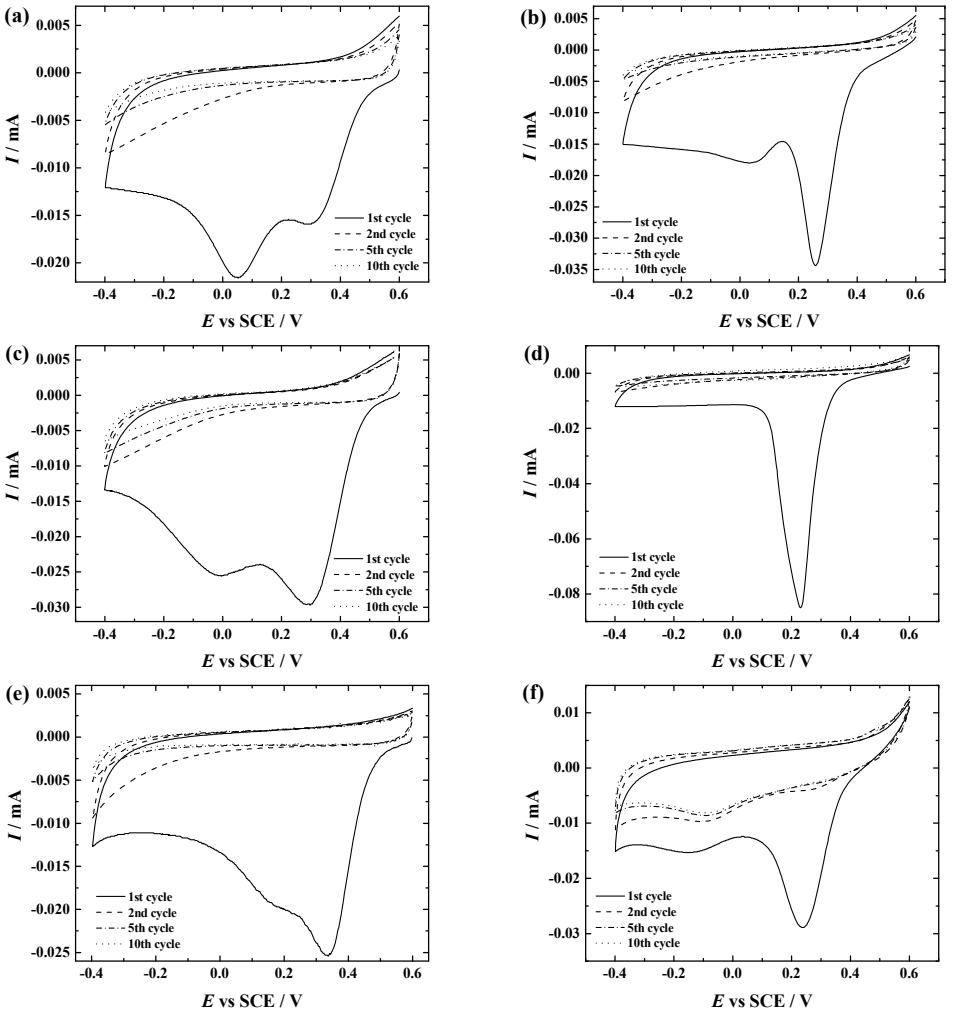

Figure 7. Electrografting of GC (a,c,e) and Au (b,d,f) electrodes by electrochemical reduction of (a,b) azobenzene diazonium salt, (c,d) Fast Garnet GBC sulphate salt and (e,f) Fast Black K salt in Ar-saturated ACN containing 0.1 M $TBABF_4$ as a supporting electrolyte. v = 100 mV s^{-1}. It should be noted that the diazonium salt concentration was 1 and 3 mM in case of GC (a,c,e) and Au (b,d,f) electrodes, respectively.

The modification curves of the electrochemical reduction of different azobenzene diazonium salts on GC are shown in Figures 7a,c,e and on Au are presented in Figures 7b,d,f. The first modification cycle showed two reduction peaks in case of ABD ($E_p \approx 0.31$ V and 0.05 V), Fast Garnet GBC sulphate salt

($E_p \approx 0.30$ V and –0.02 V) and Fast Black K salt ($E_p \approx 0.33$ V and 0.16 V) while using GC as an electrode. The reduction potential of the ABD on GC was rather similar to that reported in the literature [175]. Compared with GC electrodes, quite similar electrochemical behaviour was observed in case of Au electrodes electrografted with AB ($E_p \approx 0.26$ and 0.03 V) and FBK groups (0.23 and –0.15 V), except in case of GBC, where only one reduction peak appeared on Au at ca 0.23 V. The latter result was also confirmed by EQCM study (the discussion is given above).

As discussed in Section 6.1.1, the origin of pre-peak is still not clear, meanwhile, the second reduction peak can be attributed to the reduction of the diazonium species on GC electrode. Different explanation is given in case of electrografting of Au surfaces with aryldiazonium cations. It was proposed by Benedetto et al. [176] that the first reduction peak can be associated with the reduction of diazonium cations on Au(111) facets, while the second peak at lower potential values can be attributed to the reduction of diazonium cations on Au(100), or on Au(110), Au(311) and other crystal facets.

Although rather similar electrochemical behaviour during the electrografting between GC and Au electrodes was observed, it is important to note that the reduction potential of different azobenzene derivatives at GC electrode was a more positive (by ca 0.1 V) than that at Au electrode surface. Based on the recent reports [77, 177], the reason of this shift is the spill over of electron density into the resultant film derived from the aryl diazonium salts that occurs on gold surfaces. The negative charge makes the attachment of radicals difficult hence shifts the second peak potential to the negative values with respect to the first peak [177].

In general, for both substrates, the diazonium reduction peak(s) disappeared and peak current values decreased upon successive potential cycling (see Figure 7) indicating the formation of the aryl layer on the electrode surface [5]. However, as can be seen from the electrochemical behaviour of Fast Black K diazonium cations on Au surface, the first reduction peak vanishes for the subsequent cycles, whereas the current of the second peak only slightly decreases and does not disappear entirely. Similar electrochemical behaviour was observed by Gui *et al*. [31] where the Au surface was electrografted with 4-sulfophenyl diazonium salt. The authors suggested that the second reduction peak at lower potentials is observed because on Au(100) a smaller amount of aryl radicals is attached to this particular crystallographic facet [31].

There has been a disagreement in determining the surface concentration of azobenzene groups. Sadowska *et al*. [178] proposed that azo compounds are electroactive and therefore the surface concentration can be estimated by cyclic voltammetry. According to Brooksby and Downard [93], the azobenzene groups have no detectable electroactivity in aqueous acidic solution, whereas Šljukic *et al.* [128] have evaluated the surface concentration of physically adsorbed azobenzene in acidic solution. In the present thesis, the CV peaks were not reproducible and therefore the surface coverage of all the azobenzene

derivatives used for the modification of GC and Au substrates remained unknown.

In case of Au electrodes, the GBC and FBK film formation on Au electrode was further investigated by EQCM. Figures 8a,b present the *I–E* and Δ*m–E* potentiodynamic results for an Au electrode grafting during 10 repetitive potential cycles in 0.1 M $TBAClO_4$/ACN containing 3 mM of the Fast Garnet GBC sulphate salt and Fast Black K salt, respectively. As can be seen from Figures 8a,b, the electrochemical behaviour of Au surface grafting with Fast Garnet GBC sulphate salt and Fast Black K salt is similar to that presented in Figures 7d,f. Briefly, the first cycle showed one ($E_p \approx 0.15$ V) and two ($E_p \approx 0.10$ V and –0.05 V) reduction peaks in case of electrografting with GBC and FBK diazonium compounds, respectively.

From the EQCM results we may conclude that the aryl-film thickness increases with successive potential cycles despite the lack of an observable reduction wave. This continuing growth of the film may be attributed to the diazonium cation reduction *via* electron transfer through the grafted film although grafting at a decreased rate was observed [75].

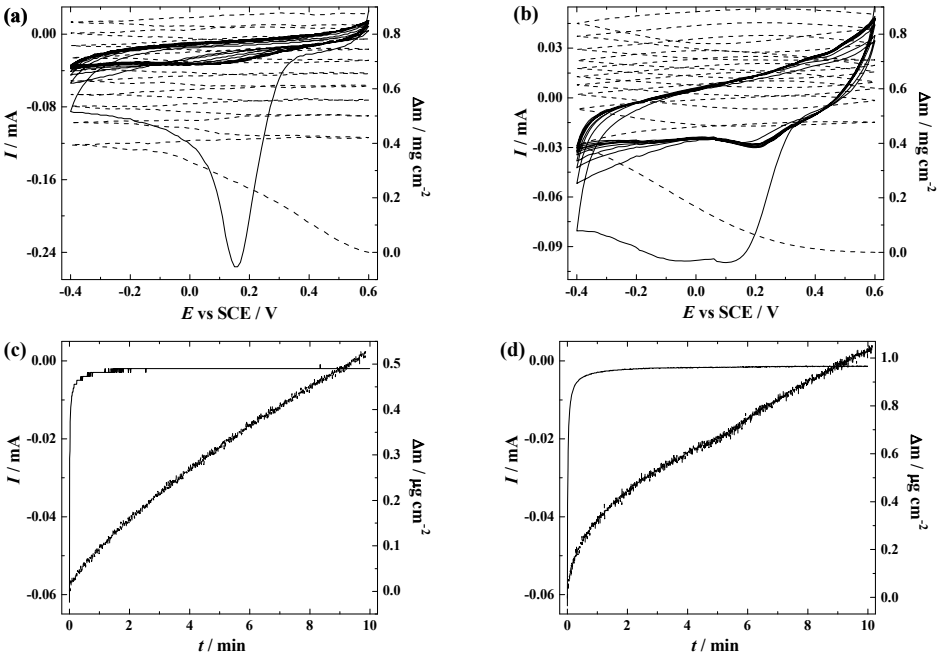

Figure 8. (a,b) *I*−*E* (solid line) and Δ*m*−*E* (dashed line) potentiodynamic profiles for ten repetitive potential cycles (v = 100 mV s^{-1}) and (c,d) dynamic profiles for the chronoamperometric experiment at −0.2 V for Au electrode in 0.1 M $TBAClO_4$/ACN containing 3 mM of Fast Garnet GBC sulphate salt and Fast Black K salt (after 10 potential scans presented).

Increases in mass densities are observed for potentials more negative than 0.57 and 0.45 V to Fast Garnet GBC diazonium cation and Fast Black K diazonium cation, respectively, which coincide with increases in currents for the first CV scans. These increases in mass densities (230 and 75 ng cm^{-2}) are linear until around 0.21 and 0.17 V which are close to the potentials of the first reduction peaks. Therefore, the attachment of GBC and FBK groups to the surface of Au is in evidence already in the first stage. After these potentials, in the negative potential scan direction, a second increase in mass densities (137 (= 367–230) and 295 (= 370–75) ng cm^{-2}) with smaller and higher inclinations (ng cm^{-2} V^{-1}), respectively, are observed until around –0.09 and –0.35 V (second stage of the attachment of GBC and FBK groups to the surface of gold film, respectively). At the end of the first potential half-cycle the increases in mass densities were very close (390 ng cm^{-2}) for both compounds, and at the end of the first potential cycle were 420 and 480 ng cm^{-2} for GBC and FBK groups, respectively. When the potential scan is reversed, the mass densities continue to increase slowly. A gradual mass density increase is observed for further potential cycling. Comparing the mass density change of the first and tenth scans, an increase in mass density of approximately 425 ng cm^{-2} (in average), for both compounds, is observed for a layer that blocks completely the reduction of the Fast Garnet GBC diazonium compound. This behaviour has been previously observed for the covalent grafting of gold with other aryldiazonium compounds [75, 104, 176, 179]. The slow mass density increase in the reverse scan has been attributed to the formation of charge-transfer complexes that precipitate on the electrode surface [104, 180–183], but further growth from the radicals generated and diffusing to the electrode surface cannot be ruled out. In case of the Fast Black K diazonium compound, the decrease in mass densities was noted after the second potential cycling at more positive potentials than 0.2 V, whereas the increase in mass densities was observed at more negative potentials than 0.2 V. This kind of behaviour can be attributed to some redox behaviour/electron hopping [183] to the film produced after reduction of Fast Black K diazonium compound.

The faradaic efficiencies were calculated from the slope of the Δm–Δq plots for different experimental conditions and values of 21 and 34% were found for the first electrografting half-cycle to Fast Garnet GBC and Fast Black K diazonium compound, respectively.

By assuming a surface concentration of 10×10^{-10} mol cm^{-2} for a monolayer [75], the corresponding mass density expected for a monolayer of GBC group is 286 ng cm^{-2} and FBK group is 209 ng cm^{-2}. The surface concentration of GBC and FBK groups on Au surface can be calculated as 13.6×10^{-10} and 18.7×10^{-10} mol cm^{-2} (390 ng cm^{-2}), respectively, indicating higher coverage than a monolayer for the first potential half-cycle.

After recording ten consecutive *I*–*E* and Δm–*E* profiles the electrode was held at a constant potential of –0.2 V for 10 min and a relatively small reduction

current was observed during the chronoamperometric experiment (Figures 8c,d) for both diazonium compounds. Surprisingly, although the currents are very small, the mass densities continue to increase (more effective to Fast Black K diazonium salt) indicating further growth of the grafted layers (i.e. multilayer growth).

6.2.2 Surface characterisation of AB-, GBC- and FBK-modified GC and Au electrodes

In order to confirm the presence of different azobenzene derivatives on aryl-modified GC and Au substrates, the XPS analysis was used. The surface morphology of aryl-modified Au electrodes was further characterised by AFM.

As all the azobenzene derivatives used include azo groups (–N=N–), then it is relevant to note that the presence of azo linkages in aryl layers was studied by Saby *et al*. [39]. They revealed that the XPS peak in the N1s region at 400 eV is attributed to –N=N– linkage. Furthermore, Liu and McCreery [62] used the electrochemical reduction method to modify the GC electrodes with aryl groups, using azobenzene as well as nitroazobenzene (NAB) diazonium salts. They investigated the aryl layers with Raman spectroscopy and also with XPS. As NAB includes nitro group besides the azo group, the high–resolution XPS spectra showed N1s peaks at 400 and 406 eV, which correspond to the azo and the nitro groups, respectively.

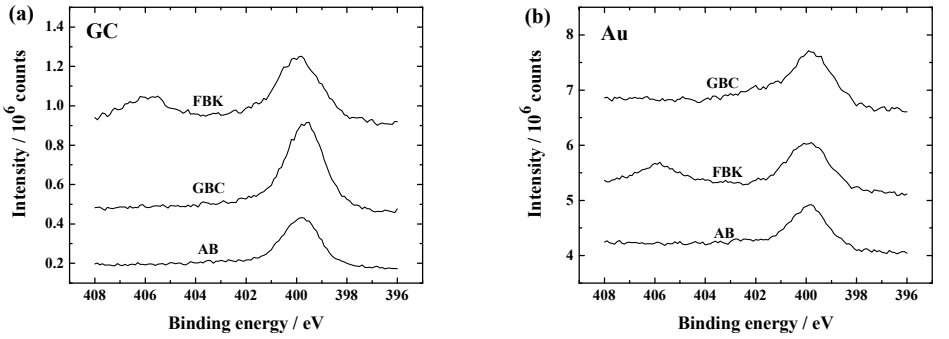

Figure 9. The XPS spectra in the N1s region for AB-, GBC- and FBK-modified: (a) GC and (b) Au electrodes. Both substrates were modified using Procedure (2).

The XPS core–level spectrum in the N1s region of AB-, GBC- and FBK-modified GC and Au electrodes is shown in Figure 9. While the XPS data for the corresponding diazonium salts using different modification procedures was rather similar, only the data of one modification procedure which involved 10 subsequent cycles were chosen for comparison. It is important to note that the XPS survey spectra of AB-, GBC- and FBK-modified Au electrodes showed

gold, carbon, oxygen and nitrogen peaks (data not shown). The appearance of the gold peak is due to the presence of the defect sites in the grafted aryl layer. However, it was of considerable interest to investigate the nitrogen groups of azobenzene derivatives attached to GC and Au surfaces *via* electrochemical reduction of the corresponding diazonium salts and therefore only the N1s core level spectra of aryl-modified GC and Au samples are presented in Figure 9.

As can be seen in Figure 9, the main peak at ca 400 eV gives evidence for the presence of azo groups as well as azo linkages (–N=N–) for AB-, GBC- and FBK-modified GC and Au electrodes. It is relevant to note that Ricci *et al*. [81] studied the formation of an azo bond during the electroreduction of diazonium salts on Au electrode surface. They revealed from the XPS study the formation of N=N bonds tethering the complexes to Au. On the other hand, for both FBK-modified surfaces, the XPS spectrum in the N1s region revealed two peaks (Figures 9a,b). The first peak around 406 eV is attributed to $–NO_2$ functionality and the second one at 400 eV corresponds to azo linkage. These observations are in good agreement with earlier reports for on different substrate materials [184]. Since all the studied aryl-compounds contain azo linkage and additionally, FBK contains a nitro group (see Scheme 3), these XPS results were rather expected. However, from the XPS data it can be concluded that the GC and Au electrodes can be successfully electrografted with AB, GBC and FBK groups.

As it was shown previously [104], the Au(111) thin-film electrodes are very suitable for detailed topographic studies of the modifier films on gold. Therefore, the surface morphology of the Au film on a mica substrate modified with different aryldiazonium compounds was further examined using AFM. Typical topographical images obtained in non-contact mode and their height profiles are presented in Figure 10. The AFM images of modified Au electrodes clearly show that the surfaces of all electrodes are fully covered with a granular layer (see Figure 10). Thickening of modifier layers can be clearly seen in all three cases. The typical pattern of Au(111) surface is clearly visible after modification with one voltammetric cycle (Figures 10a,d,g), but after 10 voltammetric scans and holding the electrode at –0.2 V for 10 min, the pattern of Au(111) is practically invisible (Figures 10c,f,i).

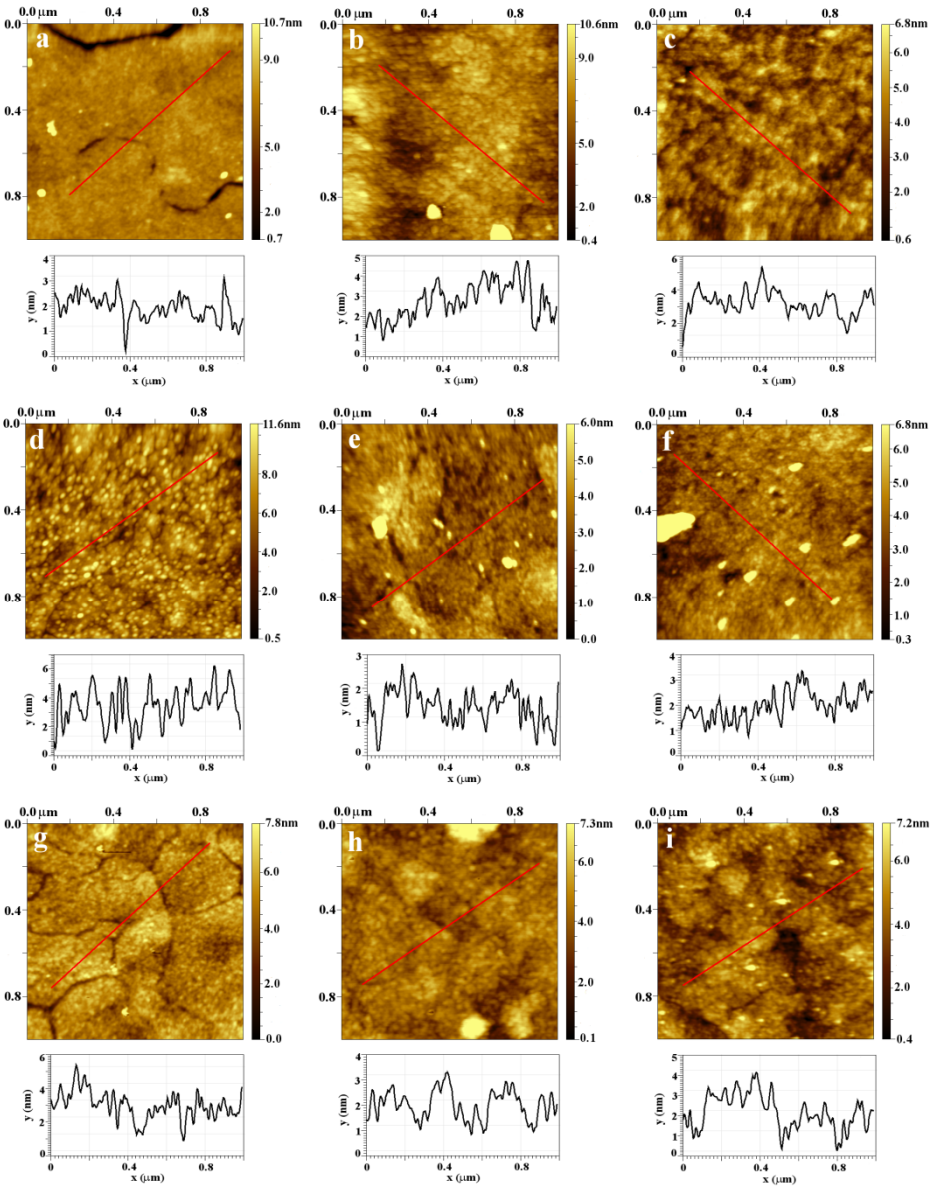

Figure 10. AFM images of Au(111) film electrodes modified with AB (a–c), GBC (d–f) and FBK (g–i) groups. The Au electrodes were electrografted using one potential cycle (a,d,g), 10 cycles (b,e,h), and 10 cycles, followed by holding the electrode at –0.2 V for 10 min (c,f,i).

The granular features of the electrodes modified by one potential cycle were uniform with average diameter of 30–50 nm for AB (Figure 10a), 35–50 nm for GBC (Figure 10d) and 25–45 nm for FBK (Figure 10g). After 10 voltammetric

scans, the dimensions of the granules increased in case of AB (35–70 nm) and FBK (40–60 nm). Different change of dimensions of the granules is detectable in case of GBC, average diameter decreases to 20–45 nm. This can be explained by differences in the growth stage of GBC film. After one cycle the upper layer of GBC film is not fully filled and separate granules can be measured, but after 10 cycles all layers are filled and granules are closely packed, therefore their sizes are reduced. This explanation is also supported by decrease in the root mean square (RMS) roughness values from 1.53 nm for electrode modified with one voltammetric cycle to 1.35 nm for an electrode modified with 10 potential cycles. For electrodes modified with AB and FBK the RMS roughness increases from 1.34 nm and 1.1 nm for electrodes modified with one cycle to 1.58 nm and 1.9 nm for electrodes modified with 10 potential cycles, respectively. The RMS roughness of modified electrodes after additional holding the electrode at –0.2 V for 10 min were 1.45 nm for AB, 1.22 nm for GBC and 0.93 nm for FBK. Decrease in RMS roughness of the modified Au electrodes during additional modification can be explained by thickening of modifier layers and close package of granules. Granule sizes do not change during this additional process for GBC (20–45 nm) and FBK (40–60 nm). Increase in granule dimensions was measured for electrodes modified with AB (50–80 nm). For comparison purposes, the RMS roughness of the unmodified Au(111) film surface was 0.2 nm.

The thickness of aryl films was estimated using the AFM scratching experiment or ellipsometry (see Table 3).

Table 3. Estimation of the AB, GBC or FBK film thickness on Au electrode by ellipsometry.

Electrode	Film thickness measured by ellipsometry (nm)
Au/AB1	12 (or 11)[a]
Au/AB2	18 (or 13)[a]
Au/AB3	21 (or 18)[a]
Au/GBC1	5
Au/GBC2	4 (or 7)[a]
Au/GBC3	11
Au/FBK1	10
Au/FBK2	12 (or 17)[a]
Au/FBK3	33

[a] Film thickness was measured by AFM

The layer thicknesses measured by AFM in case of AB were 11 nm for the electrode modified with one cycle, 13 nm for the electrode modified with 10 cycles, and 18 nm for the electrode modified with 10 cycles and additional holding of the electrode at –0.2 V for 10 min. For Au electrodes modified with

FBK and GBC groups by 10 potential cycles the thicknesses of modifier layers were 17 and 7 nm, respectively. These estimations of layer thickness were qualitatively confirmed by ellipsometric measurements (see Table 3). It should be noted that the ellipsometric thickness results for FBK layers are less reliable as modelling was performed only using a homogeneous film model. However, the comparison of measured and fitted spectra clearly indicates a more complex structure of a film.

6.2.3. Electrochemical behaviour towards the $Fe(CN)_6^{3-/4-}$ redox probe on AB-, GBC- and FBK-modified GC and Au electrodes

The electrochemical properties of GC and Au electrodes modified with different azobenzene derivatives were characterised by CV using the ferri/ferrocyanide redox probe (see Figure 11). For comparison purposes, the electrochemical experiments with polished GC and Au electrodes were also conducted. Figure 11 shows peak-shaped voltammograms for the redox reaction on bare GC and Au substrates, indicating that the electron-transfer process is under diffusion control. The ΔE_p values were ca. 76 and 60 mV for polished GC and Au electrodes, respectively. It is known that these ΔE_p values exhibit fast one-electron transfer kinetics for the $Fe(CN)_6^{3-/4-}$ redox couple.

In general, the electrochemical responses towards the ferri/ferrocyanide redox probe at the aryl-modified GC and Au electrodes are of two general types (see Figure 11). To be more specific, quite well-defined peaks were observed in case of GC grafted with AB, GBC and FBK films using short modification procedure (e.g. one cycle, Procedure 1) while the shape of CVs of aryl-modified Au electrodes was rather sigmoidal. Therefore, two main parameters, ΔE_p and I_{rel}, were used to characterise the barrier properties of the aryl films studied in case of GC/AB1, GC/GBC1 and GC/FBK1 electrodes. The parameter of I_{rel} was defined according to the equation (3) given in Section 6.1.3, with a difference that the intensity of the cathodic peak (I_{pc}) was used.

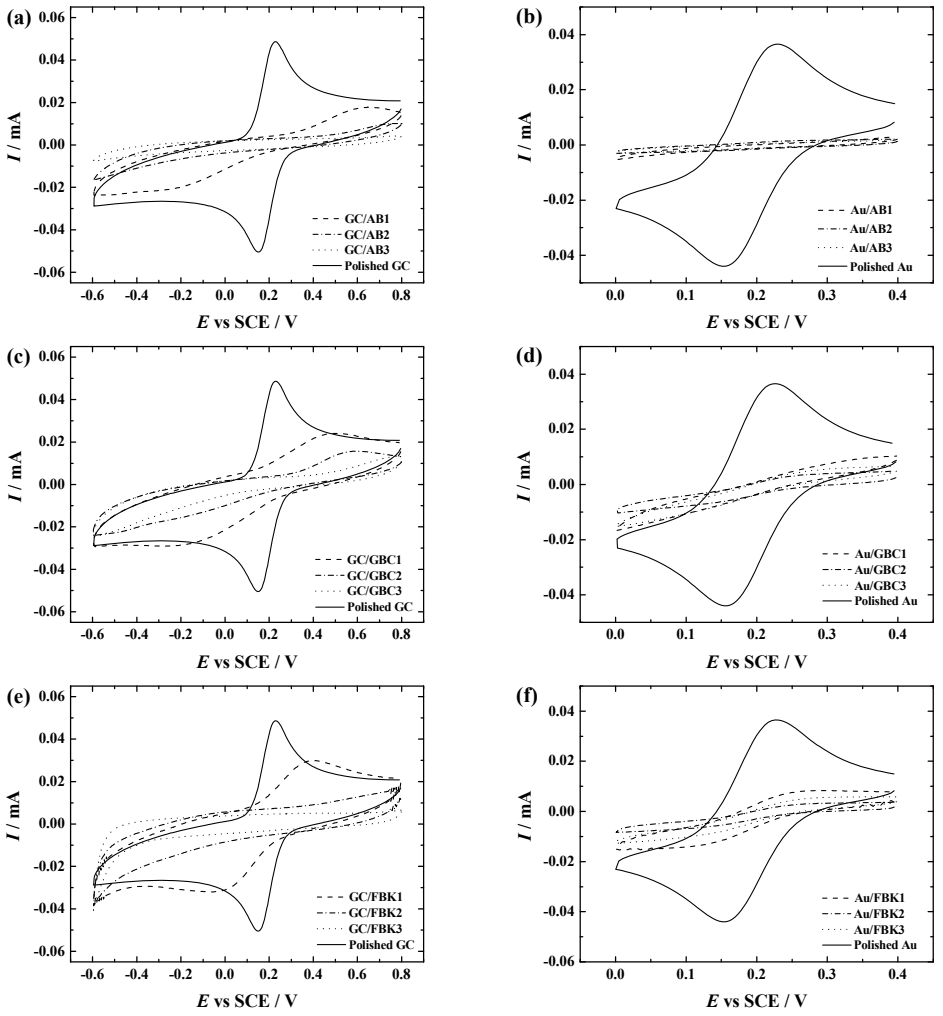

Figure 11. Cyclic voltammograms of (a,c,e) GC and (b,d,f) Au electrografted with (a,b) AB, (c,d) GBC and (e,f) FBK groups. CVs were recorded in 1 mM $K_3Fe(CN)_6$ solution containing 0.1 M K_2SO_4 as a supporting electrolyte. $v = 100$ mV s^{-1}.

The electrochemical data for aryl-modified GC electrodes are given in Table 4.

Table 4. CV results of polished and aryl–modified GC electrodes recorded in Ar-saturated 0.1 M K_2SO_4 containing 1 mM $K_3Fe(CN)_6$ (ν = 100 mV s^{-1}). The GC electrodes were modified using Procedure (1).

Electrode	I_{pc} (µA)	I_{rel} (%)	ΔE_p (V)
Polished GC	44	–	0.076
GC/AB	10	22.8	0.863
GC/GBC	12.5	28.4	0.597
GC/FBK	18	40.9	0.377

Considerable increase in the ΔE_p value for all the aryl layers studied was observed compared to the polished GC electrode (see Table 4). The increase in the value of ΔE_p reflects a significant decrease in the ET rate due to the blocking action of the grafted AB, GBC and FBK layers. It is well-known that the $Fe(CN)_6^{3-/4-}$ ions should interact with GC surface for an effective ET process to occur [16, 90]. Therefore, it is evident that the formation of an aryl layer on the GC surface should inhibit the electron transfer kinetics of this redox couple. Also, it has been previously demonstrated that using the same procedure of modification by different aryl groups results in different degrees of surface blocking [123]. Khoshroo and Rostami [185] have grafted the GC surface with FBK *via* electrochemical reduction using different diazonium reduction times and compared the electrochemical behaviour with 4–diazophenylaceticacid tetrafluroborate (PAA) modified GC electrodes. They concluded that the blocking action was less pronounced for FBK-modified electrode towards the $Fe(CN)_6^{3-/4-}$ redox couple compared to PAA-modified GC electrode although both aryl layers showed a significant blocking effect for the oxidation and reduction reactions of the $Fe(CN)_6^{3-/4-}$ redox system compared to polished GC electrode [185]. For example, using the modification time of 30 s to obtain FBK layer on the GC surface, the parameter I_{rel} was evaluated as 55.6% [185]. In this study, according to the value of I_{rel}, the best blocking action was observed for GC/AB electrode (22.8%) and the lowest, 40.9%, for GC/FBK electrode (see Table 4), when only one potential cycle was used during electrografting.

While using a shorter modification program during electrografing (e.g. only one potential cycle), the electrochemical results somewhat differed between aryl-modified Au and GC electrodes (see Figure 11). For example, for the Au/AB1 electrode, the CV did not show any peak indicating that the electron transfer process was strongly inhibited (see Figure 11b). In contrast to the results obtained on GC/AB1 electrodes, both the cathodic and anodic waves were observed (see Figure 11a). This might be explained by the circumstance that different diazonium salt concentrations were used for electrochemical grafting (1 mM and 3 mM for GC and Au substrates, respectively). Therefore, higher concentration may allow the Au surface to be better covered with aryl film. Furthermore, the electrochemical behaviour of the Au/GBC1 and Au/FBK1 electrodes was different compared to Au/AB1 and aryl-modified GC

electrodes. More specifically, the general shape of the corresponding CVs was rather sigmoidal in case of GBC- and FBK-modified Au electrodes. There were no defined peaks but the peaks were not suppressed completely. The sigmoidal shape of CV might refer that the aryl film contains pinholes where the electron transfer process between the $Fe(CN)_6^{3-/4-}$ redox species and electrode surface is possible [162].

Kariuki and McDermott [10] reported that the longer electrolysis time of diazonium salt yielded larger ΔE_p for several redox systems. Also, Khoshroo and Rostami [32, 185] studies revealed that in case of FBK film on GC or Au substrate the blocking action increased with increasing the modification time. In the present study, we also used different modification conditions (i.e. by applying 10 potential cycles beside the one cycle and furthermore, for the third modification procedure the electrode was held 10 min at a constant potential in order to improve the compactness of the aryl film) with all three diazonium salts and with both substrates (GC and Au) in order to further investigate the blocking effect. The slowing down of the electron-transfer kinetics was more evident by increasing the number of potential cycles during the electrografting of both, GC and Au surfaces. The electrochemical response of the $Fe(CN)_6^{3-/4-}$ probe was strongly suppressed (the CV peaks were not discernible, see Figures 11a,c,e) by applying modification Procedures (2) and (3) in case of GC electrodes. Therefore, the electrochemical data for the $Fe(CN)_6^{3-/4-}$ couple using CV could not be determined in order to characterise their barrier properties. Also, using a longer modification program in case of Au electrodes, the blocking effect was found to be somewhat stronger (see Figures 11b,d,f), indicating that the electrode surface is better-covered with aryl layers as it was also clearly evidenced by AFM study described above. However, the shape of CV was still rather sigmoidal in case of Au/FBK3 electrodes (see Figure 11f) compared to GC/FBK3 electrodes, where the electrochemical response of the $Fe(CN)_6^{3-/4-}$ couple was completely blocked (Figure 11e). The differences between the electrochemical behaviour of AB-modified electrode and for instance FBK-modified electrode could be explained on the basis of the structure of aryl layers. Apparently, the azobenzene groups are more closely packed than FBK groups and this provides better blocking action. From these results we may conclude that the use of subsequent cycles and increasing the duration of the grafting procedure would result in larger aryl film thickness (as was seen in case of Au electrodes by ellipsometry and AFM, Table 3) and more compact film.

In addition to the CV experiments, the RDE method was employed for aryl-modified GC electrodes to investigate the blocking action towards the $Fe(CN)_6^{3-/4-}$ redox couple in the potential range between 0.6 and –0.6 V. The corresponding RDE voltammetry curves are presented in Figure 12. Similar tendency was observed for all aryl grafted electrodes using the same modification procedure. For instance, using Procedure (3), AB, GBC as well as FBK-modified GC electrodes remarkably suppressed the reduction current. Meanwhile, the $Fe(CN)_6^{3-}$ reduction behaviour of GC/AB, GC/GBC and

GC/FBK electrodes by applying Procedure (1) differs notably as compared to the above mentioned electrodes. It can be seen that in case of GC/AB1 electrode (see Figure 12a), the reduction current is more suppressed than on GBC- and FBK-modified GC electrodes electrografted by the same procedure. However, using multiple cycles in the grafting procedure, a significant effect on the current values and on the blocking action was observed similarly to CV results.

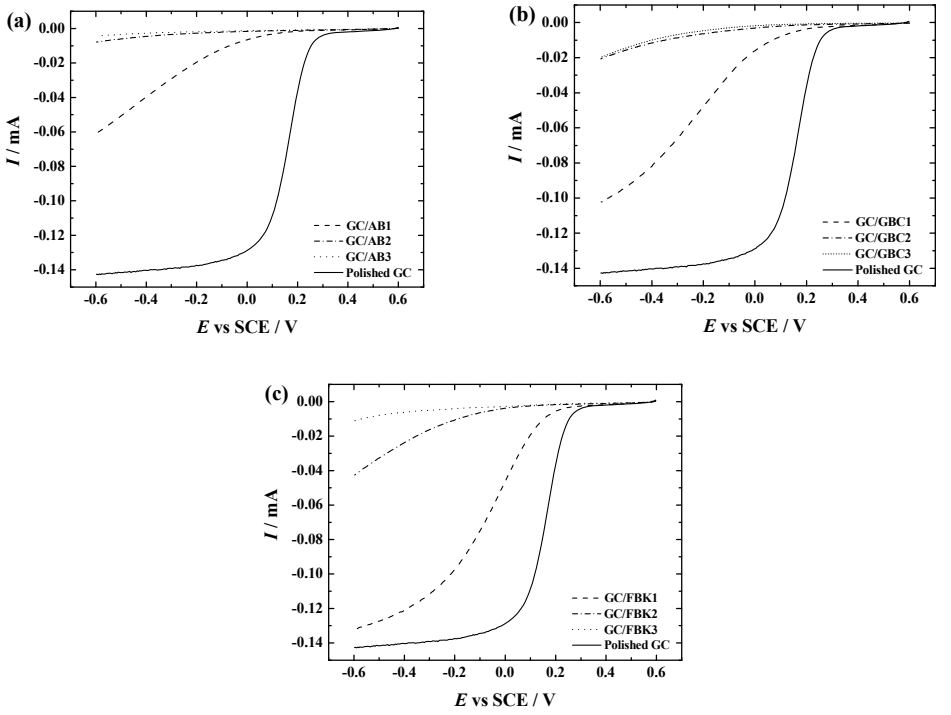

Figure 12. RDE voltammetry curves for $Fe(CN)_6^{3-}$ reduction on polished and aryl–modified GC electrodes recorded in Ar–saturated 0.1 M K_2SO_4 solution containing 1 mM $K_3Fe(CN)_6$: (a) GC/AB, (b) GC/GBC and (c) GC/FBK. $\omega = 1900$ rpm, $v = 20$ mV s^{-1}.

In addition, from the RDE data (Figure 12), the half-wave potential ($E_{1/2}$) of $Fe(CN)_6^{3-}$ reduction on polished and aryl-modified GC electrodes was calculated. The $E_{1/2}$ value for a polished GC electrode was found to be 0.16 V. In case of aryl-modified electrodes, the value of $E_{1/2}$ shifted to more negative potentials compared to polished GC which additionally refers to the inhibition of the ET rate.

To further characterise the compactness of the formed aryl layers on Au substrate and to obtain more information about the electron-transfer kinetics, the electrochemical impedance spectroscopy (EIS) was used. The EIS experiments were conducted at open circuit potential (OCP), which was 0.31 V for bare and electrografted Au electrodes in the presence of 1 mM $K_3Fe(CN)_6$. Figure 13

shows the impedance plots (Nyquist diagram) of the bare Au, Au/GBC2 and Au/FBK2 electrodes.

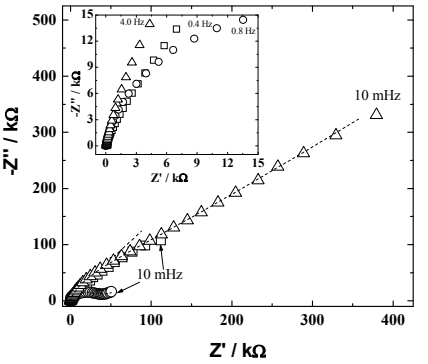

Figure 13. Impedance plane plots for bare Au (□), Au/GBC2 (○) and Au/FBK2 (△) electrodes in N_2-saturated 0.1 M K_2SO_4 solution containing 1 mM $K_3Fe(CN)_6$. Potential perturbation: 25 mV (rms). Frequency range: 100 kHz–10 mHz. Constant potential for EIS acquisition: OCP (0.31 V vs. SCE on average). Lines represent spectra (adjusted) calculated using a non-linear least-squares program, conforming to the equivalent circuit $R_s[C_{dl}(R_{ct}Q_{lf})]$, or $R_s[Q_{dl}(R_{ct}Q_{lf})]$. Calculated average values: R_s = 50 Ω, Q_{dl} = 6 μF s^{n-1}, n = 0.9, and Q_{lf} = 36 μF, n = 0.45. Inset: Impedance plane plots in the main graph restricted to 15 kΩ.

These complex plane impedance plots combine the regions of mass transfer and kinetic control at low and high frequencies, respectively [167]. When the electrochemical system is kinetically sluggish, large charge transfer resistance (R_{ct}) values are found within a well-defined semicircular region, displaying a limited frequency range in which mass transfer is a significant factor [167] (see curve ○ in Figure 13). When R_{ct} is small, the system is kinetically so facile that mass transfer always plays a role, and the semicircular region is not well defined [167] (see curve □ in Figure 13).

The simplest equivalent circuit of an electrochemical cell is a Randles equivalent circuit composed of resistors and capacitors [167]. This type of equivalent circuit was used in the present study and perfectly fitted the EIS results obtained (see the lines on the EIS curves in Figure 13). The equivalent circuit employed can be represented as $R_s[C_{dl}(R_{ct}Q_{lf})]$, or $R_s[Q_{dl}(R_{ct}Q_{lf})]$, where R_s stands for the solution resistance, Q_{dl} for the constant phase element involving an n exponent to represent C_{dl} (double layer capacitance), and Q_{lf} for a constant phase element at the low-frequency limits.

The results obtained at OCP are given in Table 5 (see also previous papers [183, 186, 187] for the assumed conditions to obtain EIS results).

Table 5. Approximate R_{ct} and k^o (or $k_{app}{}^o$) values obtained from non-linear least-squares calculations for elements of the equivalent circuit $R_s[C_{dl}(R_{ct}Q_{lf})]$, or $R_s[Q_{dl}(R_{ct}Q_{lf})]$, adjusted for EIS responses (Figure 13) provided by bare Au and Au surfaces electrografted with GBC and FBK, in N_2-saturated 0.1 M K_2SO_4 solution containing 1 mM $K_3Fe(CN)_6$.

Electrode	R_{ct} (kΩ)	k^o (or $k_{app}{}^o$)* (cm $s^{-1} \times 10^5$)
Bare Au	0.1	1700
Au/GBC2	24	7
Au/FBK2	72.6	2

*k^o (or $k_{app}{}^o$) values were obtained from R_{ct} as described in Refs. [183, 186, 187].

In order to calculate the standard heterogenous rate constant (k^o or $k_{app}{}^o$), the following equation (4) (for one-electron transfers) was used:

$$k^\circ \text{ (or } k_{app}{}^\circ) = \frac{RT}{F^2 R_{ct} A C} \quad (4)$$

where R is the universal gas constant, T is the absolute temperature, F is the Faraday constant, A is the electrode area and C is the concentration of species in the solution. From Table 5 it can be seen that the k^o (or $k_{app}{}^o$) = 0.017 cm s^{-1} was determined for bare Au which is slightly higher compared with the result (0.011 cm s^{-1}) obtained by Laforgue *et al*. [75]. Furthermore, the calculated charge transfer rates were 243 and 850 times lower ($k_{app}{}^o$ approaches 0.00007 and 0.00002 cm s^{-1}) for GBC- and FBK-modified Au electrodes, respectively, compared with bare Au, thereby showing that modification decreased drastically the charge transfer to the $Fe(CN)_6^{3-}$ probe at OCP. This behaviour is in good agreement with CV responses presented in Figures 11d,f.

The R_{ct} value obtained for bare Au (Table 5) is close to the value reported by Khoshroo and Rostami [32] and Laforgue *et al*. [75]. Also, the R_{ct} values obtained for Au/GBC2 and Au/FBK2 electrodes are close to the values reported by Khoshroo and Rostami [32]. It should be noted that we mainly compared the R_{ct} value of Au/FBK2 with that of the Au/FBK electrode obtained by Khoshroo and Rostami [32], where the Au electrode was modified in ACN or aqueous solution containing 5 mM of Fast Black K salt and electrografting was performed during 270 s at a fixed potential and with R_{ct} values obtained by Venarusso *et al*. [183] for anthraquinone-modified GC electrodes. The data given in Table 5 clearly show that the charge-transfer resistance (R_{ct}) increases with the modification of the Au surface with GBC (24 kΩ) and FBK (72.6 kΩ) layers compared to bare Au (0.1 kΩ).

It appears that the FBK film is less compact or presents more pinholes than the film of GBC, because the complex plane impedance plot presents an extended region of mass transfer (see curve △ in comparison with curve ○ in Figure 13). This can be inferred by comparing the structures of diazonium

compounds, Fast Black K and Fast Garnet GBC (see Scheme 3). See also in the next section that the blocking effect on oxygen reduction is slower on an Au surface electrografted with FBK, which results in high penetration of oxygen through this film.

On the basis of these results, the best blocking properties were obtained with AB-modified GC and Au electrodes. Moreover, we may assume that the defects are absent (at least the $Fe(CN)_6^{3-}$ ions cannot penetrate the aryl-film) in case of AB film electrografted on both (GC and Au) surfaces using a longer deposition time during electrografting because the electrochemical response of ferricyanide reduction was suppressed. Furthermore, interesting findings were obtained with GBC- and FBK-modified Au electrodes. To be more specific, the GBC films on Au electrodes are more compact inhibiting the CV response of the ferricyanide redox probe more than FBK films.

6.2.4. Oxygen reduction on AB-, GBC- and FBK-modified GC and Au electrodes

An effort has been made to study the reduction of oxygen on the GC and Au electrodes electrografted with AB, GBC and FBK groups. These experiments were performed in O_2–saturated 0.1 M KOH and two methods were employed: LSV and RDE techniques.

In earlier reports, the O_2 reduction has been widely studied for unmodified GC [121, 188, 189] and polycrystalline Au electrodes [104, 190–193].

First, the reduction of oxygen on bare and AB-, GBC- and FBK-modified GC electrodes is described. The corresponding LSV curves for bare and aryl-modified GC electrodes are shown in Figure 14, whereas the RDE voltammetry curves of GC electrodes electrografted with AB, GBC and FBK groups are shown in Figure 15. In addition, Figure 16 shows the comparative RDE voltammetry curves for polished and aryl-modified GC electrodes.

As can be seen from Figure 14, the O_2 reduction wave on bare GC starts at ca –0.2 V with a peak appearing at –0.4 V and at more negative potentials (~ –0.9 V) a second peak is observed when LSV is employed. As can be seen in Figure 16, the pre–wave at –0.5 V for unmodified GC was in evidence and the reduction wave started at ca –0.25 V when the RDE method was employed. Both, LSV and RDE results for bare GC electrodes are in good accordance with previous reports [121, 188, 189]. It has been claimed that the first O_2 reduction peak with a larger current can be associated with quinone-type centres which are present on the surface of polished GC [53, 54, 132, 194, 195]. These groups are active in the solutions of high pH [132]. At lower potentials (approximately at –0.9 V), the process of oxygen reduction is catalysed by other type of centres, however their nature is not clearly understood. It is known that the reduction of O_2 on bare GC electrodes proceeds by a two-electron pathway [53, 54].

Only some reports have been published in which the reduction of oxygen has been studied on azobenzene-modified electrodes. According to the results

reported by Šljukić *et al*. [128], the optimum pH for electrocatalysis of oxygen reduction on azobenzene- and FBK- modified GC electrodes is 2. In the latter study, the authors used the solvent evaporation method to modify the GC electrodes with azobenzene and FBK groups. The reduction of oxygen was studied in acid media (phosphate buffer solution at pH=2) and an electrocatalytic effect for modified electrodes compared to polished GC was observed [128]. Forti *et al*. [196] studied the azobenzene redox reactions on GC electrode in 0.1 M dimethylformamide and $NaClO_4$ solution (pH 7) containing 60 mM of azobenzene. They proposed that the reduction peak at –0.79 V (vs. Ag/AgCl) corresponds to the reduction of azobenzene to hydrazobenzene. They also studied the reduction of oxygen in the same solution using CV and a remarkable increase in the peak current was observed compared to the results without azobenzene, which also refers to the electrocatalytic effect in the presence of azobenzene [196].

Interesting LSV results of O_2 reduction were obtained in this study as can be seen in Figures 14a–c. In contrast to polished GC, all aryl–modified electrodes were rather inactive towards oxygen reduction in alkaline solution. The first peak shifted to more negative potentials and the E_p values were as follows: –0.51, –0.47 and –0.46 V for the AB, GBC and FBK modified electrodes, respectively using the modification Procedure (1). Some differences were observed depending on the diazonium salt and modification procedure used. For instance, the second peak was also shifted to more negative potentials for GC/AB electrodes (see Figure 14a). In case of GC/GBC and GC/FBK, the second peak was rarely observed (Figures 14b,c). Using different modification procedures, notable differences were not observed in case of GC/AB. However, the LSV behaviour of GC/GBC and GC/FBK electrodes in the presence of oxygen indicated that the blocking action depends greatly on the modification procedure. In order to evaluate the degree of blocking action, the parameter I_{rel} was used in case of the short modification program (Procedure (1)). Hence, the I_{rel} of the AB, GBC and FBK modified electrodes was estimated as 65%, 72% and 64%, respectively.

Similarly to LSV results, notable differences were observed for the GBC and FBK modified electrodes compared to the attached AB film while the RDE method was employed (see Figures 15a–c).

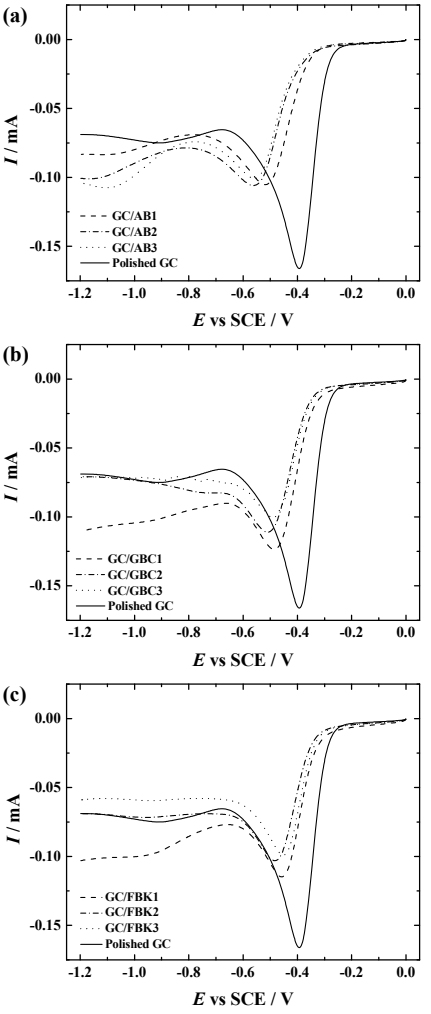

Figure 14. Linear sweep voltammograms for oxygen reduction in O_2–saturated 0.1 M KOH at a sweep rate of 100 mV s^{-1} on polished and aryl–modified GC electrodes: (a) GC/AB, (b) GC/GBC and (c) GC/FBK.

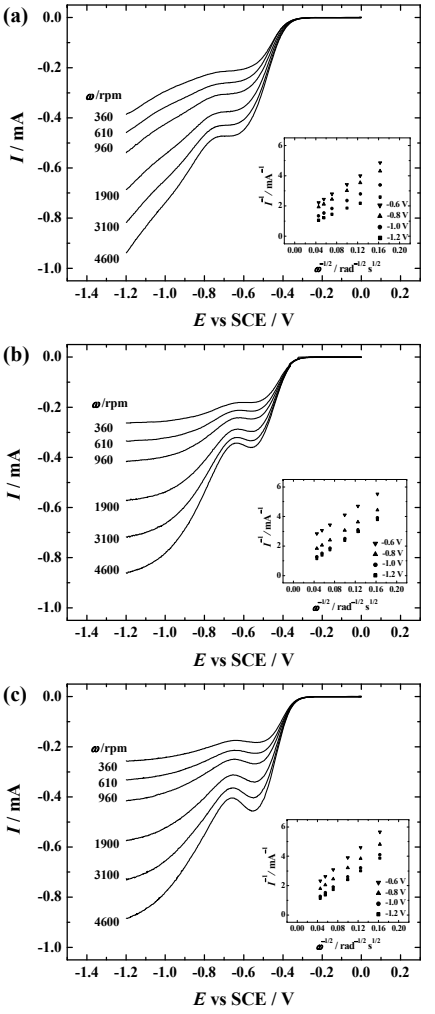

Figure 15. RDE voltammetry curves of oxygen reduction in O_2–saturated 0.1 M KOH at various rotation rates and using a sweep rate of 20 mV s^{-1}. The GC electrodes were modified with: (a) AB, (b) GBC and (c) FBK groups. In all cases, the modification Procedure (3) was used. The insets show the Koutecky-Levich plots for oxygen reduction at different potentials.

The most different behaviour was observed for GC/AB modified electrodes. For GC/AB electrodes, the pre-wave started at more negative potentials compared to other electrografted and polished GC electrodes (see Figure 16).

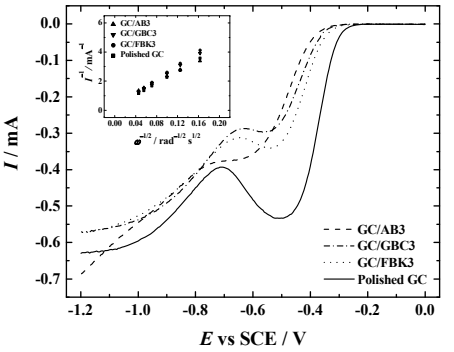

Figure 16. RDE voltammetry curves of oxygen reduction on GC/AB, GC/GBC, GC/FBK and polished GC electrodes. ω = 1900 rpm, v = 20 mV s^{-1}. The GC electrodes were modified using Procedure (3). Inset shows the dependence of I^{-1} on $\omega^{-1/2}$ for O_2 reduction in 0.1 M KOH at –1.0 V.

Also, the first reduction peak shifted negative and it was more suppressed. Surprisingly, the current values of the second reduction wave increased for this particular electrode compared to polished GC (Figure 16). Further work is needed in order to explain the reduction current increase at these more negative potentials. The onset potential of oxygen reduction shifted by up to 50 mV to more negative potentials for the GC electrodes modified with different azobenzene derivatives (see Figure 16) compared to polished GC. In case of modified GC electrodes, the pre-wave was not strongly suppressed indicating that the GC surface is not completely covered with aryl groups. However, it is difficult to estimate the uncovered area. To a certain extent, the native quinone groups are still blocked by the AB, GBC and FBK films. Recently, it has been proposed that the aryl radical formed by diazonium reduction can react with carbonyl groups [197]. This might be an alternative explanation for a decrease in the O_2 reduction current at pre-wave potentials, besides steric hindrance caused by an aryl layer.

Subsequently, the Koutecky–Levich (K-L) analysis (dependence of $I^{-1/2}$ on $\omega^{-1/2}$) was made using the following equation (5):

$$\frac{1}{I} = \frac{1}{I_k} + \frac{1}{I_d} = -\frac{1}{nFAkC^b_{O_2}} - \frac{1}{0.62nFAD^{2/3}_{O_2}v^{-1/6}C^b_{O_2}\omega^{1/2}} \qquad (5)$$

where I is the measured current, I_k and I_d are the kinetic and diffusion–limited currents, respectively, n is the number of electrons exchanged, F is the Faraday constant (96485 C mol^{-1}), A is the geometric electrode area, k is the electrochemical rate constant for O_2 reduction, $C^b_{O_2}$ is the concentration of oxygen in bulk (1.2×10^{-6} mol cm^{-3} [198]), D_{O_2} is the diffusion coefficient of

oxygen (1.9×10^{-5} cm^2 s^{-1} [198]), v is the kinematic viscosity of the solution (0.01 cm^2 s^{-1} [171]) and ω is the electrode rotation rate. According to these K-L plots (see Figures 15a-c insets), the process of oxygen reduction is under the mixed kinetic–diffusion control. The number of electrons transferred per O_2 molecule was calculated from the K–L plots. As discussed above, the reduction of oxygen follows a two–electron pathway on polished GC electrodes in alkaline solutions. In the same way, the value of n was close to two for GBC and FBK electrografted electrodes using different modification procedures. This indicates that on these electrodes the reduction of O_2 yields hydrogen peroxide as the final product. By contrast, for AB modified electrodes, the number of electrons was close to two at the pre-wave potentials, but it increased at higher negative potentials (the value of n was close to three at –1.2 V). At this stage of work it is not clear what could be the reason for the reduction current increase at these potentials.

It is well-known that a bare polycrystalline Au electrode is an active electrocatalyst for oxygen reduction in alkaline media [104, 190–193]. To be more specific, the oxygen reduction peak on bare Au electrode appeared already at ca –0.2 V (in case of LSV method, see Figure 17) or ca –0.35 V (in case of RDE method, see Figure 18). These observations are similar to that reported in the literature [192, 193]. In addition, Figure 17 displays the LSV curves of oxygen reduction on AB, GBC and FBK grafted Au electrodes using the modification Procedure (2). It was found that the cathodic peak shifted to more negative values as compared to that of bare Au for all aryl-modified electrodes and the peak currents decreased indicating that the blocking effect is obvious.

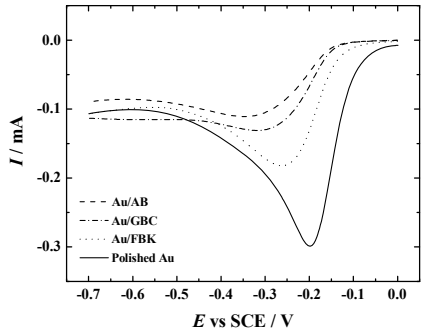

Figure 17. Linear sweep voltammograms of O_2 reduction on Au/AB, Au/GBC and Au/FBK electrodes in O_2-saturated 0.1 M KOH solution at 100 mV s^{-1}. All the aryl-modified Au electrodes were electrografted using the modification Procedure (2).

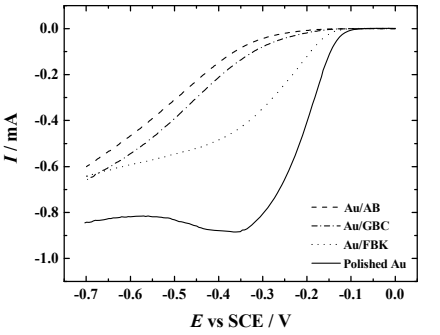

Figure 18. Comparison of the RDE voltammetry curves for oxygen reduction on Au/AB, Au/GBC and Au/FBK electrodes. Modification Procedure (1) was used. The measurements were carried out in O_2-saturated 0.1 M KOH. ω = 1900 rpm, v = 20 mV s^{-1}.

Once again, in order to evaluate the best blocking action amongst the aryl films, the parameter of I_{rel} was used. From these results, the I_{rel} for Au/AB, Au/GBC and Au/FBK was as follows: 35%, 42% and 57%. It can be assumed that due to the different structures of the surface modifiers used, the cathodic peak locations were also somewhat different. However, using different modification procedures, the cathodic peak location was almost constant, but peak currents were somewhat different (data not shown). The typical trend was that increasing the modification program, the reduction currents decreased. Still, the blocking action was not strong enough to completely suppress the oxygen reduction wave.

Another evidence for the blocking action was provided by the RDE method. Figure 18 compares the RDE voltammetry curves for oxygen reduction on polished and various aryl-modified Au electrodes at a rotation rate of 1900 rpm. For a change, the data for AB, GBC and FBK electrodes electrografted using the modification Procedure (1) are given. Similar behavioural tendencies were observed compared to LSV measurements (see Figure 17). In more specific, the blocking properties towards oxygen reduction increased as follows: Au/FBK, Au/GBC and Au/AB. This electrochemical behaviour resembles the results obtained for aryl-modified GC substrates as stated above. However, the blocking effect of the modifier films towards O_2 reduction was higher using Au as a substrate (compare Figure 18 to Figure 16). Presumably, it is due to the differences between concentrations of diazonium salts used for surface modification (as mentioned in section 6.2.3).

Figure 19 illustrates the representative current-potential curves for O_2 reduction on Au/AB electrodes at various rotation rates. The data are given for the modification by Procedure (2).

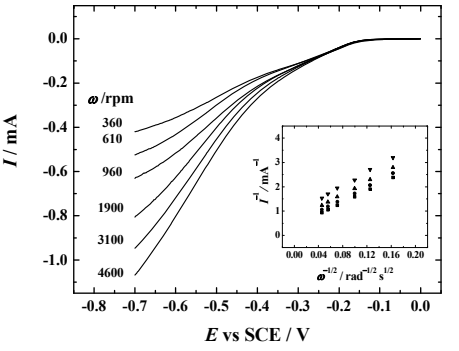

Figure 19. RDE voltammetry curves for oxygen reduction on AB-modified Au electrode in O_2-saturated 0.1 M KOH. v = 20 mV s^{-1}. The inset shows the K-L plots for oxygen reduction at different potentials. The modification Procedure (2) was used.

The inset in Figure 19 shows the K-L plots derived from the RDE data. From the K-L plots it can be concluded that the process is under the mixed kinetic diffusion control (similarly as reported for GC/AB electrodes). Identical experiments were carried out with the other azobenzene derivatives and the behavioural tendencies were rather similar (data not shown). In addition, the number of electrons transferred per O_2 molecule was calculated using the K-L equation (5). It is known that on the polished Au electrode, the *n* value is higher than two [192]. In this study, at more negative potentials, the value of *n* gradually increased indicating further reduction of H_2O_2.

Based on these experimental results described in Section 6.2.3 and 6.2.4, we may conclude that notable differences were found between the electrochemical behaviour of the modified GC and Au electrodes towards the $Fe(CN)_6^{3-}$ probe and oxygen reduction. This might be caused by differences in the hydrophilic/hydrophobic properties of aryl films and reacting species. O_2 molecule is hydrophobic and can therefore easily penetrate the aryl films studied. One should also note a difference in size between the $Fe(CN)_6^{3-}$ ion and O_2 molecule, which might affect their penetration through the aryl films.

6.2.5. GBC and FBK film degradation on GC and Au by OH• radicals

While aryl layers on GC and Au electrodes inhibited the electrochemical response of redox system, it was of special interest to see whether it is possible to degrade the aryl films by $OH^•$ radicals. In order to do that, the $OH^•$ radicals were generated by UV photolysis of H_2O_2. The degradation of GBC and FBK films on GC or Au electrodes was studied electrochemically on the basis of the response towards the $Fe(CN)_6^{4-}$ probe. In addition, XPS and AFM were used in case of GBC- and FBK-modified Au electrodes.

As the first step, GC and Au electrodes were electrografted with GBC and FBK layers similarly as described in Section 6.2.1. Briefly, the attachment of GBC and FBK groups to the GC and Au electrodes was carried out in Ar-saturated ACN containing the corresponding diazonium salts (GC: 1 mM, Au: 3 mM) and 0.1 M $TBABF_4$ as a base electrolyte. The electrochemical grafting was performed between 0.6 and –0.4 V for 10 potential cycles ($v = 100$ mV s^{-1}). The modification cycles for GC and Au electrodes were similar as previously shown (see Figures 7c,e and 7d,f). While only one modification procedure was used, the aryl-modified GC and Au electrodes are designated in this section as: GC/GBC, GC/FBK, Au/GBC and Au/FBK.

Next, the electrochemical behaviour of aryl-modified GC and Au electrodes towards the $Fe(CN)_6^{4-}$ probe before and after $OH^•$ radicals attack was studied (see Figure 20). In order to see the degradation effect of aryl film before and after the treatment with $OH^•$ radicals, the CV curves of bare GC, Au and GBC-, FBK-modified GC and Au electrodes are given for comparison. As can be seen from Figures 20a,c, the response of the $Fe(CN)_6^{4-}$ probe for aryl-modified GC

electrodes was suppressed compared with that of bare GC, which is in good agreement with the results reported in Section 6.2.3. In contrast, the shape of CVs for aryl-modified Au electrodes was rather sigmoidal (Figures 20b,d) indicating that the aryl film on Au electrode surface contained pinholes or defects. These results are in good accordance with the results obtained in Section 6.2.3. Therefore, based on the results obtained in this thesis and reports in the literature [31, 104], we may assume that the aryl layers on GC electrodes are more closely packed compared to Au electrodes and therefore the blocking effect is stronger on the modified GC electrodes than on Au surfaces.

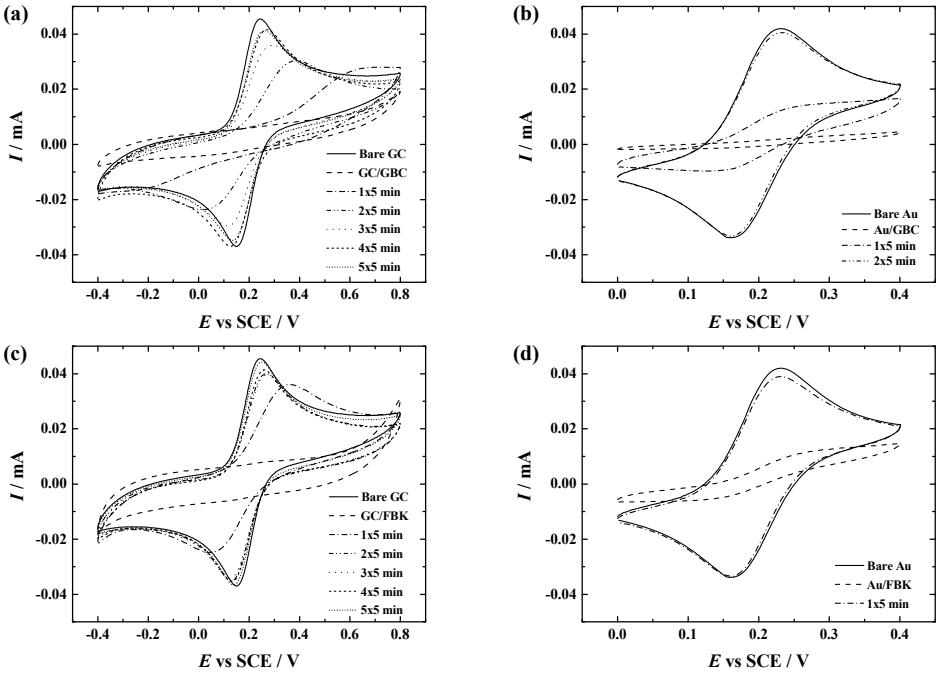

Figure 20. Cyclic voltammograms of bare and aryl-modified electrodes and after treatment with $OH^{\bullet}$ radicals for various time periods: (a) GC/GBC, (b) Au/GBC, (c) GC/FBK and (d) Au/FBK electrodes in N_2-saturated 0.1 M K_2SO_4 containing 1 mM $K_4Fe(CN)_6$. ν=100 mV s^{-1}.

Following that, the GBC- and FBK-modified GC and Au electrodes were treated with $OH^{\bullet}$ radicals *via* the combination of H_2O_2 and UV irradiation. First, 10% H_2O_2 solution and the UV treatment time of 1 min were used. It should be noted that while the effect of a 1 min treatment was very small, in further experiments the treatment time up to 5 min at a time was used. As seen in Figure 20, the 5 min treatments were repeated as long as a similar CV of bare GC or Au electrodes was obtained. For the GC/GBC and GC/FBK electrodes, the total H_2O_2/UV treatment time was 25 min and then the electrochemical

behaviour was rather similar to that of unmodified GC. Meanwhile, only 10 and 5 min of H_2O_2/UV treatment was enough to degrade the GBC and FBK layers from Au electrodes, respectively. In an earlier work [31], it has been found that the stability of aryl layers (4-sulphophenyl) is higher on carbon surfaces compared to gold surface. This could be one reason why the degradation of aryl layer was faster on Au surface than on GC surface.

By comparing the degradation process on aryl-modified GC electrodes (Figures 20a,c) with Au electrodes (Figures 20b,d), an interesting electrochemical behaviour was observed. In case of aryl-modified GC electrodes, after each treatment with $OH^{\bullet}$ radicals, the CV response returned, accompanied by an increasing electrochemical reversibility which was verified by the decrease of the ΔEp. For instance, the ΔEp values for GC/GBC electrodes were estimated as 0.32 V and 0.12 V, after 10 and 25 min treatment time, respectively. The CVs exhibited the typical response of planar infinite diffusion [199]. It is evident that multilayer films were formed during the electrografting process and the aryl layers were gradually removed by $OH^{\bullet}$ radical attack. Therefore we may conclude that in case of the aryl layers on GC, the aryl-film degradation by $OH^{\bullet}$ radicals leads to a thinning (decreasing thickness) of the film without pinhole formation. The continuous thinning of the aryl layer improved the electrochemical reversibility of $Fe(CN)_6^{4-}$, practically shifting from complete irreversibility to an almost complete regain of reversibility. This behaviour strongly reminds of the effect of alkyl chain length of SAMs on the reversibility of dissolved redox probes [200], and corroborates the interpretation that the $OH^{\bullet}$ radicals are thinning the film. In contrast to GC electrodes, the shape of CVs of aryl-modified Au electrodes before and after the H_2O_2/UV treatment (Figures 20b,d) exhibited the sigmoidal response. This electrochemical behaviour is typical for microelectrode arrays and an electrochemically reversible couple. The microelectrode behaviour taken together with the full electrochemical reversibility of $Fe(CN)_6^{4-}$ can be explained by the formation of pinholes in the film which act as microelectrodes. For instance, mixed SAMs on gold have shown a typical behaviour of microelectrode arrays [201].

To obtain more information about the degradation process, the elemental composition of aryl films before and after $OH^{\bullet}$ radical attack was investigated for the Au/GBC and Au/FBK electrodes by XPS (Figure 21).

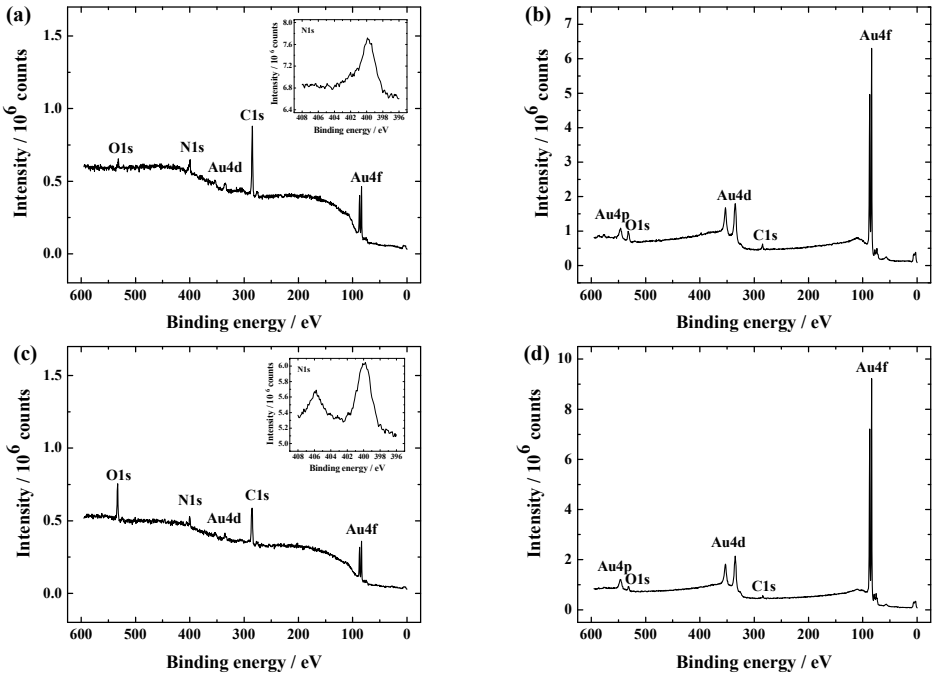

Figure 21. XPS spectra for: (a) Au/GBC, (b) Au/GBC after 10 min of H_2O_2/UV treatment, (c) Au/FBK, and (d) Au/FBK after 5 min of H_2O_2/UV treatment. The insets show the XPS spectrum in the N1s region.

First, the formation of the GBC and FBK layers on Au surface was confirmed. The survey spectrum revealed the presence of nitrogen (N1s), oxygen (O1s), carbon (C1s) and gold (Au4f, Au4d) on the electrode surface. The XPS peak at 400 eV was detected for both modifiers and it is attributed to azo groups (Figures 21a,c insets). Moreover, the attachment of FBK groups on Au electrode was further confirmed by the peak at 406 eV, which corresponds to nitro groups (Figure 21c inset). These results are in good agreement with earlier observations using different substrates [184] as well as the results obtained in Section 6.2.2. As can be seen in Figures 21b,d, no XPS peak in the N1s region was detected for GBC and FBK grafted Au electrodes after 10 and 5 min of H_2O_2/UV treatment. This indicates that after the $OH^{\bullet}$ radicals treatment for that time period, the aryl layers were degraded so much that XPS could not detect the film residue.

Figure 22 presents the AFM images of the GBC and FBK modified Au electrodes before and after the $OH^{\bullet}$ radicals attack.

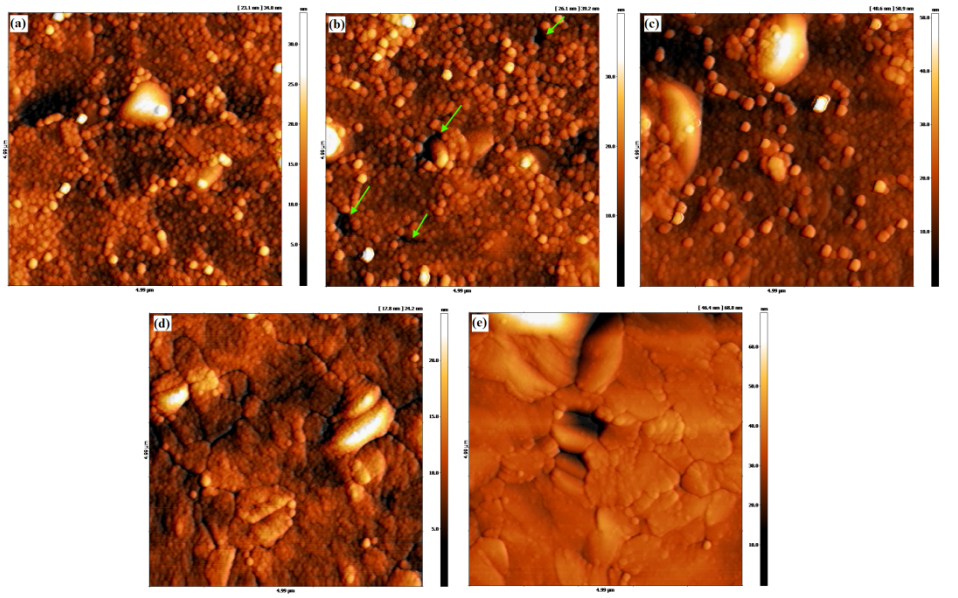

Figure 22. AFM images for Au/GBC electrodes before (a), after 5 min (b) and 10 min (c) of $OH^{\bullet}$ radicals attack. AFM micrographs for Au/FBK electrodes before (d) and after 5 min of $OH^{\bullet}$ radicals attack (e). The arrows in image (b) show the pinholes.

Figure 22a shows an AFM micrograph of a GBC covered gold surface: the GBC film has a granular structure. Figure 22b depicts the surface after 5 min of $OH^{\bullet}$ radicals attack. Small holes in the polymer are clearly detectable (see the marks). After further 5 min attack (Figure 22c) the film was obviously extremely thin and only the fact that the Au crystallites underneath could not yet be seen and some remaining grains of polymer on the surface can be taken as a proof of its existence. This explains the above mentioned XPS results. Figure 22d shows the FBK covered gold surface before $OH^{\bullet}$ radicals attack. Also, this film is rather granular, although less pronounced, and probably very thin, since the grain boundaries of the Au crystallites are still visible. With the help of AFM measurements the thickness of the formed FBK layer during modification was determined as follows: one part of an annealed gold surface was covered by a polysiloxane layer and the gold surface was modified with FBK in the described way. After the cleaning process the polysiloxane layer was removed and the thickness of the FBK layer was determined by AFM as 38 nm. Figure 3e presents the FBK film after 5 min of H_2O_2/UV treatment. The aryl film appears to be similar like the GBC film after 10 min of attack. The invisibility of the typical Au{111} triangle structures indicates that a very thin film is still present.

From these results we may conclude that the aryl films on GC and Au electrodes can be degraded by $OH^{\bullet}$ radicals. Most interestingly, the degradation of the films on these two substrates follows two different pathways: the

thickness of aryl layers on GC is decreased by $OH^{\bullet}$ and the reversibility of the dissolved redox probe $Fe(CN)_6^{4-}$ is returning, whereas the aryl film on Au shows degradation with pinhole formation, so that the electrode exhibits microelectrode behaviour and reversibility of $Fe(CN)_6^{4-}$. These observations allow assuming that treatment of blocking surface films with $OH^{\bullet}$ radicals may be a versatile tool to produce arrays of microelectrodes, and in other cases, the tuning of the reversibility of electrode systems is feasible.

6.3. Surface and electrochemical properties of AQ-modified graphene-based and HOPG electrodes

While it is known that high-quality graphene can be prepared by mechanical exfoliation of HOPG and according to our knowledge, the electrochemical grafting of CVD-grown graphene electrodes by diazonium reduction is relatively rare, the third part of this thesis involves the investigation of the electrochemical properties of bare and aryl-modified HOPG and CVD-grown graphene electrodes. First, the electrochemical behaviour of CVD graphene grown onto Ni foil with a material of similar structure (e.g. HOPG) was compared [V]. The second aim of this work was to electrochemically graft HOPG and CVD-grown graphene electrodes with thick AQ layers by diazonium reduction in order to study the electrochemical and morphological properties of AQ-modified HOPG and graphene-based electrodes [VI]. In both studies [V,VI], GC was used for comparison purposes.

6.3.1. Morphological and electrochemical properties of bare CVD-grown graphene and HOPG

Herein, a systematic study of bare CVD-grown graphene (Ni-Gra), HOPG and GC that served as reference material, is described. It should be noted, that these Ni-Gra samples were prepared in the Institute of Physics of the University of Tartu and therefore the samples are designated as “home-made” Ni-Gra.

6.3.1.1. Surface characterisation of bare CVD-grown graphene and HOPG

First, the XPS measurements of Ni foil before and after the synthesis of graphene by CVD method were performed (see Figure 23). The XPS survey spectra of Ar-purified bare Ni foil (Figure 23a) showed characteristic peaks of Ni, whereas the XPS spectra of CVD-grown graphene on Ni foil did not show any Ni peaks, only a symmetric peak at ca 284 eV was observed which corresponds to the sp^2 carbon (Figure 23b).

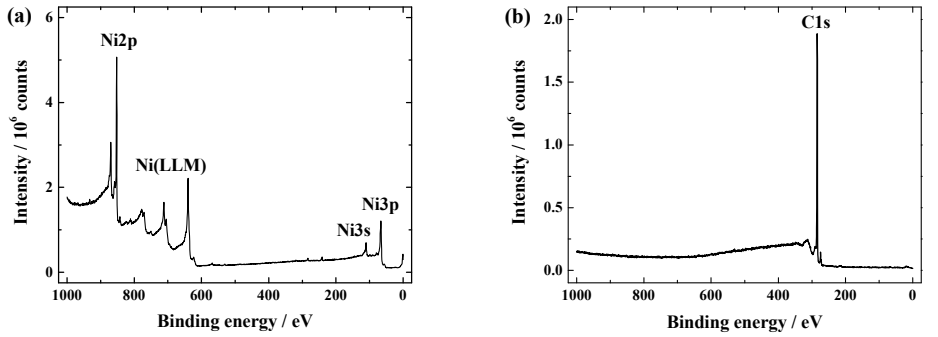

Figure 23. XPS survey spectra of (a) Ar-purified bare Ni and (b) CVD-grown graphene on Ni foil.

Figure 24 presents the Raman spectra of HOPG and CVD-grown graphene.

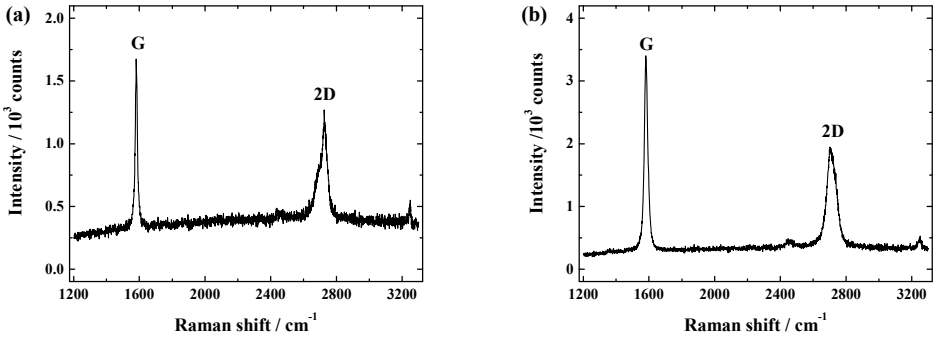

Figure 24. Raman spectra of (a) HOPG and (b) CVD-grown graphene sheet on Ni substrate.

The Raman spectra of HOPG showed a G band and a 2D band at about 1581 and 2718 cm^{-1}, respectively. Clearly, no G and 2D bands appear in the Raman spectra of bare Ni foil [202]. In this study, G band (1582 cm^{-1}) and 2D band (2711 cm^{-1}) were observed in the spectrum of the CVD-grown graphene on Ni foil (Figure 24b). These results are similar to Raman spectra of HOPG and CVD graphene films presented in Ref. [203]. The intensity of the 2D band was smaller compared with the G band (Figure 24b). According to the literature data [204], this indicates that the CVD graphene film consists more than one atomic layer of graphene, which confirms the presence of multilayer graphene.

Taking into account the Raman spectrum of CVD graphene (Figure 24b), the number of graphene layers grown on the Ni substrate was estimated to be <10. Based on the Geim and Novoselov report [205], graphene can be viewed as less than 10 layers of graphite. The absence of the D peak in the Raman spectra of CVD graphene (Figure 24b) at about 1360 cm^{-1}, which corresponds to the disorders in the graphene film, indicates that this material is almost defect-free,

well-ordered and high-quality [127, 204]. In case of HOPG (Figure 24a) the D band was also missing, which refers to the low-defect surface. This is in good accordance with the study by Pimenta *et al*. [206] who showed that on the flat HOPG surface the D band was not observed.

Next, HR-SEM studies were carried out to illustrate the morphological features of the CVD graphene film. Figure 25a exhibits a large-area HR-SEM image of graphene layers that were grown by the CVD method onto Ni foil. In closer look (Figure 25b), characteristic folds and wrinkles of the graphene layers on Ni foil were observed, whereas defects within the film were rarely visible, which is in accordance with the results of Raman spectroscopy (Figure 24b).

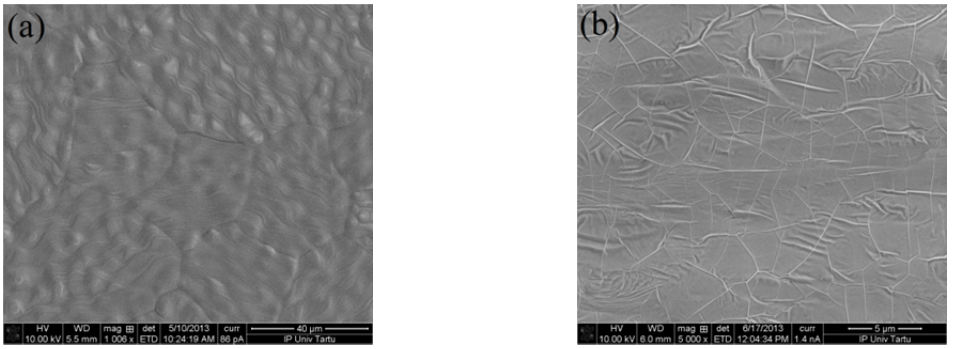

Figure 25. HR-SEM micrographs of "home-made" Ni-Gra. Scale bar: (a) 40 μm and (b) 5 μm.

AFM measurements were performed to compare the surface morphology of HOPG and CVD graphene (Figures 26a,b). In case of CVD graphene (Figure 26b), the folds and wrinkles are still visible as is also seen in SEM images. These folds and wrinkles cause an increase in the real surface area (A_r) over the geometric area. The A_r/A ratio is larger for CVD graphene than for HOPG surface (compare the height scales in Figures 26a,b).

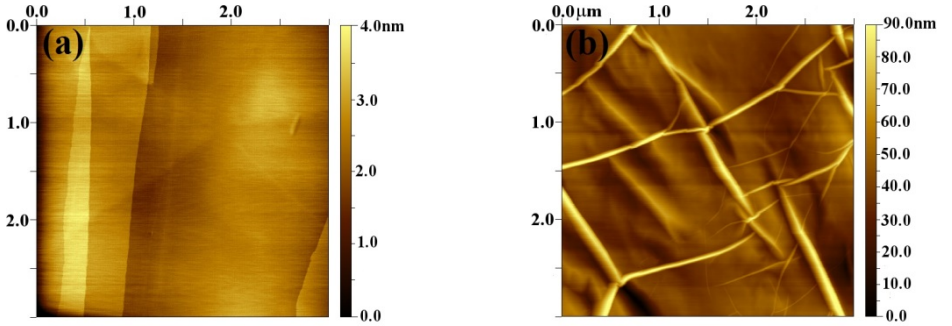

Figure 26. AFM images of (a) HOPG substrate and (b) "home-made" Ni-Gra.

6.3.1.2. Electrochemical characterisation of bare CVD-grown graphene and HOPG electrodes

Ambrosi *et al*. [202] described an easy electrochemical way of evaluating the quality of CVD-grown graphene. Specifically, this method utilises the inherent electrochemical signals of exposed sites of the underlying metal catalysts (i.e., Ni and Cu), when fractures or discontinuities of the graphene film are present [202]. Figure 27 compares the CV behaviour of Ni substrate and CVD-grown graphene in Ar-saturated 0.1 M KOH. The results obtained are similar to that reported by Ambrosi *et al*. [202]. They have studied the electrochemical behaviour of bare Ni foil and CVD graphene grown onto the Ni foil in 0.1 M NaOH in the potential range of –0.5 to 0.8 V vs. Ag/AgCl. The authors revealed that the Ni foil covered with multilayer graphene film showed extremely low redox signal generated by $Ni(OH)_2$ compared with bare Ni, indicating that the Ni foil was covered with graphene film although some holes might be present [202].

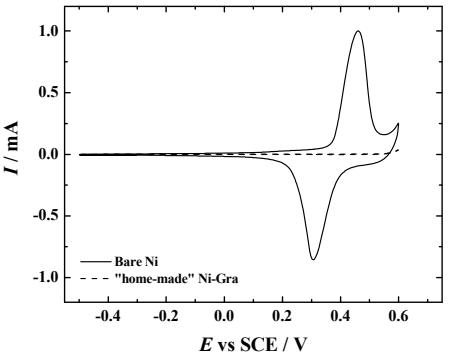

Figure 27. CV curves for bare Ni and "home-made" Ni-Gra electrodes recorded in Ar-saturated 0.1 M KOH (10th cycles are shown). $v = 100$ mV s^{-1}.

In the current study, a rather small Ni signal was observed for the CVD-grown graphene sample (Figure 27), which indicates that the underlying Ni substrate is covered with graphene sheet but some holes are still present.

In the following step, the electrochemical properties of the CVD-grown graphene were investigated using the ferricyanide probe. For comparative purposes, electrochemical testing with bare GC and HOPG electrodes was also performed. Figure 28 shows CVs of the GC, HOPG and CVD graphene electrodes registered in Ar-saturated 0.1 M K_2SO_4 solution containing 1 mM $K_3Fe(CN)_6$ at a scan rate of 100 mV s^{-1}. As mentioned before in sections 6.1.3 and 6.2.3 the peak-to-peak separation increases with decreasing the ET rate [199]. The electrochemical behaviour towards the $Fe(CN)_6^{3-/4-}$ redox probe shows that the electron transfer kinetics on HOPG and CVD-grown graphene is remarkably slower compared with bare GC (Figure 28). McCreery *et al*. [207]

studied the ET kinetics of various redox systems and the CV results revealed that the ET rates were also slower on basal plane HOPG than on GC. Similarly, Davies *et al*. [16] observed slower ET kinetics at basal plane HOPG compared with edge plane pyrolytic graphite. Recently, Ambrosi and Pumera [127] have demonstrated that the electrochemical behaviour towards ferricyanide reduction on multilayer graphene electrodes grown by the CVD method resembled that of basal plane graphite. Based on the above-mentioned results, it is important to note that the general electrochemical behaviour of CVD graphene film is similar to that of HOPG. It should also be mentioned that bare Ni substrate cannot be used for the CV experiments of the $Fe(CN)_6^{3-/4-}$ redox probe in neutral solution, because the oxidation potential of nickel is more negative than the redox potential of the $Fe(CN)_6^{3-/4-}$ couple [170]. No extra peaks were observed on the CV curves of the CVD graphene in Figure 28, which indicates that the area of the underlying Ni substrate exposed to solution is negligible, therefore confirming the CV results presented in Figure 27.

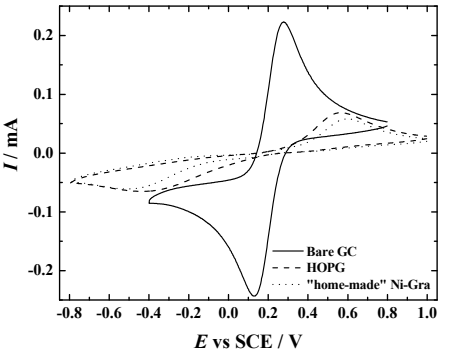

Figure 28. CVs of bare GC, HOPG and "home-made" Ni-Gra in Ar-saturated 0.1 M K_2SO_4 solution containing 1 mM $K_3Fe(CN)_6$. v = 100 mV s^{-1}.

The ORR was investigated by measuring the LSVs in O_2-saturated 0.1 M KOH at different carbon electrodes (Figure 29). In case of bare GC the oxygen reduction peaks at –0.45 and –0.9 V were observed, which is in good agreement with earlier observations shown in Section 6.2.4. On the other hand, a reduction pre-peak appeared at ca –0.5 V on HOPG, which is only 50 mV more negative compared with the first LSV peak on bare GC (Figure 29). This might be due to the fact that the reduction of oxygen on HOPG is mediated by oxygen-containing groups present on the defect sites [188]. However, as can be seen from Raman spectra (Figure 24a), these defect sites are almost missing, which confirms that we have the basal plane surface of HOPG with negligible amount of edge plane sites and therefore low density of sites for functional groups [13]. These observations are consistent with previous results using the rotating disk electrode method [208]. The pre-peak of the ORR was absent on the CVD-

graphene (Figure 29), which confirms the results of Raman spectroscopy investigations (Figure 24b). The oxygen reduction peaks for HOPG and CVD graphene appeared at approximately –0.8 and –1.1 V. This again demonstrates that the overall electrochemical behaviour for HOPG and CVD graphene is rather comparable. In general, HOPG and CVD-grown graphene electrodes were inactive compared with bare GC, which makes these substrates appropriate to study the properties of electrocatalytically active materials [208]. Furthermore, the ORR studies performed by Qu *et al*. [209] revealed that the CVD-grown graphene was a less active catalyst than commercial carbon supported Pt. Lima *et al*. [140] observed electrocatalytic effect of rGO on O_2 reduction compared with bare GC. Similar results with rGO were also obtained by Kruusenberg *et al*. [210]. This indicates that the electrocatalytic properties of rGO and the CVD-grown graphene studied in this work are remarkably different, the latter material being significantly less active for ORR than rGO.

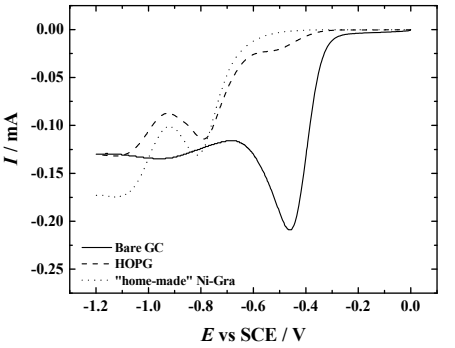

Figure 29. LSV curves for oxygen reduction at bare GC, HOPG and CVD-grown graphene in O_2-saturated 0.1 M KOH. $v = 100$ mV s^{-1}.

6.3.2. Surface and electrochemical characterisation of CVD-grown graphene and HOPG electrografted with thick anthraquinone films

In this part of the work the film formation, the electrochemical behaviour and the surface morphology of AQ-modified different carbon materials (including CVD graphene, HOPG and GC as reference substrate) is investigated. In addition to HOPG, two different sources of CVD-grown graphene are considered, i.e., commercially available Ni-Gra (graphene is synthesised by CVD method on Ni, whereas thin film of Ni itself is deposited onto silicon) and graphene synthesised by CVD on Cu foil (Cu-Gra). The Cu-Gra samples were made in Aarhus University (Denmark).

6.3.2.1. Evaluation of the quality of CVD-grown graphene

It was of special interest to see whether the quality or the nature of the commercially available Ni-Gra and Cu-Gra samples differed from the "home-made" Ni-Gra electrodes used in Section 6.3.1. First, the cyclic voltammetry was employed similarly as described in Section 6.3.1.2. As shown in Figure 30, the characteristic peaks of bare Ni are almost suppressed in case of commercially available CVD-grown graphene on Ni which is rather similar to "home-made" Ni-Gra electrode as shown in Section 6.3.1.2 (Figure 27). Also, the characteristic peaks of bare Cu are almost suppressed in case of CVD-grown graphene on Cu (see Figure 30b). In closer look (data not shown) the cyclic voltammogram of graphene (both on Ni and Cu substrate) showed an extremely low redox signals corresponding to the underlying substrate. These observations indicate that the underlying substrate is covered with graphene, although some holes might still be present [202].

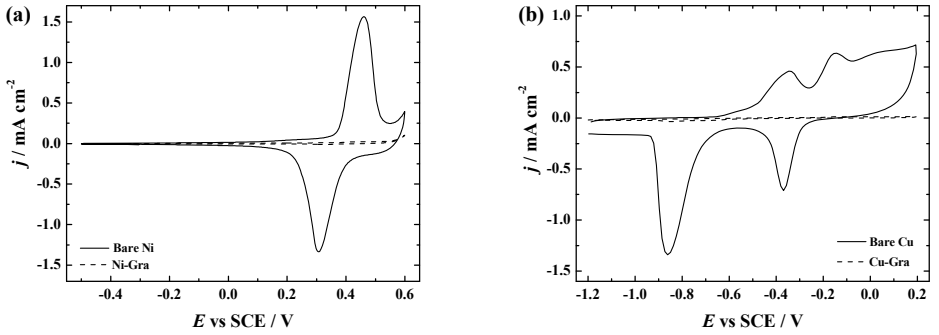

Figure 30. Cyclic voltammograms recorded in Ar-saturated 0.1 M KOH at v = 100 mV s^{-1} for (a) bare Ni and Ni-Gra and (b) bare Cu and Cu-Gra.

Also, it is important to determine whether we have mono-, few- or multilayer graphene grown by CVD. Raman spectroscopy provides useful information about the number of graphene layers as well as the presence of disorders and defects within the graphene [158, 206, 211]. According to the specification from the supplier (i.e., Graphene Supermarket) Ni-Gra is composed of patches of 1−7 layers with dimensions of 3−10 μm. This is in accordance with Raman analysis carried out by Lillethorup *et al*. [70]. With an average number of layers being 4, Ni-Gra should be considered multilayer graphene. Also, a "home-made" Ni-Gra was specified as multi-layer graphene (graphene layers were estimated to be <10) in Section 6.3.1.1.

Figure 31 shows a Raman spectrum of Cu-Gra obtained on a SiO_2/Si wafer. It should be noted that the graphene on Cu-Gra was transferred onto SiO_2/Si only for the Raman spectroscopy measurements to allow a better comparison with literature data [158]. As can be seen, the intensity ratio 2D/G is ca 2 which is expected for the monolayer graphene. However, a small D peak was also

observed from disorders or defects in the graphene which could partially expose the underlying substrate. Furthermore, Raman mapping (45×45 μm^2) of similar Cu-Gra samples showed that, primarily, monolayer graphene was present. From the results obtained we may conclude the almost 100% coverage of graphene on Cu-Gra covers the underlying substrate. However, there are some regional variations, regarding the amount of layers, which, most likely, are due to insufficient electropolishing/annealing of the Cu foil before graphene synthesis.

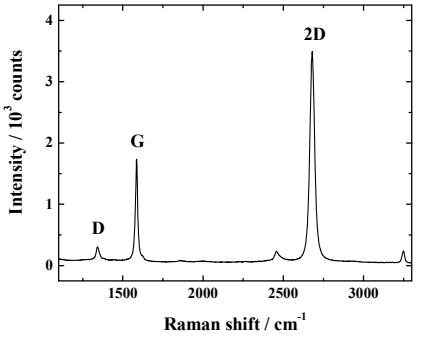

Figure 31. Raman spectrum of Cu-Gra after transferring graphene onto a SiO_2/Si wafer.

It is important to note that in case of commercially available Ni-Gra substrate (data not shown), rather small D peak in Raman spectra was observed. This is also relevant because no D peak was detected in case of "home-made" Ni-Gra (see Figure 24b). According to these observations, we might conclude that within the graphene layers, some disorders or defects might occur which may partially expose the underlying substrate surface. This was also confirmed by the electrochemical experiments stated above (see Figure 30).

It is also important to note that the Raman spectra of HOPG samples were similar to spectra already shown in Section 6.3.1.1 (see Figure 24a) with no D peak showing up). This indicates the presence of rather basal plane HOPG with a negligible amount of edge sites.

6.3.2.2. The formation of thick AQ layers onto different carbon-based electrodes

Based on the principles of redox grafting [96–98] discussed in the literature overview (Section 4.1.5.), thick conductive AQ films on GC, HOPG, Ni-Gra and Cu-Gra were prepared. First, the redox grafting of AQ moieties on GC substrate was carried out in order to see the similarities in the results reported in Refs. [96, 98]. Considering that switching potential, number of sweeps and sweep rate play a crucial role in forming the organic layer of high thickness, the redox grafting of AQD on GC was performed between 0.6 and –1.6 V for 10 cycles at a sweep rate of 1 V s^{-1} (this electrode is designated as GC/AQ). As

seen from Figure 32a, a broad peak at ca 0.2 V, assigned to the reduction of AQ diazonium compound disappeared while the current density of the redox wave at E = –0.96 V pertaining to the one-electron reduction of GC/AQ to GC/AQ$^{\bullet-}$ increased during potential cycling. The gradual increase in the latter is due to the continuous attachment of AQ groups, occurring in a mediated reduction of AQD [96–98, 212]. In general, this electrochemical behaviour is in good accordance with previous results [96].

To the best of our knowledge, the electrografting of AQ moieties on HOPG in a wide potential range has not been performed as yet. Therefore, in order to see the general electrochemical behaviour, the potential sweeping was performed from 0.6 to –2 V on HOPG (see Figure 32b inset). There is a pre-peak or shoulder on the first cycle in the potential region where the reduction of diazonium salt appears giving the aryl radical which reacts with the electrode surface. The pre-peak or shoulder has been seen earlier for other aryldiazonium salts on the basal plane of HOPG and this might be associated with reaction on the more reactive cleavage defects or the electrochemical behaviour towards aryl radical is just different compared to other materials (for instance GC or edge plane HOPG) [136]. Most likely, this can be attributed to reactions taking place at defect sites on the basal plane of HOPG. At more negative potentials, two redox waves were observed pertaining to the one-electron reduction of HOPG/AQ to HOPG/AQ$^{\bullet-}$ and the further reduction of the latter to the dianion, HOPG/AQ^{2-} [212, 213]. In addition, there is a distinct reduction peak between the two redox waves, which was not observed for GC/AQ. At this point we do not know the exact origin of this, but we speculate that it might arise from the attachment of AQ groups to the basal plane HOPG.

Based on the results reported previously [98], AQ layers of high thickness should be attainable if the switching potential of the electrografting is set before the potential of the second redox wave. For the preparation of HOPG/AQ electrodes two modification procedures with equal potential sweeping time were used: (1) 10 consecutive potential cycles recorded from 0.6 to –1.5 V at 1 V s^{-1} and (2) 20 potential cycles recorded from 0.6 to –1.5 V at v = 2 V s^{-1} (Figure 32b), to obtain HOPG/AQ1 and HOPG/AQ2, respectively. As may be noticed from Figure 32b, the diazonium reduction wave gradually diminished while the current density of the first redox wave of the AQ moiety at HOPG concomitantly increased during potential sweeping due to the continuous attachment of AQ groups by the redox catalysis effect [96–98]. Overall, this electrografting behaviour is the same as that observed for GC electrodes.

Figures 32c,d show the redox grafting of AQD on Ni-Gra and Cu-Gra, respectively, performed by potential cycling (20 cycles, v = 2 V s^{-1}). To avoid any corrosion at holes of exposed metal for the Ni-Gra and Cu-Gra electrodes, the starting potential was chosen to be 0.4 and –0.2 V, respectively. In case of Cu-Gra, the reduction peak of AQD is not observed at the starting potential, although we may assume that the aryl radical is already formed at this potential [1].

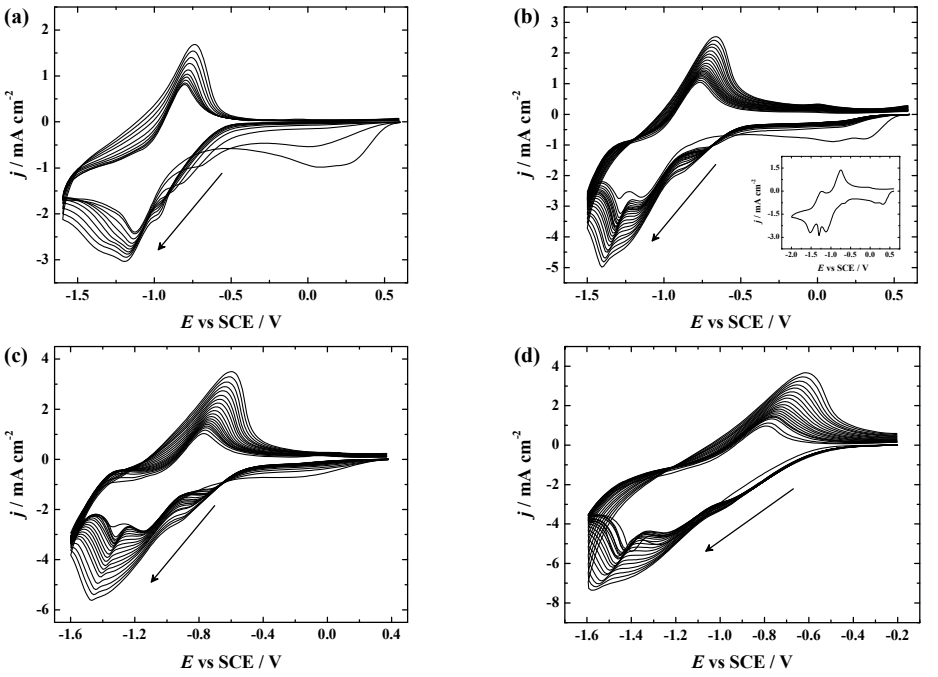

Figure 32. Redox grafting of AQ on (a) GC, (b) HOPG, (c) Ni-Gra and (d) Cu-Gra in Ar-saturated 0.1 M $TBABF_4$/ACN containing 2 mM AQD; ν = 1 V s^{-1} (a) and 2 V s^{-1} (b-d) using 10 (a) and 20 (b-d) potential cycles. In all cases, the arrow indicates the direction for increasing number of potential cycles applied during the electrografting. Inset of (b) shows the first potential cycle in a wider potential range on HOPG.

On successive potential cycles an increase in the current density of the redox wave at more negative potentials was observed for both Ni-Gra and Cu-Gra (see Figures 32c,d). This again refers to the surface-mediated reduction of the AQD as well as an increase in the number of AQ groups attached to the graphene-based electrode surfaces. As for HOPG an additional peak after the redox wave was observed at both substrates which may be attributed to the attachment of AQ groups to the basal plane surface.

6.3.2.3. Determination of surface concentration of AQ groups and film thickness

Figure 33 shows cyclic voltammograms recorded for all AQ-modified carbon electrodes in Ar-saturated 0.1 M $TBABF_4$/ACN, all exhibiting well-defined redox peaks pertaining to the AQ moieties. The surface concentration of electroactive AQ (Γ_{AQ}) on GC/AQ, HOPG/AQ, Ni-Gra/AQ, and Cu-Gra/AQ electrodes was determined electrochemically according to the equation (1) where Q is the charge consumed during the reduction of AQ to $AQ^{\bullet-}$ during the first sweep in cyclic voltammetry (obtained from an integration of the area

beneath the reduction wave) and in this case, $n = 1$. Similarly to Γ_{NP} in case of NP-modified GC electrodes (Section 6.1.1), it is important to emphasize that this measurement of Γ_{AQ} only includes electroactive AQ moieties, meaning that the real surface density could be considerably larger if the compactness of the film restricts the access of the counter ions. The availability of counter ions is a prerequisite for having electrochemical activity at all.

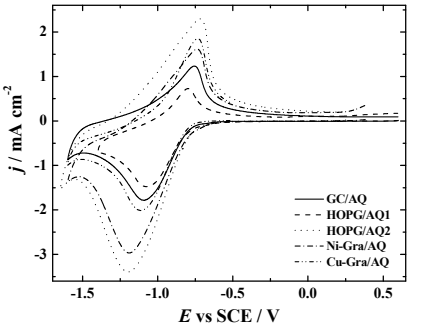

Figure 33. Cyclic voltammograms recorded in Ar-saturated 0.1 M $TBABF_4$/ACN for different carbon electrodes electrografted with AQ groups; $v = 1$ V s^{-1} for GC/AQ and HOPG/AQ1; otherwise $v = 2$ V s^{-1}.

In Table 6 the values of Γ_{AQ} are collected along with film thicknesses measured by ellipsometry or the AFM scratching method.

Table 6. Surface concentration of AQ groups (Γ_{AQ}) and thickness of AQ films on GC, HOPG, Ni-Gra and Cu-Gra.

Electrode	Γ_{AQ} (mol cm^{-2}) measured in 0.1 M $TBABF_4$/ACN	Thickness (nm)
GC/AQ[a]	4.2×10^{-9}	26.9 ± 0.9[f]
HOPG/AQ1[b]	2.1×10^{-9}	7.1 ± 0.3[f]
HOPG/AQ2[c]	9.9×10^{-9}	61.3 ± 1.2[f]; ~55[g]
Ni-Gra/AQ[d]	7.1×10^{-9}	40.7 ± 0.1[f]; ~40[g]
Cu-Gra/AQ[e]	3.5×10^{-9}	~10[g]

Modification procedures: [a] 0.6 to –1.6 V, 10 cycles, $v = 1$ V s^{-1}; [b] 0.6 to –1.5 V, 10 cycles, $v = 1$ V s^{-1}; [c] 0.6 to –1.5 V, 20 cycles, $v = 2$ V s^{-1}; [d] 0.4 to –1.6 V, 20 cycles, $v = 2$ V s^{-1}; [e] –0.2 to –1.6 V, 20 cycles, $v = 2$ V s^{-1}. [f] Measured by ellipsometry; [g] Measured by the AFM scratching technique.

First of all, it may be noted that Γ_{AQ} for GC/AQ obtained by redox grafting, involving charging and discharging of the film through scanning the potential, is ~10 times larger compared to what would generally have been obtained using

classical electrografting of AQD restricted to the potential region of the diazonium salt [53, 183, 214].

Second, Γ_{AQ} for HOPG/AQ1 is only half that for GC/AQ, although the grafting conditions were very similar. This is also reflected in the measured layer thickness which was found to be higher in case of GC/AQ compared to HOPG/AQ1 (~ 27 and 7 nm, respectively). Hence, from these results we may conclude that the electrografting of AQ proceeds more efficiently on GC compared with HOPG using similar modification procedures. The same tendency was observed earlier using NBD to modify GC and the basal plane HOPG surface with NP groups [41, 58, 66]. These results may be explained by the fact that GC has a rougher surface than HOPG and that basal plane HOPG has a negligible amount of edge sites.

Third, for HOPG/AQ2 electrodes using the same scanning time as for HOPG/AQ1 electrodes but with twice the number of cycles and twice as high a sweep rate, Γ_{AQ} and the film thickness are more than four and eight times larger, respectively, than the corresponding values for HOPG/AQ1 and they are even higher than those obtained for GC/AQ. This indicates that for a given carbon substrate the redox grafting efficiency may be enhanced by increasing the number of sweeps as well as by applying higher sweep rates [98].

Fourth, the redox grafting efficiency of AQD on Ni-Gra/AQ and Cu-Gra/AQ is smaller compared to HOPG/AQ2 with values of Γ_{AQ} and layer thicknesses being 25% and 50% lower, respectively, for the two metal-based graphene substrates. Still, the absolute values are substantial, underlining the generality of the redox catalysis approach. Furthermore, Figure 34 shows that a good correlation between Γ_{AQ} and film thickness exists. The relationship is not ideally linear as it was observed previously in case of gold surfaces redox grafted with thick AQ films [98]. However, the plot clearly confirms that thick AQ layers may be formed by redox grafting on all substrates, i.e., GC, HOPG, Ni-Gra and Cu-Gra, with almost ten times higher surface density and film thickness than in the classical diazonium grafting method.

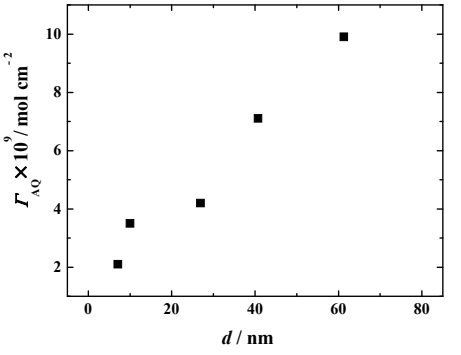

Figure 34. Relationship between the surface concentration of AQ groups, Γ_{AQ}, attached to various carbon-based electrodes and the AQ layer thickness, *d*.

6.3.2.4. Morphological studies of AQ-modified HOPG, Ni-Gra and Cu-Gra electrodes by AFM

Figure 35 shows the topographical AFM images characterising the surface morphology of the bare HOPG, Ni-Gra, and Cu-Gra along with the modified HOPG/AQ2, Ni-Gra/AQ, and Cu-Gra/AQ samples. For the bare HOPG substrate a typical smooth surface feature with large atomically flat areas is seen (Figure 35a), which is in good agreement with the AFM result obtained in Section 6.3.1.1. In comparison, for the bare Ni-Gra and Cu-Gra (Figures 35b,c) a large degree of relief surface morphology is revealed due to the influence of the underlying substrate (compare height bars in Figures 35a-c). The latter AFM images of bare Ni-Gra and Cu-Gra differ from previously shown AFM image of "home-made" Ni-Gra (see Section 6.3.1.1, Figure 26b), where folds and wrinkles were observed. This might be explained by the differences of the underlying substrate.

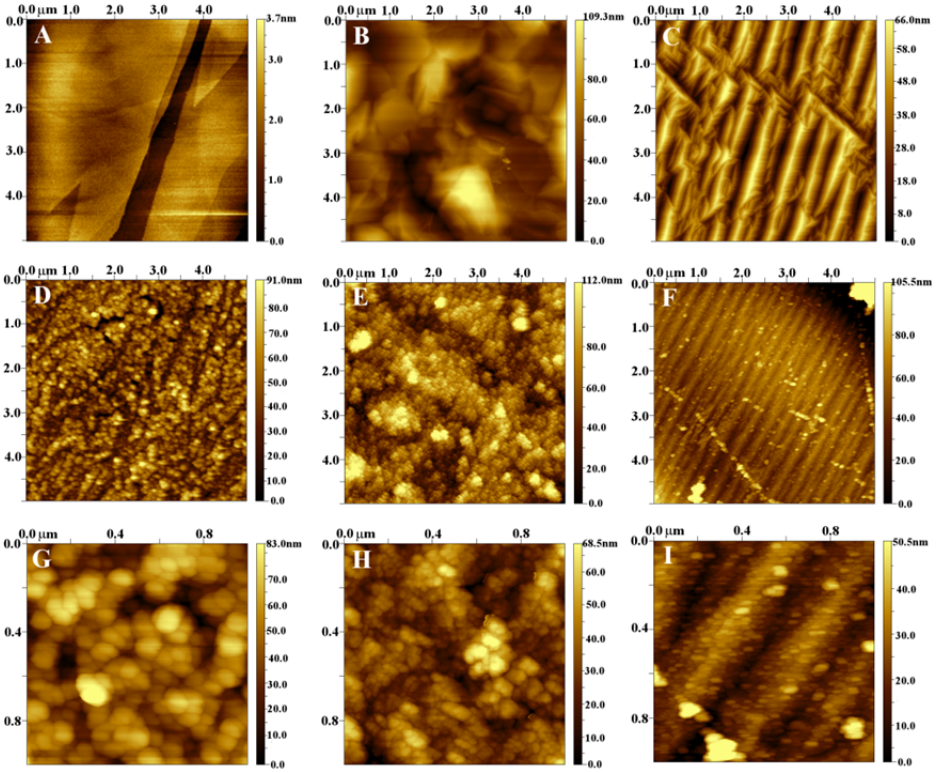

Figure 35. AFM images of (a) HOPG, (b) Ni-Gra, (c) Cu-Gra, (d,g) HOPG/AQ2, (e,h) Ni-Gra/AQ and (f,i) Cu-Gra/AQ. Scanning areas were 5×5 μm^2 for (a-f) and 1×1 μm^2 for (g-i). The various carbon-based substrates were modified using 2 mM AQD in 0.1 M $TBABF_4$/ACN by applying 20 potential cycles (ν = 2 V s^{-1}) between 0.6 and −1.5 V, 0.4 and −1.6 V and −0.2 and −1.6 V vs. SCE in case of HOPG, Ni-Gra and Cu-Gra, respectively.

AFM images of the AQ-modified electrodes clearly show that the surfaces in all cases are fully covered with a granular layer of AQ (Figures 35d-i). The typical pattern of the underlying substrate surface is evident for Cu-Gra/AQ electrodes (Figures 35f,i), whereas HOPG/AQ2 (Figures 35d,g) and Ni-Gra/AQ (Figures 35e,h) exhibit no distinct pattern in this respect. Considering that the AFM images were recorded under dried conditions, the AQ coating will be lodged as seen, e.g., for HOPG/AQ2 in Figure 35d. The AQ film thickness measured by an AFM scratching experiment was found to be 55, 40, and 10 nm for HOPG/AQ2, Ni-Gra/AQ, and Cu-Gra/AQ, respectively. This is in accordance with the AFM images of the structures taken with larger magnification (Figures 35g-i), showing gradually decreasing globules of the AQ coating. Also, the AFM-measured thicknesses of the AQ coating are, by and large, equal to the corresponding ellipsometry data (Table 6). Hence, it appears that the formation of the AQ film on mono-layered Cu-Gra is not as efficient as on multi-layered Ni-Gra or on HOPG. Furthermore, the morphology of Ni-Gra/AQ somewhat resembles that of HOPG/AQ2, although the electrochemical behaviour of these two electrodes is quite different (see next Section 6.3.2.5).

6.3.2.5. Electrochemical response of AQ-modified carbon-based electrodes towards the $Fe(CN)_6^{3-/4-}$ redox couple

Figure 36 shows the electrochemical behaviour of the $Fe(CN)_6^{3-/4-}$ redox probe on GC/AQ, HOPG/AQ1, HOPG/AQ2, Ni-Gra/AQ, and Cu-Gra/AQ electrodes. For comparative reasons, the bare electrodes are also included in these studies. As seen earlier (from Figures 11a,c,e, in Section 6.2.3), the interaction of ferricyanide ions on bare GC enables a fast heterogeneous electron transfer (Figure 36a), however the redox response of the $Fe(CN)_6^{3-/4-}$ probe on the basal plane HOPG is slower (Figure 36b) [12, 16], giving rise to a considerably larger peak-to-peak separation.

Interestingly, it was not possible to perform the experiments with bare CVD-grown graphene on Ni electrodes in neutral pH as shown previously. This observation is contradictory to our previous results of electrochemical behaviour of bare "home-made" Ni-Gra towards ferricyanide reduction (see Section 6.3.1.2, Figure 28). This discrepancy could arise due to the differences of graphene layers between commercially available (ca 4) and "home-made" Ni-Gra samples (below 10 graphene layers).

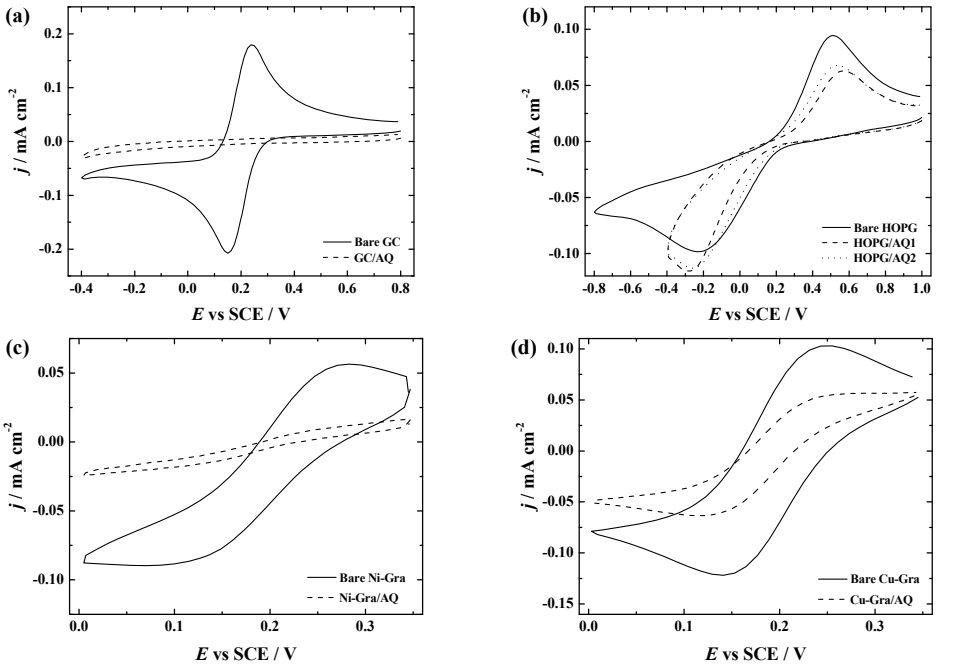

Figure 36. Electrochemical response towards the $Fe(CN)_6^{3-/4-}$ redox probe on bare and AQ-modified (a) GC, (b) HOPG, (d) Ni-Gra and (d) Cu-Gra in Ar-saturated (a,b) 0.1 M K_2SO_4 or (c,d) 0.1 M KOH solution containing 1 mM $K_3Fe(CN)_6$. v = 100 mV s^{-1}.

Hence, the electrochemical behaviour of the $Fe(CN)_6^{3-/4-}$ couple at Ni-Gra and Cu-Gra were studied in 0.1 M KOH containing 1 mM $K_3Fe(CN)_6$ (Figures 36c,d) to avoid oxidation of the underlying metals that would, otherwise, take place at neutral pH [215]. Both voltammograms recorded showed a sigmoidal shape with small current density values and larger peak-to-peak separations compared, for example, to bare Ni in the same solution [216]. This definitely refers that graphene is present on Ni surface. Interestingly, Shul *et al*. [217] have reported that even $Fe(CN)_6^{3-}$ may oxidise the surface of Cu to preclude any further measurements. However, as seen the voltammogram of Cu-Gra (Figure 36d) showed the expected electrochemical response of the $Fe(CN)_6^{3-/4-}$ redox system, implying that the monolayer graphene is protecting the Cu surface.

From previous study on GC/AQ [214] it is known that the electrochemical response of $Fe(CN)_6^{3-/4-}$ is strongly inhibited, if $\Gamma_{AQ} > 10^{-9}$ mol cm^{-2}. This is also observed herein (Figure 35a). In contrast, for both HOPG/AQ1 and HOPG/AQ2 the response comes through and, moreover, the peak separation is decreased compared to that for bare HOPG, indicating slightly faster ET kinetics. According to a study by Liu and McCreery [66] on the electrochemical reduction of NBD on GC and basal plane HOPG, NP radicals formed during the electrografting process would be sufficiently reactive to attack both edge and

basal plane sites on HOPG. In particular, the attack of the radicals on edges was assumed to be fast, thereby damaging the carbon lattice to create even more edge sites [66]. If this is happening herein as well, this would certainly make the electron transfer kinetics of the $Fe(CN)_6^{3-/4-}$ redox probe faster on HOPG/AQ than HOPG itself. At the same time the AQ layer is expected to be more porous on HOPG/AQ than GC/AQ because of the fewer nucleation sites in the former case. As a result, the electron transfer of $Fe(CN)_6^{3-/4-}$ ions may take place directly on uncovered edge sites at the HOPG. Importantly, this would also provide an explanation why the electrochemical behaviour of $Fe(CN)_6^{3-/4-}$ on HOPG/AQ1 and HOPG/AQ2 is so similar, despite the AQ film being more than eight times thicker in the latter case (see Table 6).

On Ni-Gra/AQ the electrochemical signal of the $Fe(CN)_6^{3-/4-}$ redox probe was almost completely suppressed (Figure 36c), implying that the ET is strongly inhibited. For Cu-Gra/AQ the current density values also decreased but in this case the sigmoidal shape of the voltammogram remained. This would suggest that Cu-Gra/AQ having a thinner film is covered with AQ layers of higher porosity or containing pinholes. In general we may conclude that the AQ film on HOPG, Ni-Gra and Cu-Gra is not as closely packed as on GC surface.

6.3.2.6. Oxygen reduction on AQ-modified carbon-based electrodes

Figure 37 shows the linear sweep voltammograms for the reduction of O_2 on bare and AQ-modified GC, HOPG, Ni-Gra and Cu-Gra electrodes in alkaline solution. Several O_2 reduction studies have been performed on AQ-modified GC electrodes [53–55, 121, 130, 131, 134, 195, 218], only very recently the ORR was investigated on GC substrates modified with thick AQ films (up to $\Gamma_{AQ} = 6\times10^{-9}$ mol cm^{-2}) [219]. In the latter study, the results of kinetic parameters revealed that in spite of the thick AQ film on GC electrode, these electrodes are not advantageous for the electrocatalysis of O_2 reduction and a good electrocatalytic effect can be observed already for the Γ_{AQ} values of 10^{-9} mol cm^{-2} [219]. As can be seen from Figure 37a, these results are in good agreement with those obtained in our previous study [219]. Briefly, the O_2 reduction wave on AQ grafted GC electrode started at more negative potential (ca –0.3 V) compared to bare GC (ca –0.2 V). Furthermore, the O_2 reduction wave which is usually caused by the native quinone-type groups present on the bare GC surface [53, 54] shifted to more negative direction on GC/AQ electrodes (Figure 37a) indicating that the electrochemically grafted AQ groups inhibit O_2 reduction on GC electrodes at these potentials. However, at lower potentials (E < –0.6 V) the reduction current densities were larger on AQ-modified GC electrode compared to bare GC and this is due to the electrocatalytic effect of AQ groups attached to GC electrode surface during the electrografting process (Figure 37a) [131, 219].

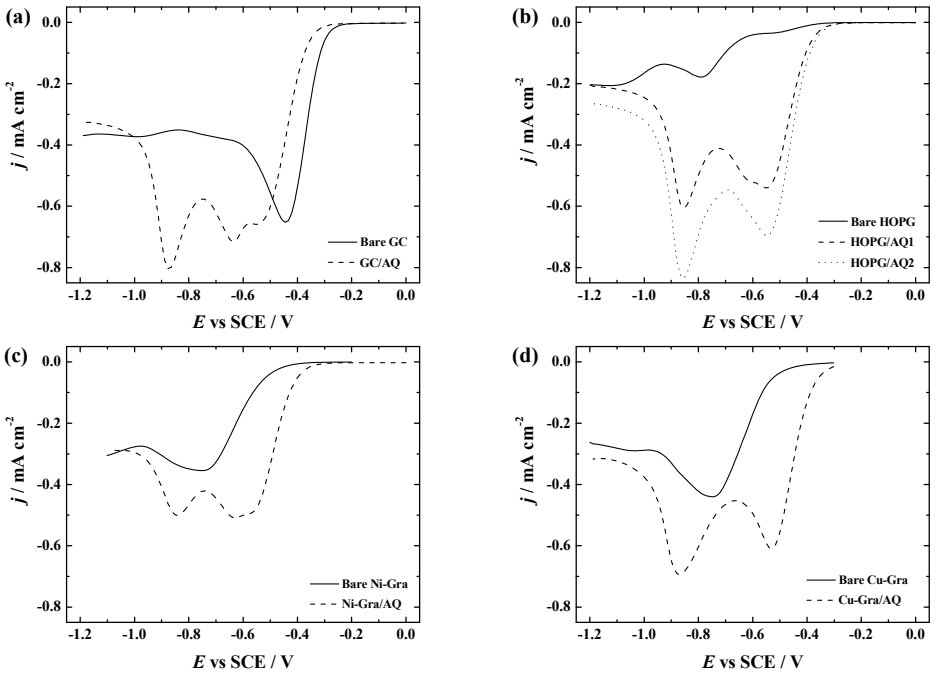

Figure 37. LSVs of O_2 reduction on bare and AQ-modified (a) GC, (b) HOPG, (c) Ni-Gra, and (d) Cu-Gra in O_2-saturated 0.1 M KOH; ν = 100 mV s^{-1}.

The LSV curves for O_2 reduction on bare HOPG, Ni-Gra and Cu-Gra (Figures 37b-d) all show a major reduction wave at ca –0.75 V and a minor wave at around –1.1 V. This shows that the ORR activity is significantly lower compared to that of bare GC which is consistent with earlier studies [135, 208]. The small pre-peak seen in Figure 37b at –0.55 V on bare HOPG is suggested to occur from O_2 reduction at quinone-type groups present on HOPG defect sites. Moreover, its relatively low intensity implies that mainly the basal plane is exposed [208]. The pre-peak is absent in case of CVD-grown graphene on Ni or Cu substrate (Figures 37c,d) implying that graphene sheets cover the corresponding underlying surface without edge sites. These findings also indicate that the substrates (basal plane HOPG and CVD-grown graphene electrodes) are suitable to study the properties of electrocatalytically active functional groups as reported earlier [53, 54, 134, 135, 195, 218] and therefore anthraquinone is a good candidate for that.

As can be seen in Figure 37b, the O_2 reduction wave started at a more positive potential (at ca –0.3 V) for AQ-modified HOPG compared to bare HOPG. Sarapuu *et al*. [135] studied the reduction of O_2 in 0.1 M KOH at AQ-modified basal plane HOPG with very low surface concentration of AQ groups (8×10^{-11} mol cm^{-2}). The authors revealed that in case of HOPG/AQ electrodes, the first O_2 reduction peak was around –0.8 V and larger current values were

observed compared to bare HOPG, suggesting the catalytic effect due to the presence of surface-confined AQ [135]. In contrast to the latter study, the first oxygen reduction peak of the AQ-modified HOPG electrodes was already observed at ca –0.55 V (see Figure 37b). At this point we do not know the exact reason for this observation. However there might be several reasons for that. First the presence of this cathodic peak might be associated with edge plane sites which might have been formed during the grafting of HOPG surface with AQ moieties as suggested above. Therefore the native quinone-type functionalities which are present only on defect sites of HOPG enhance the electrocatalytic activity for O_2 reduction at these potentials. Another explanation might also be attributed to the thicker AQ layer on HOPG (Figure 37b). Then in this case, the O_2 reduction peak observed at bare HOPG (ca –0.8 V) has been shifted to more positive potentials (–0.55 V) because of the AQ-modified HOPG electrodes. For example, Kocak *et al*. [136] performed the O_2 reduction studies in 0.1 M acetate buffer (pH=5) at basal plane and edge plane HOPG modified with AQ through $–NH_2CH_2C_6H_4–$ linker. Amongst other things the authors investigated the influence of edge plane HOPG electrodes of different AQ coverage on the ORR and the results showed that as the surface concentration of AQ groups increased the reduction peak shifted to a more positive direction and the peak current increased as well [136]. A similar tendency was observed in this study (Figure 37b). Therefore it may be concluded that the current density values depend on the surface concentration of the AQ groups as observed earlier [136].

Compared with bare CVD-grown graphene substrates, the AQ-modified graphene-based electrodes greatly increase the ORR current density values (see Figures 37c,d). In both cases, the oxygen reduction peaks shifted to more positive potentials (at around –0.55 V) compared to the bare substrates where the first peak potential was at ca –0.8 V (Figures 37c,d). Similarly to GC/AQ electrodes, a reduction peak close to –0.9 V was observed for all the AQ-modified carbon-based electrodes (see Figures 37b-d). This peak is most probably due to the electrocatalysis by the surface-bound AQ groups.

However, there is an additional peak at ca –0.65 V in case of GC, HOPG and Ni-Gra grafted with AQ groups. Unfortunately the reason for that remains unclear, but according to the study by Kullapere *et al*. [121] this peak might indicate the involvement of the AQ sites in the reduction of oxygen.

On the basis of these results we may conclude that all HOPG and graphene-based electrodes modified with thick AQ films display enhanced ORR performance compared to bare substrates. This is caused by the intrinsic electro-catalytic property of AQ groups for O_2 reduction in alkaline media.

7. SUMMARY

In this PhD thesis, a variety of aryl groups, for example 4-nitrophenyl (NP), 4-carboxyphenyl (CP), azobenzene (AB), 2-methyl-4([2-methylphenyl]azo)-benzene (GBC), 2,5-dimethoxy-4-([4-nitrophenyl]azo)benzene (FBK) and 9,10-anthraquinone (AQ) groups were electrografted onto different electrode surfaces (e.g. GC, Au, HOPG and CVD-grown graphene on Ni or Cu) *via* electrochemical reduction of the corresponding diazonium salts and these aryl-modified electrodes were systematically investigated using various surface analytical and electrochemical methods.

In the first part of the work, the electrochemical behaviour of ABTS on aryl-modified GC electrodes was studied. GC electrodes were electrografted with NP or CP groups and in addition, the electrochemical reduction of the NP films was used to prepare 4-aminophenyl (AP) modified GC electrodes. First, the X-ray photoelectron spectroscopy (XPS) results confirmed the presence of NP or AP layers on GC surfaces. Thereafter, the oxidation of ABTS was studied in aqueous solutions of different pH (pH=4–8). The cyclic voltammetry (CV) and rotating disk electrode (RDE) results revealed that the response of ABTS was independent of pH for bare GC and GC/NP electrodes (modified by 20 electrografting cycles), whereas a slight pH-dependence was observed for other electrodes (especially for CP-modified GC electrodes). In general, the strongest blocking action was observed for the NP-modified GC electrodes of higher surface coverage and the lowest for reduced NP films (modified by a single electrografting cycle) [I].

In the next part of the work, three different azobenzene diazonium compounds (AB, GBC and FBK) were strongly attached to GC and Au electrodes *via* electrochemical grafting in order to compare the surface grafting and electrochemical behaviour of these aryl-modified electrodes. After electrochemical grafting, the presence of azo groups as well as azo linkages within aryl films was observed for all aryl-modified GC and Au electrodes and additionally, the nitro functionality for the FBK-modified GC and Au electrodes was detected by XPS. Furthermore, in case of aryl-modified Au electrodes, the atomic force microscopy (AFM) and electrochemical quartz crystal microbalance results showed that potential cycling during surface modification enables the formation of multilayer films. For all aryl-modified GC and Au substrates, the results indicated that the blocking action towards the $Fe(CN)_6^{3-}$ probe was far more evident than for oxygen reduction, which might be explained by differences in size between the $Fe(CN)_6^{3-/4-}$ ions and O_2 molecule. Also, the hydrophobic/hydrophilic interactions between the aryl film and redox probe may influence the electron transfer rate. Based on the performance of aryl-modified electrodes for oxygen reduction by linear sweep voltammetry and RDE, the aryl layers on GC or Au surface tend to be loosely packed which means that the electrochemical grafting of aryldiazonium salts does not provide an efficient barrier for ORR. It should also be noted that even though a higher

diazonium salt concentration was used in case of Au surfaces, the blocking effect of aryl-modified Au electrodes was not as strong as compared with aryl-modified GC electrodes [II,III]. Afterwards, the aryl films on GC and Au substrate were treated with $OH^{\bullet}$ radicals generated by UV photolysis of H_2O_2. It was found that the treatment with $OH^{\bullet}$ radicals was effective to degrade aryl films on both GC and Au substrate and the aryl layers were removed more quickly from Au surface than from the GC surface [IV].

In the final part of the work, the surface characterisation and electrochemical behaviour of bare and anthraquinone-grafted different carbon substrates, including GC that served as a reference material, HOPG and the novel carbon material, CVD-grown graphene, were studied. First, the Raman spectroscopy, high-resolution scanning electron microscopy and AFM confirmed that multilayer graphene was formed on the Ni foil by the CVD method [V], whereas based on the Raman spectroscopy results, CVD graphene grown on Cu foil was rather a monolayer [VI]. In addition, electrochemical experiments revealed that the electrochemical behaviour of bare HOPG can be assimilated to CVD-grown graphene on Ni foil [V]. Next, it was demonstrated that thick AQ films can be electrografted onto different carbon substrates, including HOPG and CVD-grown graphene on Ni and Cu substrate. The AQ layer thickness on different carbon substrates varied in the range of 7–60 nm (measured by ellipsometry or the AFM scratching method). The general electrografting behaviour was similar for HOPG and the graphene-based substrates, but it was shown to be highly dependent on the potential range, the sweep rate and the number of potential cycles applied. For example, the experimental results showed that the electrochemical response of $Fe(CN)_6^{3-/4-}$ was completely blocked on AQ-grafted GC electrode and strongly suppressed on AQ-grafted CVD grown graphene on Ni substrate. Meanwhile, for AQ-grafted CVD grown graphene on Cu substrate and in particular HOPG electrodes the signal was only slightly suppressed. This could be explained by the formation of a more densely packed AQ film on GC than on HOPG or CVD graphene. Interestingly, the oxygen reduction studies revealed good electrocatalytic activity of AQ-modified HOPG and graphene electrodes compared with the bare substrates [VI].

In conclusion, it is clear that the diazonium reduction is an efficient method for surface modification because it can be applied to all types of electrodes (including CVD-grown graphene) studied in this thesis. Unfortunately, the nature of the bonding which occurs during elecrografting between the electrode surface (e.g Au, HOPG and CVD-grown graphene electrodes) and the aryl group is not fully understood and therefore it is still under investigation. The experimental results clearly indicated that the aryl films were strongly bonded to the Au surface as these survived an ultrasonic treatment. Moreover, the experimental results revealed that the aryl modifiers changed the electrochemical properties of the bulk electrode materials and the electrochemical behaviour of aryl-modified electrodes greatly depended on the diazonium salt, electrografting procedures and substrate material.

8. REFERENCES

[1] M.M. Chehimi, Aryl diazonium salts: new coupling agents in polymer and surface science, Wiley-VCH, Weinheim, 2012.
[2] J.J. Gooding, *Electroanalysis* 20 (2008) 573.
[3] S. Mahouche-Chergui, S. Gam-Derouich, C. Mangeney, M.M. Chehimi, *Chem. Soc. Rev*. 40 (2011) 4143.
[4] D. Bélanger, J. Pinson, *Chem. Soc. Rev*. 40 (2011) 3995.
[5] J. Pinson, F. Podvorica, *Chem. Soc. Rev*. 34 (2005) 429.
[6] Z. Salmi, S. Gam-Derouich, S. Mahouche-Chergui, M. Turmine, M.M. Chehimi, *Chem. Pap*. 66 (2012) 369.
[7] R.L. McCreery, *Chem. Rev*. 108 (2008) 2646.
[8] A.J. Downard, *Int. J. Nanotechnol*. 6 (2009) 233.
[9] R.L. McCreery, in: A. Wieckowski (Ed.), Interfacial electrochemistry, Marcel Dekker Inc., New York, 1999, pp. 631–647.
[10] J.K. Kariuki, M.T. McDermott, *Langmuir* 17 (2001) 5947.
[11] S.H. DuVall, R.L. McCreery, *Anal. Chem.* 71 (1999) 4594.
[12] R.L. McCreery, M.T. McDermott, *Anal. Chem.* 84 (2012) 2602.
[13] K.R. Kneten, R.L. McCreery, *Anal. Chem.* 64 (1992) 2518.
[14] M.T. McDermott, K. Kneten, R.L. McCreery, *J. Phys. Chem.* 96 (1992) 3124.
[15] R.S. Robinson, K. Sternitzke, M.T. McDermott, R.L. McCreery, *J. Electrochem. Soc*. 138 (1991) 2412.
[16] T.J. Davies, R.R. Moore, C.E. Banks, R.G. Compton, *J. Electroanal. Chem*. 574 (2004) 123.
[17] J.K. Kariuki, M.T. McDermott, *Langmuir* 15 (1999) 6534.
[18] X.K. Lu, M.F. Yu, H. Huang, R.S. Ruoff, *Nanotechnology* 10 (1999) 269.
[19] K.S. Novoselov, A.K. Geim, S.V. Morozov, D. Jiang, Y. Zhang, S.V. Dubonos, I.V. Grigorieva, A.A. Firsov, *Science* 306 (2004) 666.
[20] K.S. Novoselov, D. Jiang, F. Schedin, T.J. Booth, V.V. Khotkevich, S.V. Morozov, A.K. Geim, *Proc. Natl. Acad. Sci. USA* 102 (2005) 10451.
[21] S. Bae, H. Kim, Y. Youngbin, X. Xu, J.-S. Park, Y. Zheng, J. Balakrishnan, T. Lei, H.-R. Kim, Y.-I. Song,Y.-J. Kim, K.S. Kim, B. Ozyilmaz, J.-H. Ahn, B.H. Hong, S. Iijima, *Nat. Nanotechnol.* 5 (2010) 574.
[22] S.H. Hur, J.-N. Park, *Asia-Pac. J. Chem. Eng.* 8 (2013) 218.
[23] M. Song, D. Cai, in: V. Mittal (Ed.), Polymer-graphene nanocomposites, Royal Society of Chemistry, Cambridge, UK, 2012, p. 280.
[24] Y. Zhang, L. Gomez, F.N. Ishikawa, A. Madaria, K. Ryu, C. Wang, A. Badmaev, C. Zhou, *J. Phys. Chem. Lett.* 1 (2010) 3101.
[25] A. Bianco, H.-M. Cheng, T. Enoki, Y. Gogotsi, R.H. Hurt, N. Koratkar, T. Kyotani, M. Monthioux, C.R. Park, J.M.D. Tascon, J. Zhang, *Carbon* 65 (2013) 1.
[26] X. Huang, Z. Zeng, Z. Fan, J. Liu, H. Zhang, *Adv. Mater.* 24 (2012) 5979.
[27] S. Chen, L. Brown, M. Levendorf, W. Cai, S.-Y. Ju, J. Edgeworth, X. Li, C.W. Magnuson, A. Velamakanni, R.D. Piner, J. Kang, J. Park, R.S. Ruoff, *ACS Nano* 5 (2011) 1321.
[28] D. Prasai, J.C. Tuberquia, R.R. Harl, G.K. Jennings, K.I. Bolotin, *ACS Nano* 6 (2012) 1102.
[29] J. Liu, J. Tang, J.J. Gooding, *J. Mater. Chem*. 22 (2012) 12435.

[30] R. Munoz, C. Gomez-Aleixandre, *Chem. Vap. Dep*. 19 (2013) 297.
[31] A.L. Gui, G. Liu, M. Chockalingam, G. Le Saux, J.B. Harper, J.J. Gooding, *Electroanalysis* 22 (2010) 1283.
[32] M. Khoshroo, A.A. Rostami, *J. Electroanal. Chem*. 647 (2010) 117.
[33] H. Zollinger, Diazo Chemistry, Wiley, New York, 2004.
[34] J.A. Delaire, K. Nakatani, *Chem. Rev*. 100 (2000) 1817.
[35] T. Ikeda, O. Tsutsumi, *Science* 268 (1995) 1873.
[36] E. Merino, Chem. *Soc. Rev*. 40 (2011) 3835.
[37] S. Griveau, S. Aroua, D. Bediwy, R. Cornut, C. Lefrou, F. Bedioui, *J. Electroanal. Chem*. 647 (2010) 93.
[38] A.L. Gui, G. Liu, M. Chockalingam, G. Le Saux, E. Luais, J.B. Harper, J.J. Gooding, *Electroanalysis* 22 (2010) 1824.
[39] C. Saby, B. Ortiz, G.Y. Champagne, D. Bélanger, *Langmuir* 13 (1997) 6805.
[40] P.A. Brooksby, A.J. Downard, *Langmuir* 20 (2004) 5038.
[41] M. Delamar, R. Hitmi, J. Pinson, J.M. Savéant, *J. Am. Chem. Soc*. 114 (1992) 5883.
[42] S.S.C. Yu, E.S.Q. Tan, R.T. Jane, A.J. Downard, *Langmuir* 23 (2007) 11074.
[43] A.J. Gross, S.S.C. Yu, A.J. Downard, *Langmuir* 26 (2010) 7285.
[44] G. Liu, T. Bocking, J.J. Gooding, *J. Electroanal. Chem*. 600 (2007) 335.
[45] A.-E. Radi, V. Lates, J.-L. Marty, *Electroanalysis* 20 (2008) 2557.
[46] C. Combellas, M. Delamar, F. Kanoufi, J. Pinson, F.I. Podvorica, *Chem. Mater*. 17 (2005) 3968.
[47] C. Fernandez, M. Soledad Larrechi, M. Pilar Callao, *TRAC-Trends Anal. Chem*. 29 (2010) 1202.
[48] G.G. Wildgoose, M. Pandurangappa, N.S. Lawrence, L. Jiang, T.G.J. Jones, R.G. Compton, *Talanta* 60 (2003) 887.
[49] V.G.H. Lafitte, W. Wang, A.S. Yashina, N.S. Lawrence, *Electrochem. Commun*. 10 (2008) 1831.
[50] Y. Dou, S. Haswell, J. Greenman, J. Wadhawan, *Electrochem. Commun*. 11 (2009) 1976.
[51] C. Feng, L. Ma, F. Li, H. Mai, X. Lang, S. Fan, *Biosens. Bioelectron.* 25 (2010) 1516.
[52] A. Salimi, H. Eshghi, H. Sharghi, S.M. Golabi, M. Shamsipur, *Electroanalysis* 11 (1999) 114.
[53] A. Sarapuu, K. Vaik, D.J. Schiffrin, K. Tammeveski, *J. Electroanal. Chem*. 541 (2003) 23.
[54] K. Tammeveski, K. Kontturi, R.J. Nichols, R.J. Potter, D.J. Schiffrin, *J. Electroanal. Chem*. 515 (2001) 101.
[55] G. Maia, F.C. Maschion, S.T. Tanimoto, K. Vaik, U. Mäeorg, K. Tammeveski, *J. Solid State Electrochem*. 11 (2007) 1411.
[56] S. Valarselvan, P. Manisankar, *Electrochim. Acta* 56 (2011) 6945.
[57] Q. Li, M.C. Henstridge, C. Batchelor-McAuley, N.S. Lawrence, R.S. Hartshorne, R.G. Compton, *Phys. Chem. Chem. Phys*. 15 (2013) 7854.
[58] P. Allongue, M. Delamar, B. Desbat, O. Fagebaume, R. Hitmi, J. Pinson, J.M. Saveant, *J. Am. Chem. Soc*. 119 (1997) 201.
[59] F. Barriere, A.J. Downard, *J. Solid State Electrochem*. 12 (2008) 1231.
[60] E. Bekyarova, M.E. Itkis, P. Ramesh, C. Berger, M. Sprinkle, W.A. de Heer, R.C. Haddon, *J. Am. Chem. Soc*. 131 (2009) 1336.
[61] A.J. Downard, *Electroanalysis* 12 (2000) 1085.

[62] Y.C. Liu, R.L. McCreery, *Anal. Chem*. 69 (1997) 2091.
[63] A.M. Nowak, R.L. McCreery, *Anal. Chem*. 76 (2004) 1089.
[64] C. Combellas, F. Kanoufi, J. Pinson, F.I. Podvorica, *Langmuir* 21 (2005) 280.
[65] C. Combellas, F. Kanoufi, J. Pinson, F.I. Podvorica, *J. Am. Chem. Soc.* 130 (2008) 8576.
[66] Y.C. Liu, R.L. McCreery, *J. Am. Chem. Soc.* 117 (1995) 11254.
[67] K. Ray, R.L. McCreery, *Anal. Chem*. 69 (1997) 4680.
[68] P.M. Kirkman, A.G. Güell, A.S. Cuharuc, P.R. Unwin, *J. Am. Chem. Soc*. 136 (2014) 36.
[69] H. Ma, L. Lee, P.A. Brooksby, S.A. Brown, S.J. Fraser, K.C. Gordon, Y.R. Leroux, P. Hapiot, A.J. Downard, *J. Phys. Chem. C* 118 (2014) 5820.
[70] M. Lillethorup, M. Kongsfelt, M. Ceccato, B.B.E. Jensen, B. Jorgensen, S.U. Pedersen, K. Daasbjerg, *Small* 10 (2014) 922.
[71] P. Huang, L. Jing, H. Zhu, X. Gao, *Acc. Chem. Res.* 46 (2013) 43.
[72] D.-e. Jiang, B.G. Sumpter, S. Dai, *J. Phys. Chem. B* 110 (2006) 23628.
[73] F.M. Koehler, A. Jacobsen, K. Ensslin, C. Stampfer, W.J. Stark, *Small* 6 (2010) 1125.
[74] E. Ahlberg, B. Helgee, V.D. Parker, *Acta Chem. Scand. B* 34 (1980) 181.
[75] A. Laforgue, T. Addou, D. Bélanger, *Langmuir* 21 (2005) 6855.
[76] L. Laurentius, S.R. Stoyanov, S. Gusarov, A. Kovalenko, R. Du, G.P. Lopinski, M.T. McDermott, *ACS Nano* 5 (2011) 4219.
[77] G.Z. Liu, J.Q. Liu, T. Bocking, P.K. Eggers, J.J. Gooding, Chem. Phys. 319 (2005) 136.
[78] D.M. Shewchuk, M.T. McDermott, *Langmuir* 25 (2009) 4556.
[79] A. Celiktas, M.A. Ghanem, P.N. Bartlett, *J. Electroanal. Chem*. 670 (2012) 42.
[80] D.E. Jiang, B.G. Sumpter, S. Dai, *J. Am. Chem. Soc.* 128 (2006) 6030.
[81] A.M. Ricci, L.P. Mendez De Leo, F.J. Williams, E.J. Calvo, *ChemPhysChem* 13 (2012) 2119.
[82] L. Lee, P.A. Brooksby, A.J. Downard, *Electrochem. Commun.* 19 (2012) 67.
[83] F. Scholz, G.L. de Lara Gonzalez, L.M. de Carvalho, M. Hilgemann, K.Z. Brainina, H. Kahlert, R.S. Jack, D.T. Minh, *Angew. Chem. Int. Ed.* 46 (2007) 8079.
[84] E. Brillas, I. Sires, M.A. Oturan, *Chem. Rev*. 109 (2009) 6570.
[85] A.M. Nowicka, U. Hasse, M. Hermes, F. Scholz, *Angew. Chem. Int. Ed*. 49 (2010) 1061.
[86] A.M. Nowicka, U. Hasse, G. Sievers, M. Donten, Z. Stojek, S. Fletcher, F. Scholz, *Angew. Chem. Int. Ed*. 49 (2010) 3006.
[87] M. Fau, A. Kowalczyk, P. Olejnik, A.M. Nowicka, *Anal. Chem*. 83 (2011) 9281.
[88] H.H. Yang, R.L. McCreery, *Anal. Chem*. 71 (1999) 4081.
[89] A.J. Downard, M.J. Prince, *Langmuir* 17 (2001) 5581.
[90] P.H. Chen, R.L. McCreery, *Anal. Chem*. 68 (1996) 3958.
[91] B. Feier, D. Floner, C. Cristea, R. Sandulescu, F. Geneste, *Electrochem. Commun*. 31 (2013) 13.
[92] F. Anariba, S.H. DuVall, R.L. McCreery, *Anal. Chem*. 75 (2003) 3837.
[93] P.A. Brooksby, A.J. Downard, *J. Phys. Chem. B* 109 (2005) 8791.
[94] A.O. Solak, L.R. Eichorst, W.J. Clark, R.L. McCreery, *Anal. Chem*. 75 (2003) 296.
[95] A.J. Downard, *Langmuir* 16 (2000) 9680.

[96] M. Ceccato, A. Bousquet, M. Hinge, S.U. Pedersen, K. Daasbjerg, *Chem. Mater.* 23 (2011) 1551.
[97] S. Chernyy, A. Bousquet, K. Torbensen, J. Iruthayaraj, M. Ceccato, S.U. Pedersen, K. Daasbjerg, *Langmuir* 28 (2012) 9573.
[98] A. Bousquet, M. Ceccato, M. Hinge, S.U. Pedersen, K. Daasbjerg, *Langmuir* 28 (2012) 1267.
[99] G.G. Wildgoose, P. Abiman, R.G. Compton, *J. Mater. Chem*. 19 (2009) 4875.
[100] Y.-S. Sun, *Instrum. Sci. Technol.* 42 (2014) 109.
[101] A. Bismarck, A. Menner, J. Barner, A.F. Lee, K. Wilson, J. Springer, J.P. Rabe, A.S. Sarac, *Surf. Coat. Technol.* 145 (2001) 164.
[102] J.F. Wall, J.C. Brumfield, R.W. Murray, E.A. Irene, *J. Electrochem. Soc*. 141 (1994) 306.
[103] L.M. Malard, M.A. Pimenta, G. Dresselhaus, M.S. Dresselhaus, *Phys. Rep*. 473 (2009) 51.
[104] M. Kullapere, M. Marandi, L. Matisen, F. Mirkhalaf, A.E. Carvalho, G. Maia, V. Sammelselg, K. Tammeveski, *J. Solid State Electrochem*. 16 (2012) 569.
[105] S.S.C. Yu, A.J. Downard, *e-J. Surf. Sci. Nanotech*. 3 (2005).
[106] G.T.R. Palmore, H.H. Kim, *J. Electroanal. Chem*. 464 (1999) 110.
[107] E. Nazaruk, K. Sadowska, J.F. Biernat, J. Rogalski, G. Ginalska, R. Bilewicz, *Anal. Bioanal. Chem.* 398 (2010) 1651.
[108] P. Giardina, V. Faraco, C. Pezzella, A. Piscitelli, S. Vanhulle, G. Sannia, *Cell. Mol. Life Sci.* 67 (2010) 369.
[109] M. Fernandez-Fernandez, M. Angeles Sanroman, D. Moldes, *Biotechnol. Adv*. 31 (2013) 1808.
[110] S.L. Scott, W.J. Chen, A. Bakac, J.H. Espenson, *J. Phys. Chem*. 97 (1993) 6710.
[111] R. Bourbonnais, D. Leech, M.G. Paice, *Biochim. Biophys. Acta* 1379 (1998) 381.
[112] S. Tsujimura, B. Tatsumi, J. Ogawa, S. Shimizu, K. Kano, T. Ikeda, *J. Electroanal. Chem*. 496 (2001) 69.
[113] D. Quan, Y. Kim, W. Shin, *J. Electroanal. Chem*. 561 (2004) 181.
[114] H. Zeng, Z.-q. Tang, L.-w. Liao, J. Kang, Y.-x. Chen, *Chin. J. Chem. Phys*. 24 (2011) 653.
[115] M. Di Fusco, G. Favero, F. Mazzei, *J. Phys. Chem. B* 115 (2011) 972.
[116] C. Vaz-Dominguez, S. Campuzano, O. Rudiger, M. Pita, M. Gorbacheva, S. Shleev, V.M. Fernandez, A.L. De Lacey, *Biosens. Bioelectron.* 24 (2008) 531.
[117] M. Sosna, J.-M. Chretien, J.D. Kilburn, P.N. Bartlett, *Phys. Chem. Chem. Phys.* 12 (2010) 10018.
[118] M. Pita, C. Gutierrez-Sanchez, D. Olea, M. Velez, C. Garcia-Diego, S. Shleev, V.M. Fernandez, A.L. De Lacey, *J. Phys. Chem*. C 115 (2011) 13420.
[119] C. Gutierrez-Sanchez, M. Pita, C. Vaz-Dominguez, S. Shleev, A.L. De Lacey, *J. Am. Chem. Soc*. 134 (2012) 17212.
[120] P. Olejnik, B. Palys, A. Kowalczyk, A.M. Nowicka, *J. Phys. Chem. C* 116 (2012) 25911.
[121] M. Kullapere, G. Jürmann, T.T. Tenno, J.J. Paprotny, F. Mirkhalaf, K. Tammeveski, *J. Electroanal. Chem.* 599 (2007) 183.
[122] S. Schauff, M. Ciorca, A. Laforgue, D. Bélanger, *Electroanalysis* 21 (2009) 1499.
[123] M. Kullapere, F. Mirkhalaf, K. Tammeveski, *Electrochim. Acta* 56 (2010) 166.
[124] D.A.C. Brownson, C.E. Banks, *Phys. Chem. Chem. Phys.* 14 (2012) 8264.

[125] D.A.C. Brownson, D.K. Kampouris, C.E. Banks, *Chem. Soc. Rev*. 41 (2012) 6944.
[126] D.A.C. Brownson, R.V. Gorbachev, S.J. Haigh, C.E. Banks, *Analyst* 137 (2012) 833.
[127] A. Ambrosi, M. Pumera, *J. Phys. Chem. C* 117 (2013) 2053.
[128] B. Sljukic, C.E. Banks, R.G. Compton, *Phys. Chem. Chem. Phys*. 6 (2004) 4034.
[129] D.-W. Wang, D. Su, *Energy Environ. Sci*. 7 (2014) 576.
[130] M. Kullapere, J.-M. Seinberg, U. Mäeorg, G. Maia, D.J. Schiffrin, K. Tammeveski, *Electrochim. Acta* 54 (2009) 1961.
[131] J.-M. Seinberg, M. Kullapere, U. Mäeorg, F.C. Maschion, G. Maia, D.J. Schiffrin, K. Tammeveski, *J. Electroanal. Chem.* 624 (2008) 151.
[132] G. Jürmann, D.J. Schiffrin, K. Tammeveski, *Electrochim. Acta* 53 (2007) 390.
[133] E. Lobyntseva, T. Kallio, N. Alexeyeva, K. Tammeveski, K. Kontturi, *Electrochim. Acta* 52 (2007) 7262.
[134] F. Mirkhalaf, K. Tammeveski, D.J. Schiffrin, *Phys. Chem. Chem. Phys*. 6 (2004) 1321.
[135] A. Sarapuu, K. Helstein, D.J. Schiffrin, K. Tammeveski, *Electrochem. Solid-State Lett.* 8 (2005) E30.
[136] I. Kocak, M.A. Ghanem, A. Al-Mayouf, M. Alhoshan, P.N. Bartlett, *J. Electroanal. Chem*. 706 (2013) 25.
[137] S. Ernst, L. Aldous, R.G. Compton, *Chem. Phys. Lett*. 511 (2011) 461.
[138] C. Zhu, S. Dong, Nanoscale 5 (2013) 1753.
[139] E.P. Randviir, C.E. Banks, *Electroanalysis* 26 (2014) 76.
[140] F. Lima, G.V. Fortunato, G. Maia, *RSC Adv.* 3 (2013) 9550.
[141] Y. Matsumoto, H. Tateishi, M. Koinuma, Y. Kamei, C. Ogata, K. Gezuhara, K. Hatakeyama, S. Hayami, T. Taniguchi, A. Funatsu, *J. Electroanal. Chem.* 704 (2013) 233.
[142] D.A.C. Brownson, D.K. Kampouris, C.E. Banks, *J. Power Sources* 196 (2011) 4873.
[143] K. Tiido, N. Alexeyeva, M. Couillard, C. Bock, B.R. MacDougall, K. Tammeveski, *Electrochim. Acta* 107 (2013) 509.
[144] M. Vikkisk, I. Kruusenberg, U. Joost, E. Shulga, I. Kink, K. Tammeveski, *Appl. Catal. B* 147 (2014) 369.
[145] S. Ratso, I. Kruusenberg, M. Vikkisk, U. Joost, E. Shulga, I. Kink, T. Kallio, K. Tammeveski, *Carbon* 73 (2014) 361.
[146] Y. Zhou, G. Zhang, J. Chen, G.e. Yuan, L. Xu, L. Liu, F. Yang, *Electrochem. Commun.* 22 (2012) 69.
[147] G. Yuan, G. Zhang, J. Chen, L. Fu, L. Xu, F. Yang, *J. Solid State Electrochem.* 17 (2013) 2711.
[148] H.O. House, E. Feng, N.P. Peet, *J. Org. Chem*. 36 (1971) 2371.
[149] M. D'Amours, D. Bélanger, *J. Phys. Chem*. B 107 (2003) 4811.
[150] M.F.W. Dunker, E.B. Starkey, G.L. Jenkins, *J. Am. Chem. Soc*. 58 (1936) 2308.
[151] T. Kim, J. Jung, S. Son, S. Yoon, M. Kim, J.-S. Bae, *Fiber. Polym*. 9 (2008) 538.
[152] K.H. Saunders, R.L.M. Allen, The aromatic diazo compounds, Edward Arnold, 1985.
[153] E.B. Starkey, in: A.H. Blatt (Ed.), Organic syntheses, John Wiley & Sons, New York, 1943, p. 225.
[154] E. Rochlin, Z. Rappoport, *J. Org. Chem*. 68 (2003) 216.

[155] R.M. Silverstein, G.C. Bassler, T.C. Morrill, Spectrometric identification of organic compounds, Wiley, New York, 1991.
[156] A. Reina, S. Thiele, X. Jia, S. Bhaviripudi, M.S. Dresselhaus, J.A. Schaefer, J. Kong, *Nano Res.* 2 (2009) 509.
[157] B. Zhang, W.H. Lee, R. Piner, I. Kholmanov, Y. Wu, H. Li, H. Ji, R.S. Ruoff, *ACS Nano* 6 (2012) 2471.
[158] X. Li, W. Cai, J. An, S. Kim, J. Nah, D.Yang, R. Piner, A. Velamakanni, I. Jung, E. Tutuc, S.K. Banerjee, L. Colombo, R.S. Ruoff, *Science* 324 (2009) 1312.
[159] E.D. Palik, Handbook of optical constants of solids, Academic Press, New York, 1985.
[160] Z. Ustundag, M.O. Caglayan, R. Guzel, E. Piskin, A.O. Solak, *Analyst* 136 (2011) 1464.
[161] D.A. Buttry, M.D. Ward, *Chem. Rev.* 92 (1992) 1355.
[162] B. Ortiz, C. Saby, G.Y. Champagne, D. Bélanger, *J. Electroanal. Chem.* 455 (1998) 75.
[163] S. Baranton, D. Bélanger, *J. Phys. Chem. B* 109 (2005) 24401.
[164] E. Repo, E. Ahlberg, L. Murtomäki, K. Kontturi, D.J. Schiffrin, *Electrochim. Acta* 54 (2009) 6584.
[165] M. Delamar, G. Desarmot, O. Fagebaume, R. Hitmi, J. Pinson, J.M. Saveant, *Carbon* 35 (1997) 801.
[166] S. Ranganathan, R.L. McCreery, *Anal. Chem.* 73 (2001) 893.
[167] A.J. Bard, L.R. Faulkner, Electrochemical methods: Fundamentals and applications, Wiley, New York, 2001.
[168] M.G. Paulik, P.A. Brooksby, A.D. Abell, A.J. Downard, *J. Phys. Chem. C* 111 (2007) 7808.
[169] P. Mendes, M. Belloni, M. Ashworth, C. Hardy, K. Nikitin, D. Fitzmaurice, K. Critchley, S. Evans, J. Preece, *ChemPhysChem* 4 (2003) 884.
[170] A. Adenier, E. Cabet-Deliry, A. Chausse, S. Griveau, F. Mercier, J. Pinson, C. Vautrin-Ul, *Chem. Mater*. 17 (2005) 491.
[171] D.R. Lide, CRC handbook of physics and chemistry, CRC Press, Boca Raton, 2001.
[172] B.S. Flavel, D.J. Garrett, J. Lehr, J.G. Shapter, A.J. Downard, *Electrochim. Acta* 55 (2010) 3995.
[173] J. Lyskawa, D. Bélanger, *Chem. Mater*. 18 (2006) 4755.
[174] P. Abiman, A. Crossley, G.G. Wildgoose, J.H. Jones, R.G. Compton, *Langmuir* 23 (2007) 7847.
[175] T. Itoh, R.L. McCreery, *Anal. Bioanal. Chem*. 388 (2007) 131.
[176] A. Benedetto, M. Balog, P. Viel, F. Le Derf, M. Salle, S. Palacin, *Electrochim. Acta* 53 (2008) 7117.
[177] A.A. Isbir-Turan, Z. Uestuendag, A.O. Solak, E. Kilic, A. Avseven, *Thin Solid Films* 517 (2009) 2871.
[178] K. Sadowska, K.P. Roberts, R. Wiser, J.F. Biernat, E. Jablonowska, R. Bilewicz, *Carbon* 47 (2009) 1501.
[179] J. Haccoun, C. Vautrin-Ul, A. Chausse, A. Adenier, *Prog. Org. Coat*. 63 (2008) 18.
[180] H.A. Menezes, G. Maia, J. Electroanal. Chem. 586 (2006) 39.
[181] M. Kullapere, M. Marandi, V. Sammelselg, H.A. Menezes, G. Maia, K. Tammeveski, *Electrochem. Commun*. 11 (2009) 405.

[182] M. Kullapere, J. Kozlova, L. Matisen, V. Sammelselg, H.A. Menezes, G. Maia, D.J. Schiffrin, K. Tammeveski, *J. Electroanal. Chem*. 641 (2010) 90.
[183] L.B. Venarusso, K. Tammeveski, G. Maia, *Electrochim. Acta* 56 (2011) 8926.
[184] G.G. Wildgoose, N.S. Lawrence, H.C. Leventis, L. Jiang, T.G.J. Jones, R.G. Compton, *J. Mater. Chem*. 15 (2005) 953.
[185] M. Khoshroo, A.A. Rostami, *J. Electroanal. Chem*. 624 (2008) 205.
[186] S.R. Santos, G. Maia, *Electrochim. Acta* 71 (2012) 116.
[187] A.H.H. Tanji, F. Lima, S.R. Santos, G. Maia, *J. Phys. Chem. C* 116 (2012) 18857.
[188] J. Xu, W.H. Huang, R.L. McCreery, *J. Electroanal. Chem*. 410 (1996) 235.
[189] H.H. Yang, R.L. McCreery, *J. Electrochem. Soc.* 147 (2000) 3420.
[190] R.W. Zurilla, R.K. Sen, E.B. Yeager, *J. Electrochem. So*c. 125 (1978) 1103.
[191] A. Kuzume, E. Herrero, J.M. Feliu, E. Ahlberg, R.J. Nichols, D.J. Schiffrin, *Phys. Chem. Chem. Phys*. 7 (2005) 1293.
[192] A. Sarapuu, M. Nurmik, H. Mändar, A. Rosental, T. Laaksonen, K. Kontturi, D.J. Schiffrin, K. Tammeveski, *J. Electroanal. Chem*. 612 (2008) 78.
[193] F. Mirkhalaf, K. Tammeveski, D.J. Schiffrin, *Phys. Chem. Chem. Phys*. 11 (2009) 3463.
[194] M.S. Hossain, D. Tryk, E. Yeager, *Electrochim. Acta* 34 (1989) 1733.
[195] K. Vaik, D.J. Schiffrin, K. Tammeveski, *Electrochem. Commun*. 6 (2004) 1.
[196] J.C. Forti, J.A. Nunes, M.R.V. Lanza, R. Bertazzoli, *J. Appl. Electrochem*. 37 (2007) 527.
[197] B. Batanero, R. Saez, F. Barba, *Electrochim. Acta* 54 (2009) 4872.
[198] R.E. Davis, G.L. Horvath, C.W. Tobias, *Electrochim. Acta* 12 (1967) 287.
[199] R.G. Compton, C.E. Banks, Understanding Voltammetry, Imperial College Press, London, 2011.
[200] L.H. Guo, J.S. Facci, G. McLendon, *J. Phys. Chem*. 99 (1995) 8458.
[201] S. Campuzano, M. Pedrero, C. Montemayor, E. Fatas, J.M. Pingarron, *J. Electroanal. Chem*. 586 (2006) 112.
[202] A. Ambrosi, A. Bonanni, Z. Sofer, M. Pumera, *Nanoscale* 5 (2013) 2379.
[203] A.N. Obraztsov, A.V. Tyurnina, E.A. Obraztsova, A.A. Zolotukhin, B. Liu, K.-C. Chin, A.T.S. Wee, *Carbon* 46 (2008) 963.
[204] A.C. Ferrari, *Solid State Commun*. 143 (2007) 47.
[205] A.K. Geim, K.S. Novoselov, *Nat. Mater*. 6 (2007) 183.
[206] M.A. Pimenta, G. Dresselhaus, M.S. Dresselhaus, L.G. Cancado, A. Jorio, R. Saito, *Phys. Chem. Chem. Phys*. 9 (2007) 1276.
[207] R.L. McCreery, K.K. Cline, C.A. McDermott, M.T. McDermott, *Colloids Surf. A* 93 (1994) 211.
[208] A. Sarapuu, K. Helstein, K. Vaik, D.J. Schiffrin, K. Tammeveski, *Electrochim. Acta* 55 (2010) 6376.
[209] L. Qu, Y. Liu, J.-B. Baek, L. Dai, *ACS Nano* 4 (2010) 1321.
[210] I. Kruusenberg, J. Mondal, L. Matisen, V. Sammelselg, K. Tammeveski, *Electrochem. Commun*. 33 (2013) 18.
[211] A.C. Ferrari, J.C. Meyer, V. Scardaci, C. Casiraghi, M. Lazzeri, F. Mauri, S. Piscanec, D. Jiang, K.S. Novoselov, S. Roth, A.K. Geim, *Phys. Rev. Lett*. 97 (2006) 187401.
[212] D. Ajloo, B. Yoonesi, A. Soleymanpour, *Int. J. Electrochem. Sci*. 5 (2010) 459.
[213] M.W. Lehmann, D.H. Evans, *J. Electroanal. Chem*. 500 (2001) 12.
[214] R. Reilson, M. Kullapere, K. Tammeveski, *Electroanalysis* 22 (2010) 513.

[215] A. Adenier, C. Combellas, F. Kanoufi, J. Pinson, F.I. Podvorica, *Chem. Mater*. 18 (2006) 2021.
[216] M. Kullapere, L. Matisen, A. Saar, V. Sammelselg, K. Tammeveski, *Electrochem. Commun*. 9 (2007) 2412.
[217] G. Shul, R. Parent, H.A. Mosqueda, D. Bélanger, *ACS Appl. Mater. Interfaces* 5 (2013) 1468.
[218] K. Vaik, A. Sarapuu, K. Tammeveski, F. Mirkhalaf, D.J. Schiffrin, *J. Electroanal. Chem*. 564 (2004) 159.
[219] M. Mooste, E. Kibena, A. Sarapuu, L. Matisen, K. Tammeveski, *J. Electroanal. Chem*. 702 (2013) 8.

9. SUMMARY IN ESTONIAN

Klaassüsinik- ja kuldelektroodide ning kõrgorienteeritud pürolüütilise grafiidi ja keemilisel aurufaasist sadestamise meetodil valmistatud grafeeni elektrokeemiline modifitseerimine diasooniumisoolade redutseerumise meetodil

Doktoritöö eesmärk oli erinevate elektroodide modifitseerimine diasooniumisoolade elektrokeemilise redutseerumise meetodil, et uurida arüülkiledega kaetud elektroodide elektrokeemilisi omadusi.

Doktoritöös kasutati alusmaterjalina klaassüsinikku (GC) [I,II,IV–VI] ja kuldelektroode (Au) [III,IV], kõrgorienteeritud pürolüütilist grafiiti (HOPG) [V,VI] ja viimastel aastatel palju huvi tekitanud keemilisel aurufaasist sadestamise meetodil valmistatud grafeeni [V,VI]. Vastavalt eesmärgile, modifitseeriti eelpool mainitud elektroodid diasooniumisoolade elektrokeemilise redutseerumise meetodil erinevate arüülrühmadega: 4-nitrofenüül- (NP) [I], 4-karboksüfenüül- (CP) [I], asobenseen- (AB) [II,III], 2-metüül-4([2-metüülfenüül]aso)benseen- (GBC) [II–IV], 2,5-dimetoksü-4-([4-nitrofenüül]aso)benseen- (FBK) [II–IV] ja 9,10-antrakinoonrühmadega (AQ) [VI], kasutades vastavaid diasooniumisoolasid.

Doktoritöö esimeses osas keskenduti 2,2`-asino-bis(3-etüülbensotiasoliin-6-sulfoonhappe) diammooniumsoola (ABTS) elektrokeemilise käitumise uurimisele erineva pH väärtusega lahustes (pH=4–8) NP või CP rühmadega modifitseeritud GC elektroodidel. Lisaks kasutati NP kilega kaetud GC elektroodide puhul elektrokeemilist redutseerumist, et saada elektroodi pinnale aminofenüülrühmad (AP). Röntgenfotoelektronspektroskoopilise (XPS) analüüsi tulemused näitasid vastavate arüülrühmade (NP või AP) esinemist GC elektroodi pinnal. Tsüklilise voltamperomeetria (CV) ja pöörleva ketaselektroodi (RDE) eksperimentide põhjal võis järeldada, et ABTS-i redoks-protsess oli pH-st sõltumatu nii puhtal kui ka NP-modifitseeritud GC elektroodidel, kui modifitseerimisel kasutati suuremat potentsiaali tsüklite arvu. Samas suurimat pH efekti täheldati CP-modifitseeritud GC elektroodide korral.

Doktoritöö teises osas modifitseeriti GC ja Au elektroodid AB, GBC ja FBK diasooniumiühenditega, et võrrelda arüülrühmadega kaetud GC ja Au elektroodide pinna morfoloogiat ning elektrokeemilist käitumist heksatsüanoferraat(III)ioonide redutseerumisel ja hapniku redutseerumisel leeliselises lahuses. Pärast modifitseerimist kasutati arüülkilede iseloomustamiseks XPS-analüüsi, mille tulemused näitasid nii asorühmade kui ka asosildade teket kõigil arüülkiledega modifitseeritud GC ja Au elektroodidel ning lisaks ka nitrorühmade olemasolu FBK-modifitseeritud elektroodidel. Lisaks kinnitasid aatomjõumikroskoopia (AFM) ja kvartsmikrokaalude meetodil saadud tulemused arüülmodifikaatorite polükihtide moodustumist kuldelektroodi pinnal. CV ja RDE tulemused näitasid, et mõlema substraadi

puhul (GC või Au) oli kõige tugevamalt $Fe(CN)_6^{3-/4-}$ redokspaari signaal maha surutud asobenseeniga modifitseeritud elektroodide korral, aga hapniku redutseerumisel ei olnud kõigil juhtudel arüülkilede blokeerivad omadused piisavalt efektiivsed, et redutseerumisprotsessi täielikult inhibeerida. Kokkuvõtvalt võib öelda, et arüülrühmadega modifitseeritud GC elektroodide puhul oli nii heksatsüanoferraat(III)ioonide laenguülekande- kui ka hapniku redutseerumise protsess rohkem inhibeeritud kui sarnaselt modifitseeritud Au elektroodide korral [II,III]. Kuna arüülkiled GC ja Au pinnal blokeerisid muuhulgas heksatsüanoferraat(III)ioonide laenguülekannet ning pärast eksperimente oli näha, et arüülkilede eemaldamiseks nii GC kui ka Au pinnalt oli vaja rakendada mehaanilist töötlemist, oli huvipakkuv edasi uurida, kuidas mõjutab $OH^{\bullet}$ radikaalidega töötlemine asobenseeni derivaatidega modifitseeritud GC ja Au elektroodide omadusi. Arüülkilede lagundamiseks kasutati $OH^{\bullet}$ radikaalide tekitamiseks vesinikperoksiidi ja ultraviolettkiirgust. Eksperimentaalsed tulemused näitasid, et $OH^{\bullet}$ radikaalidega töötlemine lagundab GC ja Au elektroodidel arüülkilesid, kusjuures Au elektroodidel toimus arüülkilede lagundamine kiiremini kui GC elektroodidel [IV].

Doktoritöö viimases osas uuriti antrakinooniga (AQ) modifitseeritud ja modifitseerimata HOPG ja uudse nanomaterjali, grafeeni, morfoloogilisi ning elektrokeemilisi omadusi. Võrdlusena kasutati ka klaassüsinikelektroodi. Ramani spektroskoopia, kõrglahutusega skaneeriva elektronmikroskoopia ja AFM tulemused kinnitasid mitmekihilise grafeeni olemasolu nikkelfooliumil [V], kusjuures Ramani spektroskoopia mõõtmised täheldasid pigem monokihi esinemist vaskfooliumil [VI]. Tsüklilised voltamperogrammid näitasid, et puhta HOPG ja mitmekihilise grafeeni elektrokeemiline käitumine oli omavahel sarnane ning eelpool toodud materjalid olid pigem inaktiivsed, võrreldes puhta GC elektroodiga [V]. Järgnevalt uuriti esmakordselt paksude antrakinooni kilede moodustumist HOPG ja keemilisel aurufaasist sadestamise meetodil valmistatud grafeeni (nii Ni kui ka Cu alusel) pinnal. Olenevalt alusmaterjalist, mõõdeti AQ kile paksuseks 7–60 nm kasutades AFM kraapimise tehnikat või ellipsomeetriat. Lähtudes AFM ja elektrokeemiliste eksperimentide tulemustest võib väita, et arüülkilede struktuur ning elektrokeemilised omadused sõltuvad suuresti alusmaterjalist (GC, HOPG, ühe- või mitmekihiline grafeen). Näiteks heksatsüanoferraat(III)ioonide laenguülekandeprotsess oli AQ-modifitseeritud GC elektroodide korral täielikult maha surutud ning suurel määral ka AQ-modifitseeritud mitmekihilise grafeeni puhul. Samas kui modifitseerimisel kasutati alusmaterjalina HOPG või ühekihilist grafeeni, oli antud elektroodidel $Fe(CN)_6^{3-/4-}$ redokspaari signaal oluliselt vähem inhibeeritud. Huvitavaid tulemusi saadi ka hapniku redutseerumise uurimisel leeliselises lahuses. Nimelt näitasid AQ-modifitseeritud HOPG ja grafeen väga head elektrokatalüütilist efekti võrreldes modifitseerimata substraatidega [VI].

10. ACKNOWLEDGEMENTS

First, I would like to thank my supervisor, Assoc. Prof. Kaido Tammeveski, for his assistance, guidance, support and patience during the past four years over my PhD studies and for providing great input into this work.

I would also like to thank Assoc. Prof. Uno Mäeorg for his guidance and assistance in synthesising different diazonium compounds, Prof. Väino Sammelselg for supporting with different electrode materials, Dr. Leonard Matisen for the XPS measurements, Dr. Margus Marandi for the AFM measurements, Dr. Aarne Kasikov for the ellipsometry measurements and Jekaterina Kozlova for making the CVD-grown graphene substrates on Ni foil as well as performing the HR-SEM and Raman spectroscopy measurements.

I am very grateful for our research collaborators, Prof. Kim Daasbjerg and Assoc. Prof. Steen U. Pedersen from Aarhus University (Denmark) and Prof. Fritz Scholz and Dr. Ulrich Hasse from the University of Greifswald (Germany) for the international research opportunity, their helpful advice, discussions and making my stay abroad wonderful. In addition, I would also like to thank Bjarke B. E. Jensen, Anders B. Mortensen, Mikkel Kongsfelt and Mie Lillethorup from Aarhus University for making the CVD-grown graphene substrates on Cu foil, for performing the Raman spectroscopy measurements and for helping to synthesise the 9,10-anthraquinone-1-diazonium compound. I am also grateful to Dr. Gilberto Maia and Dr. Luna B. Venarusso from Universidade Federal de Mato Grosso do Sul (Brazil) for the international collaboration as well as for performing the EQCM and EIS measurements.

My special gratitude goes to my fellow co-workers and friends from the Institute of Chemistry (University of Tartu), Department of Chemistry and Interdisciplinary Nanoscience Center (Aarhus University) and Institute of Biochemistry (University of Greifswald) for the discussions, support, lab assistance and a nice atmosphere in the office and the lab.

I would like to express my personal and sincere gratitude to my parents, Eike Kibena and Ennu Kibena, and to my fiancé, Tanel Põldsepp, for their continuous support throughout my studies and for believing in me. In addition, I am grateful to my friends from Estonia and elsewhere for their support.

This work has been supported by the Estonian Science Foundation (Grants Nos. 9323 and 8666), the Estonian Ministry of Education and Research (IUT20-16, IUT02-24 and TK117) and partially supported by the grant of the Rector of the University of Greifswald for supporting the cooperation with Baltic countries, the Danish Council for Independent Research (DFF-1323-00136), Archimedes Foundation, DoRa scholarships and graduate school „Functional materials and technologies“ receiving funding from the European Social Fund under project 1.2.0401.09-0079 in Estonia.

11. PUBLICATIONS

CURRICULUM VITAE

Name:	Elo Kibena
Born:	22.04.1986
Citizenship:	Estonian
Address:	Institute of Chemistry, University of Tartu Ravila 14a, 50411 Tartu, Estonia
Phone:	+372 737 5174
E-mail:	elo.kibena@ut.ee

Education:

2010–	Institute of Chemistry, University of Tartu, PhD student
2008–2010	Institute of Chemistry, University of Tartu, Master´s degree in environmental technology
2005–2008	Türi College, University of Tartu, Diploma of professional higher education in environmental science

Professional employment:

07.2011–	Institute of Chemistry, University of Tartu, chemist (0.5)
09.2010–06.2011	Institute of Chemistry, University of Tartu, chemist (0.25)

Major scientific publications:

1. E. Kibena, M. Marandi, V. Sammelselg, K. Tammeveski, B.B.E. Jensen, A.B. Mortensen, M. Lillethorup, M. Kongsfelt, S.U. Pedersen, K. Daasbjerg, Electrochemical behaviour of HOPG and CVD-grown graphene electrodes modified with thick anthraquinone films by diazonium reduction (2014, submitted).
2. E. Kibena, M. Mooste, J. Kozlova, M. Marandi, V. Sammelselg, K. Tammeveski, Surface and electrochemical characterisation of CVD grown graphene sheets, *Electrochemistry Communications* 35 (2013) 26–29.
3. E. Kibena, K. Tammeveski, L. Matisen, U. Hasse, F. Scholz, $OH^{\bullet}$ radical degradation of blocking aryl layers on glassy carbon and gold electrodes leads to film thinning on glassy carbon and pinhole films on gold, *Electrochemistry Communications* 29 (2013) 33–36.
4. E. Kibena, M. Marandi, U. Mäeorg, L.B. Venarusso, G. Maia, L. Matisen, A. Kasikov, V. Sammelselg, K. Tammeveski, Electrochemical modification of gold electrodes with azobenzene derivatives by diazonium reduction, *ChemPhysChem* 14 (2013) 1043–1054.
5. E. Kibena, U. Mäeorg, L. Matisen, P. Sulamägi, K. Tammeveski, A study of glassy carbon electrodes modified with azobenzene derivatives, *Journal of Electroanalytical Chemistry* 686 (2012) 46–53.

6. E. Kibena, U. Mäeorg, L. Matisen, K. Tammeveski, Electrochemical behaviour of ABTS on aryl-modified glassy carbon electrodes, *Journal of Electroanalytical Chemistry* 661 (2011) 343–350.
7. M. Mooste, E. Kibena, J. Kozlova, A. Kasikov, M. Marandi, L. Matisen, V. Sammelselg, K. Tammeveski, Electrografting and morphological studies of CVD-grown graphene modified by electroreduction of corresponding diazonium salts (manuscript under preparation).
8. M. Mooste, E. Kibena, A. Sarapuu, L. Matisen, K. Tammeveski, Oxygen reduction on thick anthraquinone films electrografted to glassy carbon, *Journal of Electroanalytical Chemistry* 702 (2013) 8–14.
9. M. Mooste, E. Kibena, A. Sarapuu, U. Mäeorg, G. Maia, K. Tammeveski, Electrocatalysis of oxygen reduction on glassy carbon electrodes modified with anthraquinone moieties, *Journal of Solid State Electrochemistry* 18 (2014) 1725–1733.
10. E. Kibena, M. Raud, E. Jõgi, T. Kikas, Semi-specific *Microbacterium phyllosphaerae*-based microbial sensor for biochemical oxygen demand measurements in dairy wastewater, *Environmental Science and Pollution Research* 20 (2013) 2492–2498.
11. M. Raud, E. Linde, E. Kibena, S. Velling, T. Tenno, E. Talpsep, T. Kikas, Semi-specific biosensors for measuring BOD in dairy wastewater, *Journal of Chemical Technology and Biotechnology* 85 (2010) 957–961.

ELULOOKIRJELDUS

Nimi:	Elo Kibena
Sünniaeg:	22.04.1986
Kodakondsus:	Eesti
Aadress:	Tartu Ülikool, Keemia instituut Ravila 14a, 50411 Tartu, Eesti
Telefon:	+372 737 5174
E-post:	elo.kibena@ut.ee

Haridus:

2010–	Tartu Ülikool, Keemia instituut, doktoriõppe üliõpilane
2008–2010	Tartu Ülikool, Keemia instituut, magistrikraad keskkonna-tehnoloogias
2005–2008	Tartu Ülikooli Türi Kolledž, rakenduslik kõrgharidus keskkonnateaduses

Teenistuskäik:

07.2011–	Tartu Ülikool, Keemia instituut, keemik (0.5)
09.2010–06.2011	Tartu Ülikool, Keemia instituut, keemik (0.25)

Olulisemad publikatsioonid:

1. E. Kibena, M. Marandi, V. Sammelselg, K. Tammeveski, B.B.E. Jensen, A.B. Mortensen, M. Lillethorup, M. Kongsfelt, S.U. Pedersen, K. Daasbjerg, Electrochemical behaviour of HOPG and CVD-grown graphene electrodes modified with thick anthraquinone films by diazonium reduction (2014, käsikiri saadetud avaldamiseks).
2. E. Kibena, M. Mooste, J. Kozlova, M. Marandi, V. Sammelselg, K. Tammeveski, Surface and electrochemical characterisation of CVD grown graphene sheets, *Electrochemistry Communications* 35 (2013) 26–29.
3. E. Kibena, K. Tammeveski, L. Matisen, U. Hasse, F. Scholz, $OH^{\bullet}$ radical degradation of blocking aryl layers on glassy carbon and gold electrodes leads to film thinning on glassy carbon and pinhole films on gold, *Electrochemistry Communications* 29 (2013) 33–36.
4. E. Kibena, M. Marandi, U. Mäeorg, L.B. Venarusso, G. Maia, L. Matisen, A. Kasikov, V. Sammelselg, K. Tammeveski, Electrochemical modification of gold electrodes with azobenzene derivatives by diazonium reduction, *ChemPhysChem* 14 (2013) 1043–1054.
5. E. Kibena, U. Mäeorg, L. Matisen, P. Sulamägi, K. Tammeveski, A study of glassy carbon electrodes modified with azobenzene derivatives, *Journal of Electroanalytical Chemistry* 686 (2012) 46–53.

6. E. Kibena, U. Mäeorg, L. Matisen, K. Tammeveski, Electrochemical behaviour of ABTS on aryl-modified glassy carbon electrodes, *Journal of Electroanalytical Chemistry* 661 (2011) 343–350.
7. M. Mooste, E. Kibena, J. Kozlova, A. Kasikov, M. Marandi, L. Matisen, V. Sammelselg, K. Tammeveski, Electrografting and morphological studies of CVD-grown graphene modified by electroreduction of corresponding diazonium salts (artikli käsikiri on valmimisel).
8. M. Mooste, E. Kibena, A. Sarapuu, L. Matisen, K. Tammeveski, Oxygen reduction on thick anthraquinone films electrografted to glassy carbon, *Journal of Electroanalytical Chemistry* 702 (2013) 8–14.
9. M. Mooste, E. Kibena, A. Sarapuu, U. Mäeorg, G. Maia, K. Tammeveski, Electrocatalysis of oxygen reduction on glassy carbon electrodes modified with anthraquinone moieties, *Journal of Solid State Electrochemistry* 18 (2014) 1725–1733.
10. E. Kibena, M. Raud, E. Jõgi, T. Kikas, Semi-specific *Microbacterium phyllosphaerae*-based microbial sensor for biochemical oxygen demand measurements in dairy wastewater, *Environmental Science and Pollution Research* 20 (2013) 2492–2498.
11. M. Raud, E. Linde, E. Kibena, S. Velling, T. Tenno, E. Talpsep, T. Kikas, Semi-specific biosensors for measuring BOD in dairy wastewater, *Journal of Chemical Technology and Biotechnology* 85 (2010) 957–961.

DISSERTATIONES CHIMICAE UNIVERSITATIS TARTUENSIS

1. **Toomas Tamm.** Quantum-chemical simulation of solvent effects. Tartu, 1993, 110 p.
2. **Peeter Burk.** Theoretical study of gas-phase acid-base equilibria. Tartu, 1994, 96 p.
3. **Victor Lobanov.** Quantitative structure-property relationships in large descriptor spaces. Tartu, 1995, 135 p.
4. **Vahur Mäemets.** The ^{17}O and ^{1}H nuclear magnetic resonance study of H_2O in individual solvents and its charged clusters in aqueous solutions of electrolytes. Tartu, 1997, 140 p.
5. **Andrus Metsala.** Microcanonical rate constant in nonequilibrium distribution of vibrational energy and in restricted intramolecular vibrational energy redistribution on the basis of slater's theory of unimolecular reactions. Tartu, 1997, 150 p.
6. **Uko Maran.** Quantum-mechanical study of potential energy surfaces in different environments. Tartu, 1997, 137 p.
7. **Alar Jänes.** Adsorption of organic compounds on antimony, bismuth and cadmium electrodes. Tartu, 1998, 219 p.
8. **Kaido Tammeveski.** Oxygen electroreduction on thin platinum films and the electrochemical detection of superoxide anion. Tartu, 1998, 139 p.
9. **Ivo Leito.** Studies of Brønsted acid-base equilibria in water and non-aqueous media. Tartu, 1998, 101 p.
10. **Jaan Leis.** Conformational dynamics and equilibria in amides. Tartu, 1998, 131 p.
11. **Toonika Rinken.** The modelling of amperometric biosensors based on oxidoreductases. Tartu, 2000, 108 p.
12. **Dmitri Panov.** Partially solvated Grignard reagents. Tartu, 2000, 64 p.
13. **Kaja Orupõld.** Treatment and analysis of phenolic wastewater with microorganisms. Tartu, 2000, 123 p.
14. **Jüri Ivask.** Ion Chromatographic determination of major anions and cations in polar ice core. Tartu, 2000, 85 p.
15. **Lauri Vares.** Stereoselective Synthesis of Tetrahydrofuran and Tetrahydropyran Derivatives by Use of Asymmetric Horner-Wadsworth-Emmons and Ring Closure Reactions. Tartu, 2000, 184 p.
16. **Martin Lepiku.** Kinetic aspects of dopamine D_2 receptor interactions with specific ligands. Tartu, 2000, 81 p.
17. **Katrin Sak.** Some aspects of ligand specificity of P2Y receptors. Tartu, 2000, 106 p.
18. **Vello Pällin.** The role of solvation in the formation of iotsitch complexes. Tartu, 2001, 95 p.

19. **Katrin Kollist.** Interactions between polycyclic aromatic compounds and humic substances. Tartu, 2001, 93 p.
20. **Ivar Koppel.** Quantum chemical study of acidity of strong and superstrong Brønsted acids. Tartu, 2001, 104 p.
21. **Viljar Pihl.** The study of the substituent and solvent effects on the acidity of OH and CH acids. Tartu, 2001, 132 p.
22. **Natalia Palm.** Specification of the minimum, sufficient and significant set of descriptors for general description of solvent effects. Tartu, 2001, 134 p.
23. **Sulev Sild.** QSPR/QSAR approaches for complex molecular systems. Tartu, 2001, 134 p.
24. **Ruslan Petrukhin.** Industrial applications of the quantitative structure-property relationships. Tartu, 2001, 162 p.
25. **Boris V. Rogovoy.** Synthesis of (benzotriazolyl)carboximidamides and their application in relations with *N*- and *S*-nucleophyles. Tartu, 2002, 84 p.
26. **Koit Herodes.** Solvent effects on UV-vis absorption spectra of some solvatochromic substances in binary solvent mixtures: the preferential solvation model. Tartu, 2002, 102 p.
27. **Anti Perkson.** Synthesis and characterisation of nanostructured carbon. Tartu, 2002, 152 p.
28. **Ivari Kaljurand.** Self-consistent acidity scales of neutral and cationic Brønsted acids in acetonitrile and tetrahydrofuran. Tartu, 2003, 108 p.
29. **Karmen Lust.** Adsorption of anions on bismuth single crystal electrodes. Tartu, 2003, 128 p.
30. **Mare Piirsalu.** Substituent, temperature and solvent effects on the alkaline hydrolysis of substituted phenyl and alkyl esters of benzoic acid. Tartu, 2003, 156 p.
31. **Meeri Sassian.** Reactions of partially solvated Grignard reagents. Tartu, 2003, 78 p.
32. **Tarmo Tamm.** Quantum chemical modelling of polypyrrole. Tartu, 2003. 100 p.
33. **Erik Teinemaa.** The environmental fate of the particulate matter and organic pollutants from an oil shale power plant. Tartu, 2003. 102 p.
34. **Jaana Tammiku-Taul.** Quantum chemical study of the properties of Grignard reagents. Tartu, 2003. 120 p.
35. **Andre Lomaka.** Biomedical applications of predictive computational chemistry. Tartu, 2003. 132 p.
36. **Kostyantyn Kirichenko.** Benzotriazole – Mediated Carbon–Carbon Bond Formation. Tartu, 2003. 132 p.
37. **Gunnar Nurk.** Adsorption kinetics of some organic compounds on bismuth single crystal electrodes. Tartu, 2003, 170 p.
38. **Mati Arulepp.** Electrochemical characteristics of porous carbon materials and electrical double layer capacitors. Tartu, 2003, 196 p.

39. **Dan Cornel Fara.** QSPR modeling of complexation and distribution of organic compounds. Tartu, 2004, 126 p.
40. **Riina Mahlapuu.** Signalling of galanin and amyloid precursor protein through adenylate cyclase. Tartu, 2004, 124 p.
41. **Mihkel Kerikmäe.** Some luminescent materials for dosimetric applications and physical research. Tartu, 2004, 143 p.
42. **Jaanus Kruusma.** Determination of some important trace metal ions in human blood. Tartu, 2004, 115 p.
43. **Urmas Johanson.** Investigations of the electrochemical properties of polypyrrole modified electrodes. Tartu, 2004, 91 p.
44. **Kaido Sillar.** Computational study of the acid sites in zeolite ZSM-5. Tartu, 2004, 80 p.
45. **Aldo Oras.** Kinetic aspects of dATPαS interaction with $P2Y_1$ receptor. Tartu, 2004, 75 p.
46. **Erik Mölder.** Measurement of the oxygen mass transfer through the air-water interface. Tartu, 2005, 73 p.
47. **Thomas Thomberg.** The kinetics of electroreduction of peroxodisulfate anion on cadmium (0001) single crystal electrode. Tartu, 2005, 95 p.
48. **Olavi Loog.** Aspects of condensations of carbonyl compounds and their imine analogues. Tartu, 2005, 83 p.
49. **Siim Salmar.** Effect of ultrasound on ester hydrolysis in aqueous ethanol. Tartu, 2006, 73 p.
50. **Ain Uustare.** Modulation of signal transduction of heptahelical receptors by other receptors and G proteins. Tartu, 2006, 121 p.
51. **Sergei Yurchenko.** Determination of some carcinogenic contaminants in food. Tartu, 2006, 143 p.
52. **Kaido Tämm.** QSPR modeling of some properties of organic compounds. Tartu, 2006, 67 p.
53. **Olga Tšubrik.** New methods in the synthesis of multisubstituted hydrazines. Tartu. 2006, 183 p.
54. **Lilli Sooväli.** Spectrophotometric measurements and their uncertainty in chemical analysis and dissociation constant measurements. Tartu, 2006, 125 p.
55. **Eve Koort.** Uncertainty estimation of potentiometrically measured ph and pK_a values. Tartu, 2006, 139 p.
56. **Sergei Kopanchuk.** Regulation of ligand binding to melanocortin receptor subtypes. Tartu, 2006, 119 p.
57. **Silvar Kallip.** Surface structure of some bismuth and antimony single crystal electrodes. Tartu, 2006, 107 p.
58. **Kristjan Saal.** Surface silanization and its application in biomolecule coupling. Tartu, 2006, 77 p.
59. **Tanel Tätte.** High viscosity $Sn(OBu)_4$ oligomeric concentrates and their applications in technology. Tartu, 2006, 91 p.

60. **Dimitar Atanasov Dobchev**. Robust QSAR methods for the prediction of properties from molecular structure. Tartu, 2006, 118 p.
61. **Hannes Hagu**. Impact of ultrasound on hydrophobic interactions in solutions. Tartu, 2007, 81 p.
62. **Rutha Jäger.** Electroreduction of peroxodisulfate anion on bismuth electrodes. Tartu, 2007, 142 p.
63. **Kaido Viht.** Immobilizable bisubstrate-analogue inhibitors of basophilic protein kinases: development and application in biosensors. Tartu, 2007, 88 p.
64. **Eva-Ingrid Rõõm.** Acid-base equilibria in nonpolar media. Tartu, 2007, 156 p.
65. **Sven Tamp.** DFT study of the cesium cation containing complexes relevant to the cesium cation binding by the humic acids. Tartu, 2007, 102 p.
66. **Jaak Nerut.** Electroreduction of hexacyanoferrate(III) anion on Cadmium (0001) single crystal electrode. Tartu, 2007, 180 p.
67. **Lauri Jalukse.** Measurement uncertainty estimation in amperometric dissolved oxygen concentration measurement. Tartu, 2007, 112 p.
68. **Aime Lust.** Charge state of dopants and ordered clusters formation in CaF_2:Mn and CaF_2:Eu luminophors. Tartu, 2007, 100 p.
69. **Iiris Kahn**. Quantitative Structure-Activity Relationships of environmentally relevant properties. Tartu, 2007, 98 p.
70. **Mari Reinik.** Nitrates, nitrites, N-nitrosamines and polycyclic aromatic hydrocarbons in food: analytical methods, occurrence and dietary intake. Tartu, 2007, 172 p.
71. **Heili Kasuk.** Thermodynamic parameters and adsorption kinetics of organic compounds forming the compact adsorption layer at Bi single crystal electrodes. Tartu, 2007, 212 p.
72. **Erki Enkvist.** Synthesis of adenosine-peptide conjugates for biological applications. Tartu, 2007, 114 p.
73. **Svetoslav Hristov Slavov**. Biomedical applications of the QSAR approach. Tartu, 2007, 146 p.
74. **Eneli Härk.** Electroreduction of complex cations on electrochemically polished Bi(*hkl*) single crystal electrodes. Tartu, 2008, 158 p.
75. **Priit Möller.** Electrochemical characteristics of some cathodes for medium temperature solid oxide fuel cells, synthesized by solid state reaction technique. Tartu, 2008, 90 p.
76. **Signe Viggor.** Impact of biochemical parameters of genetically different pseudomonads at the degradation of phenolic compounds. Tartu, 2008, 122 p.
77. **Ave Sarapuu.** Electrochemical reduction of oxygen on quinone-modified carbon electrodes and on thin films of platinum and gold. Tartu, 2008, 134 p.
78. **Agnes Kütt.** Studies of acid-base equilibria in non-aqueous media. Tartu, 2008, 198 p.

79. **Rouvim Kadis.** Evaluation of measurement uncertainty in analytical chemistry: related concepts and some points of misinterpretation. Tartu, 2008, 118 p.
80. **Valter Reedo.** Elaboration of IVB group metal oxide structures and their possible applications. Tartu, 2008, 98 p.
81. **Aleksei Kuznetsov.** Allosteric effects in reactions catalyzed by the cAMP-dependent protein kinase catalytic subunit. Tartu, 2009, 133 p.
82. **Aleksei Bredihhin.** Use of mono- and polyanions in the synthesis of multisubstituted hydrazine derivatives. Tartu, 2009, 105 p.
83. **Anu Ploom.** Quantitative structure-reactivity analysis in organosilicon chemistry. Tartu, 2009, 99 p.
84. **Argo Vonk.** Determination of adenosine A_{2A}- and dopamine D_1 receptor-specific modulation of adenylate cyclase activity in rat striatum. Tartu, 2009, 129 p.
85. **Indrek Kivi.** Synthesis and electrochemical characterization of porous cathode materials for intermediate temperature solid oxide fuel cells. Tartu, 2009, 177 p.
86. **Jaanus Eskusson.** Synthesis and characterisation of diamond-like carbon thin films prepared by pulsed laser deposition method. Tartu, 2009, 117 p.
87. **Marko Lätt.** Carbide derived microporous carbon and electrical double layer capacitors. Tartu, 2009, 107 p.
88. **Vladimir Stepanov.** Slow conformational changes in dopamine transporter interaction with its ligands. Tartu, 2009, 103 p.
89. **Aleksander Trummal.** Computational Study of Structural and Solvent Effects on Acidities of Some Brønsted Acids. Tartu, 2009, 103 p.
90. **Eerold Vellemäe.** Applications of mischmetal in organic synthesis. Tartu, 2009, 93 p.
91. **Sven Parkel.** Ligand binding to 5-HT_{1A} receptors and its regulation by Mg^{2+} and Mn^{2+}. Tartu, 2010, 99 p.
92. **Signe Vahur.** Expanding the possibilities of ATR-FT-IR spectroscopy in determination of inorganic pigments. Tartu, 2010, 184 p.
93. **Tavo Romann**. Preparation and surface modification of bismuth thin film, porous, and microelectrodes. Tartu, 2010, 155 p.
94. **Nadežda Aleksejeva.** Electrocatalytic reduction of oxygen on carbon nanotube-based nanocomposite materials. Tartu, 2010, 147 p.
95. **Marko Kullapere.** Electrochemical properties of glassy carbon, nickel and gold electrodes modified with aryl groups. Tartu, 2010, 233 p.
96. **Liis Siinor.** Adsorption kinetics of ions at Bi single crystal planes from aqueous electrolyte solutions and room-temperature ionic liquids. Tartu, 2010, 101 p.
97. **Angela Vaasa.** Development of fluorescence-based kinetic and binding assays for characterization of protein kinases and their inhibitors. Tartu 2010, 101 p.

98. **Indrek Tulp.** Multivariate analysis of chemical and biological properties. Tartu 2010, 105 p.
99. **Aare Selberg.** Evaluation of environmental quality in Northern Estonia by the analysis of leachate. Tartu 2010, 117 p.
100. **Darja Lavõgina.** Development of protein kinase inhibitors based on adenosine analogue-oligoarginine conjugates. Tartu 2010, 248 p.
101. **Laura Herm.** Biochemistry of dopamine D_2 receptors and its association with motivated behaviour. Tartu 2010, 156 p.
102. **Terje Raudsepp.** Influence of dopant anions on the electrochemical properties of polypyrrole films. Tartu 2010, 112 p.
103. **Margus Marandi.** Electroformation of Polypyrrole Films: *In-situ* AFM and STM Study. Tartu 2011, 116 p.
104. **Kairi Kivirand.** Diamine oxidase-based biosensors: construction and working principles. Tartu, 2011, 140 p.
105. **Anneli Kruve.** Matrix effects in liquid-chromatography electrospray mass-spectrometry. Tartu, 2011, 156 p.
106. **Gary Urb.** Assessment of environmental impact of oil shale fly ash from PF and CFB combustion. Tartu, 2011, 108 p.
107. **Nikita Oskolkov.** A novel strategy for peptide-mediated cellular delivery and induction of endosomal escape. Tartu, 2011, 106 p.
108. **Dana Martin.** The QSPR/QSAR approach for the prediction of properties of fullerene derivatives. Tartu, 2011, 98 p.
109. **Säde Viirlaid.** Novel glutathione analogues and their antioxidant activity. Tartu, 2011, 106 p.
110. **Ülis Sõukand.** Simultaneous adsorption of Cd^{2+}, Ni^{2+}, and Pb^{2+} on peat. Tartu, 2011, 124 p.
111. **Lauri Lipping.** The acidity of strong and superstrong Brønsted acids, an outreach for the "limits of growth": a quantum chemical study. Tartu, 2011, 124 p.
112. **Heisi Kurig.** Electrical double-layer capacitors based on ionic liquids as electrolytes. Tartu, 2011, 146 p.
113. **Marje Kasari.** Bisubstrate luminescent probes, optical sensors and affinity adsorbents for measurement of active protein kinases in biological samples. Tartu, 2012, 126 p.
114. **Kalev Takkis.** Virtual screening of chemical databases for bioactive molecules. Tartu, 2012, 122 p.
115. **Ksenija Kisseljova**. Synthesis of aza-β^3-amino acid containing peptides and kinetic study of their phosphorylation by protein kinase A. Tartu, 2012, 104 p.
116. **Riin Rebane.** Advanced method development strategy for derivatization LC/ESI/MS. Tartu, 2012, 184 p.

117. **Vladislav Ivaništšev.** Double layer structure and adsorption kinetics of ions at metal electrodes in room temperature ionic liquids. Tartu, 2012, 128 p.
118. **Irja Helm.** High accuracy gravimetric Winkler method for determination of dissolved oxygen. Tartu, 2012, 139 p.
119. **Karin Kipper.** Fluoroalcohols as Components of LC-ESI-MS Eluents: Usage and Applications. Tartu, 2012, 164 p.
120. **Arno Ratas.** Energy storage and transfer in dosimetric luminescent materials. Tartu, 2012, 163 p.
121. **Reet Reinart-Okugbeni**. Assay systems for characterisation of subtype-selective binding and functional activity of ligands on dopamine receptors. Tartu, 2012, 159 p.
122. **Lauri Sikk.** Computational study of the Sonogashira cross-coupling reaction. Tartu, 2012, 81 p.
123. **Karita Raudkivi.** Neurochemical studies on inter-individual differences in affect-related behaviour of the laboratory rat. Tartu, 2012, 161 p.
124. **Indrek Saar.** Design of GalR2 subtype specific ligands: their role in depression-like behavior and feeding regulation. Tartu, 2013, 126 p.
125. **Ann Laheäär.** Electrochemical characterization of alkali metal salt based non-aqueous electrolytes for supercapacitors. Tartu, 2013, 127 p.
126. **Kerli Tõnurist.** Influence of electrospun separator materials properties on electrochemical performance of electrical double-layer capacitors. Tartu, 2013, 147 p.
127. **Kaija Põhako-Esko.** Novel organic and inorganic ionogels: preparation and characterization. Tartu, 2013, 124 p.
128. **Ivar Kruusenberg.** Electroreduction of oxygen on carbon nanomaterial-based catalysts. Tartu, 2013, 191 p.
129. **Sander Piiskop.** Kinetic effects of ultrasound in aqueous acetonitrile solutions. Tartu, 2013, 95 p.
130. **Ilona Faustova**. Regulatory role of L-type pyruvate kinase N-terminal domain. Tartu, 2013, 109 p.
131. **Kadi Tamm.** Synthesis and characterization of the micro-mesoporous anode materials and testing of the medium temperature solid oxide fuel cell single cells. Tartu, 2013, 138 p.
132. **Iva Bozhidarova Stoyanova-Slavova.** Validation of QSAR/QSPR for regulatory purposes. Tartu, 2013, 109 p.
133. **Vitali Grozovski**. Adsorption of organic molecules at single crystal electrodes studied by *in situ* STM method. Tartu, 2014, 146 p.
134. **Santa Veikšina**. Development of assay systems for characterisation of ligand binding properties to melanocortin 4 receptors. Tartu, 2014, 151 p.
135. **Jüri Liiv.** PVDF (polyvinylidene difluoride) as material for active element of twisting-ball displays. Tartu, 2014, 111 p.

136. **Kersti Vaarmets.** Electrochemical and physical characterization of pristine and activated molybdenum carbide-derived carbon electrodes for the oxygen electroreduction reaction. Tartu, 2014, 131 p.
137. **Lauri Tõntson**. Regulation of G-protein subtypes by receptors, guanine nucleotides and Mn^{2+}. Tartu, 2014, 105 p.
138. **Aiko Adamson.** Properties of amine-boranes and phosphorus analogues in the gas phase. Tartu, 2014, 85 p.